Physically-Based Numerical Modelling to Identify Permafrost Degradation due to Climate Change in Northern Manitoba

By

Bekalu Getachew Erkabu

A thesis submitted to

the Faculty of Graduate Studies of

the University of Manitoba

in partial fulfillment of

the requirements for the degree of

Master of Science

Department of Civil Engineering
Price Faculty of Engineering
University of Manitoba
Winnipeg, Manitoba

May 2021

Abstract

A critical factor in permafrost degradation is the hydrological processes' changes, which result from free-flowing water, such as soil water or groundwater, and their associated flow paths. Hydrological models calibrated under current climate conditions are less likely to accurately predict the water budget of a catchment under permafrost degradation under future climate conditions. However, such models are used to help manage large watersheds in northern Canada, which are used for hydropower generation, and are essential for strategic planning on the future supply of energy. This research was conducted to understand and identify the potential impact of permafrost thawing on the hydrological regime within the Nelson-Churchill River Basin (NCRB) due to climate change. Numerical models were developed using HYDRUS-1D and Hansson's module to analyze potential changes in ground temperature resulting from climate change to establish detailed physical-based understanding of the changes in the active layer. The calibration process was carried out using soil temperature data for 2014-2015 and validated by 2011-2012 data. Data from two Global Circulation Models (GCMs), namely, CanESM2 (Canadian Center for Climate Modelling Second Generation Earth System Model) and MIROC5 (Model for Interdisciplinary Research on Climate), were used to analyze potential future changes in active layer thickness due to climate change under two emission scenarios (RCP8.5 and RCP4.5). The investigation showed that permafrost remained stable in sites with peat layers. The lower emission scenario forcing predicted up to 1 m increase in active layer thickness whereas up to 5 meters increase of the active layer thickness was observed for both GCMs under high emission scenarios by 2080.

Acknowledgments

I would like to express my gratitude to every individual who played a vital role throughout my study and conducting this research. To my advisor Dr. Hartmut Holländer, PEng., I am grateful to be part of your team. I am thankful for your professional guidance, advice, and encouragement throughout this research and my stay at the University of Manitoba. I would also like to thank my advisory committee members Dr. Pooneh Maghoul, PEng., and Dr. Siri Ranjan, PEng.

I would like to thank Efrem T/Mariam, PEng, Kristina Koenig, PEng, Michael Vieira, PEng, Shane Wruth, PEng, Dr. Getnet Muluye, PEng, and other members of the Hydroclimatic studies of Manitoba Hydro that supported this research idea from its inception and professionally advised and guided me till completion.

This research would not have been possible without the financial support of NSERC and in-kind support of Manitoba Hydro.

My sincere gratitude also goes to members of the Ethio-Eritrean EGM chapter, Dr. Sitotaw Zeleke PEng., and Dr. Tebikachew Betru, who have always encouraged, supported, and mentored me since the day I arrived in Manitoba. Thank you! May God bless you and your families.

To my friends, Gebeyehu Ayele, Semhar Ekubamichael, Naeem Ahmed, Moges Dagne, and Nurelegn Hussein, I am thankful for their unconditional love and support. To Miad Jarrahi and Bernard Ayumu, thank you for your guidance and constructive discussions during my study.

Finally, words would not describe my gratitude towards Hailemelecot Ayenachew, my brothers and my sisters despite the long distance.

Contributions of authors

Bekalu G. Erkabu, Hartmut M. Holländer. *Physical-Based Numerical Modelling to Identify Permafrost Degradation due to Climate Change in Northern Manitoba*

I. Bekalu G. Erkabu: Developed and implemented the methodology for evaluating permafrost degradation due to climate change and wrote the paper
II. Hartmut M. Holländer: Supervised this research and assisted with the editing of the paper

Table of Contents

List of Tables

List of Figures

List of Appendices

List of All Variables

b_1	empirical parameters [-]
b_2	empirical parameters [-]
b_3	empirical parameters [-]
C_i	volumetric heat capacities of ice [$ML^{-1}T^{-2}K^{-1}$]
C_n	volumetric heat capacities of the solid [$ML^{-1}T^{-2}K^{-1}$]
C_p	volumetric heat capacity of the soil [$ML^{-1}T^{-2}K^{-1}$]
C_v	volumetric heat capacities of vapour [$ML^{-1}T^{-2}K^{-1}$]
C_w	volumetric heat capacities of the liquid [$ML^{-1}T^{-2}K^{-1}$]
o	organic matter [-]
t	time [T]
θ_i	volumetric ice content [-]
θ_r	residual water content [-]
θ_s	saturated water content [-]
θ_v	volumetric water content [-]
λ	latent heat of fusion of water [L^2T^{-2}]
$\lambda(\theta)$	coefficient of the apparent thermal conductivity [$MLT^{-3}K^{-1}$]
$\lambda_0(\theta)$	thermal conductivity [$MLT^{-3}K^{-1}$]
L_0	volumetric latent heat of the water [$ML^{-1}T^{-2}$]
L_f	latent heat of freezing [L^2T^{-2}]
L_w	latent heat due to the vaporization of water [$ML^{-1}T^{-2}$]

ρ_i	density of ice [ML^{-3}]
ρ_T	density of soil water at temperature T [ML^{-3}]
ρ_w	density of liquid water [ML^{-3}]

List of Acronyms

1D	One-Dimensional
2D	Two-Dimensional
3D	Three-Dimensional
ATL	Active layer thickness
B01	Borehole 1
B02	Borehole2
B03	Borehole 3
B04	Borehole 4
B05	Borehole 5
B06	Borehole 6
B07	Borehole 7
B08	Borehole 8
CMIP5	Coupled Model Intercomparison Phase 5
RCP4.5	Representative concentration pathways
RCP8.5	Representative concentration pathways
RMSE	Root Mean Square Error

1 Introduction

1.1 Overview

Permafrost present in one-quarter of the exposed land in the Northern Hemisphere (Zhang et al. 1999). It is defined as ground that remains at or below 0°C for two or more consecutive years (Dobinski 2011, Walvoord and Kurylyk 2016). Permafrost is divided into continuous, discontinuous, and sporadic zones depending on its areal extent and continuity (Dobinski 2011, Walvoord and Kurylyk 2016). Its' distribution at the regional and continental scale is strongly related to mean annual air temperature (Bonnaventure and Lewkowicz 2013). Other factors also play vital role in permafrost distribution for example, elevation, depth, and duration of snow cover, slope, aspect, geology and vegetation (Carturan et al. 2016, Dobinski 2011, Zhao et al. 2017). Permafrost presence has significant impact on the ecological, biological and hydrological processes in the region and it controls the fundamental characteristics of the water cycle (Zhang et al. 2017b).

The current climate warming is causing an increase in the thaw depth of the permafrost layer, resulting in degradation of permafrost (Kurylyk et al. 2016) and also, a considerable degradation of permafrost is projected by the end of the 21st century as a consequence of global warming (Chadburn et al. 2017, Koven et al. 2013, Shojae Ghias et al. 2019, Wagner et al. 2018). This trend results in a reduction of the areal extent (Bonnaventure and Lewkowicz 2011) and an increase of the active layer (Biskaborn et al. 2019, Boike et al. 2019) in the remaining permafrost areas. Camill (2005) examined the rates of discontinuous permafrost thawing in Northern Manitoba and concluded that temperature warming by a rate of 4-8°C would eliminate most of the present range

of sporadic and discontinuous permafrost by the end of 21st century. Such predictions are in line with current measurements of permafrost temperatures in boreholes (Boike et al. 2019).

As this climate warming trend continues, permafrost degradation is leading to catastrophic structural foundation damage, roads, bridges, and runways failure in the cold regions (Anisimov and Reneva 2006, Bao et al. 2019). It is also impacting hydrological cycles (Shojae Ghias et al. 2019, Walvoord and Kurylyk 2016) resulting in increasing winter baseflow (Duan et al. 2017), and the release of greenhouse gas into the atmosphere (Byun et al. 2017, Plaza et al. 2019, Shmelev et al. 2017). The hydrology in the Northern Hemisphere was greatly affected by permafrost degradation (Quinton et al. 2019). The flow patterns in the unsaturated zone and snowmelt water partitioning into runoff and infiltration were highly affected by the changing temperature of this region. Stone et al. (2019) demonstrated that the degradation of discontinuous permafrost in the Northwest Territories, Canada resulted in the reduction of discharge and increase of landscape evapotranspiration.

The hydrology of cold regions is changing and Canada is prone to these changes (Derksen et al. 2018, Quinton et al. 2019). Numerical model developments, laboratory, and field-based approaches to capture relevant physical processes in the cold region are important as these developments the increase understanding of the impact of climate change on permafrost degradation and their role in infrastructure and ecological hazards (Connon et al. 2014, Shojae Ghias et al. 2019). Recent developments on groundwater flow models were applied to investigate the complex interactions between climate change, permafrost and hydrogeology (Bense et al. 2009, Bense et al. 2012, Cheng and Jin 2013, McKenzie and Voss 2013).

1.2 Research motivation

Manitoba Hydro has established climate change strategies to understand the changing climate, which incorporates measuring and reporting greenhouse gas (GHG) emissions to support GHG policy and market development. This can help adapt and plan further strategies to shape the organization's response to climate change (Manitoba Hydro 2020).

The scope of the climate change studies at Manitoba Hydro includes all the river basins in the Nelson- Churchill Watershed, which on average, supply approximately 95% of Manitoba Hydro's energy in the form of water. A series of comprehensive studies have been initiated to increase knowledge of the implications of future climate change on future water supply, energy demand and extreme events in the watershed, aiming to incorporate outcomes of the studies into long-term planning and operations and consequently adapt infrastructure and business practices as required (Manitoba Hydro 2020).

The climate change study incorporated hydroclimatic analysis and monitoring. Historical hydrology and climate data were collected to characterize the hydrological and climatic conditions in a watershed. The main aim was to provide a foundation for understanding future hydroclimatic variability and changes. Climate change scenarios, hydrological modeling, future runoff scenarios, and uncertainty in future projections are implemented in different hydrological models (Manitoba Hydro 2020).

Hydrological models calibrated under current climate conditions are less likely to accurately predict the water budget of a catchment under permafrost degradation in future climate conditions. Therefore, in addition to the required ensemble of modeling for the climate projections, different scenarios regarding additional hydrological processes, such as freezing and thawing, need to be considered. Changes in hydrological processes and their impact on hydrological modeling can be

found in Abolt et al. (2017) and in Holländer et al. (2009), where changes in soil crusting resulted in inaccurate forecasts of discharge from an experimental catchment.

1.3 Scope and Objectives

This research aims to understand and identify the potential impacts of permafrost thawing on the hydrological regime of the Nelson-Churchill River Basin (NCRB) due to climate change. The study evaluates permafrost degradation in northern Manitoba by two vadose-zone numerical models: HYDRUS-1D and Hansson module. The specific objectives include 1) evaluation of soil temperature data to identify permafrost zones and active layer thickness and 2) numerical investigation of the effects of climate change on permafrost degradation under different emission scenarios at a local scale.

1.4 Thesis organization

The remaining parts of the thesis are organized as follows; a literature review in the second chapter; a detailed description of the study area, data, methods, results, and discussion in the third chapter; the last chapter presents conclusions and recommendations for future studies.

2 Literature Review

2.1 Climate change

Climate change refers to a change in the state of the climate that can be identified by changes in the mean and/or the variability of its properties and that persists for an extended period, typically decades or longer (IPCC 2018). The observed rapid rate of warming exhibited in the arctic in recent years is attributed mainly to climate change (Anisimov and Reneva 2006). Current warming rates and future climate change projections in this region present anticipated vulnerabilities of different dimensions ranging from physical, ecological, social, and economic factors (Anisimov and Reneva 2006, Derksen et al. 2018, Luedtke and Howkins 2012). In the high arctic, permafrost temperature has increased by 0.3℃ to 0.5℃ per decade, and in Canada, regional observation in the central Mackenzie Valley has shown a warming rate of 0.1℃ per decade (Derksen et al. 2018).

Enhancing a better perspective and quantifying the extent of climate change impact has been possible through the development of general circulation models (GCMs), which are used to simulate both the temporal and spatial patterns of the observed climate. GCMs have been developed to simulate the present climate and used to predict future climate change. The commonly used GCMs includes the Canadian Climate Center (CCC) model, Canadian Environmental system (CanESM2, Arora et al. (2011)), and Model for Interdisciplinary Research On Climate (MIROC5, Watanabe et al. (2010)). Other prominent GCMs are compiled in Table 1. These GCMs run based on different emission scenarios commonly known as representative concentration pathways (RCP) (Moss et al. 2010, van Vuuren et al. 2011).

Table 1. Lists of CMIP5 Global Circulation Models (GCMs)

Model Name	Institutions
BCC-CSM1.1	Beijing Climate Center
BNU-ESM	Beijing Normal University
CCSM3	National Center for atmospheric research
CGCM3_1	Canadian Center for Climate Modelling and Analysis
CMCC-CM CMCC-CMS	Centro Euro-Mediteraneo per I Cambiamenti Climatici
CNRM-CM5	Centre National de Recherches Meteorologiques and Centre Europeen de Recherche et Formation Avancees en Calcul Scientific
CSIRO-Mk3.6.0	Queensland Climate Change Centre of Excellence and
CSIRO-Mk3L 1.2	Commonwealth Scientific and Industrial Research Organization
FGOALS-g2	LASG (Institute of Atmospheric Physics)- CESS (Tsinghua University)
GFDL-CM3 GFDL-ESM2G GFDL-ESM2M	NOAA Geophysical Fluid Dynamics Laboratory
HadCM3 HadGEM1	Hadley Center for Climate Prediction and Research
INM-CM4	Russian Institute for Numerical Mathematics
IPSL-CM4	Institut Pierre Simon Laplace (IPSL)
MIROC-ESM-CHEM MIROC-ESM MIROC4h	University of Tokyo, National Institute for Environmental Studies and Japan Agency for Marine-Earth Science and Technology
MPI-ESM-LR MPI-ESM-MR MPI-ESM-P	Max Planck Institute for Meteorology
MRI-CGCM3 MRI-ESM1	Meteorological Research Institute
NorESM1-M	Norwegian Climate Centre

The RCPs are named according to radiative, forcing the target level for 2100 (Moss et al. 2010). The estimates are based on the forcing of greenhouse gases and other agents (van Vuuren et al. 2011). RCPs represent socio-economic and emission scenarios used as inputs for climate

models to explore plausible future conditions (IPCC 2018). The RCPs include one mitigation scenario leading to a very low forcing level (RCP2.6), two medium stabilization scenarios (RCP4.5/RCP6) and a very high baseline emission scenarios (RCP8.5)(van Vuuren et al. 2011).

RCP2.6 emission and concentration pathway is representative of the literature on mitigation scenarios aiming to limit the increase of global mean temperature to 2°C (Vuuren et al. 2011). The RCP2.6 scenarios were shown to be technically feasible in the IMAGE integrated assessment modeling framework from a medium emission baseline scenario (Vuuren et al. 2006, Vuuren et al. 2007). It peaks in radiative forcing at ~ 3 W/m^2 (~490 ppm CO_2 equivalence) before 2100 and declines.

RCP4.5 was developed by the Global Change Assessment Model (GCAM) modeling team at the Pacific Northwest National Laboratory's Joint Global Change Research Institute (JGCRI) in the United States(Thomson et al. 2011). It is a stabilization scenario in which total radiative forcing is stabilized shortly after 2100, without overshooting the long-run radiative forcing target level to 4.5 W/m^2 (~650 ppm CO_2 equivalence) (Clarke et al. 2007, Smith and Wigley 2006, Wise et al. 2009).

RCP6.0 was developed by the Asian-Pacific Integrated (AIM) modeling team (Masui et al. 2011). It is a stabilization scenario in which total radiative forcing is stabilized shortly after 2100, without overshooting the long-run radiative forcing target level to 6.0 W/m^2 (~850 ppm CO_2 equivalence) (Fujino et al. 2006, Hijioka et al. 2008).

RCP8.5 was developed using the MESSAGE model and the IIASA Integrated Assessment Framework by the International Institute for Applied Systems Analysis (IIASA), Austria. This RCP is characterized by increasing greenhouse gas emissions over time, representing scenarios

rising radiative forcing pathway leading to 8.5 W/m^2 (~1370 ppm CO_2 equivalence) by 2100 (Riahi et al. 2007, Riahi et al. 2011).

An extensive amount of research has been conducted on identifying influences of climate change on different aspects of the hydrological cycle (precipitation, runoff, evapotranspiration, etc.) in many geographic areas (Adane et al. 2019, Booshehrian et al. 2019, Bush et al. 2019, IPCC 2018, Salem et al. 2018, Sannel et al. 2016, Way and Lewkowicz 2018). Climate change projections indicated an increase in the probability of drought in the Mediterranean basin and the Middle East (IPCC 2018), and variability in extreme events. Changes in future climate will alter regional hydrologic cycles and will subsequently have an impact on water resource availability (Kundzewicz and Somlyódy 1997).

Climate warming is alarming and resulted in permafrost temperature globally increase by 0.29 ± 0.12°C from 2007 to 2016 (Biskaborn et al. 2019). For the same period, an increase of temperature by 0.39 ± 0.15°C and 0.20 ± 0.10 °C in continuous and discontinuous permafrost zones were observed, respectively (Biskaborn et al. 2019). Research conducted in a different part of the globe depicts this; a study conducted in Samoylov Island, Siberia, showed that permafrost warmed by 1.3°C (Boike et al. 2019). Similar permafrost warming was observed in Marre Sale, northwestern Siberia, by 0.9°C (Biskaborn et al. 2019). In Tarfala Valley, Sweden, Hällberg (2018) conducted a basal temperature snow survey and developed a model showing the current permafrost extent in the study area. He explored the impact of climate change under different warming scenarios on permafrost extent and concluded that in 20 years, an increasing ground surface temperature by +1°C will result in degradation of 97.6% of the continuous permafrost. Liu et al. (2017) conducted a study to indicate permafrost warming in the context of step-wise climate change in Tien Shan mountain, China. They found that the active layer had increased by 0.45 m,

the permafrost also warmed by +0.6°C, and the permafrost base moved by 14 m during 1992 – 2011 and indicated this could be due to a step-wise change in air temperature.

Guo et al. (2012) conducted a study on the Tibetan Plateau focusing on the period 1980 – 2100 under the A1B green gas emission scenario using the CLM4 model (Community Land Model version 4) (Oleson et al. 2010) that included an explicit frozen soil process based on a heat conduction equation without phase change and latent heat impact. The phase change was calculated in a second step by applying a method presented by Press et al. (1992). The predicted results were close to the observations for the area evaluated. Future projection scenarios showed that by 2050 the areas under permafrost would reduce by nearly 40% and by the end of the century by more than 80%. The active layer thickness increased nearly by 1 m and 2 m for the 2050s' and 2080s' projections, respectively. The study also identified that the surface runoff would decrease, whereas the subsurface runoff would increase, both relative to precipitation and evapotranspiration. The of decrease in ground ice due to permafrost degradation allowed larger fraction of liquid water to readily drain and reallocating runoff. The study did not quantify the change in discharge. This study stands exemplary for large-scale modeling attempts.

Notably, the impact of a warming climate on permafrost has been indicated in Canada. Haynes et al. (2019) conducted a study in Scotty Creek, Northwest Territories and concluded that the discontinuous permafrost in the region is experiencing rapid warming and resulting in a land cover change from forest peatland permafrost terrain to treeless wetland. A similar conclusion was drawn by Beck et al. (2015) using remote sensing data for Umiujaq, sub-arctic Quebec, from 1986 to 2009. Bonnaventure and Lewkowicz (2013) had conducted a study on the impacts of mean annual air temperature change on a regional permafrost probability model for southern Yukon and northern British Columbia, Canada. They indicated that an increase in air temperature resulted in

a decrease of permafrost areal extent, e.g., +5K increase air temperature resulted in a reduction of permafrost coverage from 58% to 9% of the study area. Gray et al. (2017) investigated a 37-year geothermal record from a 29 m deep borehole in permafrost on Mont Jacques-Cartier, Quebec, Canada. They concluded that regardless of fluctuations, overall warming trend was observed. Booshehrian et al. (2019) conducted a case study in Nunavut, Canada, numerically computed hydraulic variations, and the ground water flow change in continuous permafrost due to climate change. Their result implicated that an increase of 7°C in mean annual ground surface temperature led to permafrost disappearance. In the recent Canadian Changing Climate Report, Derksen et al. (2018) has presented a review indicating that snow, ice, and permafrost are changing across Canada because of increasing temperatures and changes in precipitation.

2.2 Permafrost

Permafrost is a ground that remains at or below 0°C for at least two consecutive years (Dobinski 2011, Walvoord and Kurylyk 2016). In exclusively physical terms, based on temperature criterion, permafrost is defined as a thermal state of the lithosphere and anything inside it (Ballantyne 2008, Brown 1974, Dobinski 2011). Permafrost distribution at the regional and continental scale is strongly related to the mean annual air temperature. However, other factors are also important (Bonnaventure and Lewkowicz 2013, Palmer et al. 2012), including elevation, depth, and duration of snow cover, slope, aspect, geology and vegetation (Carturan et al. 2016, Dobinski 2011, Zhao et al. 2017). Permafrost is divided into continuous, discontinuous, and sporadic zones depending on its areal extent and continuity (Anisimov and Reneva 2006, Anisimov et al. 2002, Beilman et al. 2001, Brown 1970, Dobinski 2011).

The surface layer, which thaws seasonally, is called the active layer. It can thaw and refreeze more deeply or shallowly, depending on how warm the summer is (Dobinski 2011, Streletskiy et al. 2017). In cold regions, the active layer plays significant roles in the ecological, hydrological, biochemical and pedogenic processes taking place within the active layer (Hinzman et al. 1991, Walvoord and Kurylyk 2016) for the transmission of heat into/out the lithosphere. Although it is not a part of permafrost, it plays a key role in its interaction with the atmosphere (Dobinski 2011). The active layer thickness depends on some critical factors such as the ground surface temperature, thermal properties of the ground and its cover, soil moisture content, snow cover, etc. (Ballantyne 2008, Willeit and Ganopolski 2015). According to Kujala et al. (2008), peat exhibiting excellent insulation properties in summer reduces the thickness of an active layer and increases the penetration of cold in winter when its thermal permeability is significantly higher. Peat's thermal property depends on its water content and temperature (Kujala et al. 2008), and it slightly changes with temperature but showed a considerable increase with the peats water content (lower for natural unfrozen peat and higher for saturated).

As polar amplification of climate change continues, terrain within the discontinuous permafrost zones where permafrost is warm and hence sensitive is likely to undergo considerable change (Bense et al. 2012, Bonnaventure and Lewkowicz 2013, Camill 2005, Lacelle et al. 2010), resulting in increasing winter baseflow (Duan et al. 2017), the release of greenhouse gases to the atmosphere (Anisimov and Reneva 2006, Beermann et al. 2017a, Beilman et al. 2001, Bense et al. 2012, Derksen et al. 2018, Plaza et al. 2019, Wagner et al. 2018), decrease bearing capacity beyond safety range and ground deformation (Arenson et al. 2016, Bao et al. 2019, Davies et al. 2001, Draebing et al. 2017).

Recently, efforts to incorporate permafrost models into hydrologic studies (Bense et al. 2012, Brunner and Simmons 2012, Carturan et al. 2016, Kurylyk et al. 2014, Zhang et al. 2000), geotechnical (Brown 1970, Rudy et al. 2017), and ecosystem models (Rivkina et al. 2018, Way and Lewkowicz 2018) has been carried out and are continuing. Such coupled models are computationally expensive (Anisimov and Reneva 2006). Predictive permafrost models forced with various climatic scenarios to see the impact on active-layer thickness (Anisimov et al. 2002, Boucher-Brossard et al. 2017, Changwei and Gough 2013, Dyke and Sladen 2010, Fagan and Nelson 2017, Gray et al. 2017, Ishikawa et al. 2018, Lewkowicz et al. 2016, Rühaak et al. 2015) have indicated a significant increase in the active-layer thickness in the future. Several reviews of previous works published on permafrost modeling can be found (Derksen et al. 2018, Riseborough et al. 2008).

2.3 Permafrost models

Permafrost models are a subset of a more general class of (geo)thermal models and focus on ground freezing and thawing in determining the important model parameters (Riseborough et al. 2008). Analytical models, e.g., n-factors (Lunardini 1978), TTOP model (Smith and Riseborough 1996), are of limited help since they were derived from idealized conditions. Statistical-empirical permafrost models, e.g., the PERMAMAP approach of (Hoelzle and Haeberli 1995), require significant changes in parameters that are easily measured, such as altitude, slope, and solar radiation. However, significant changes, e.g. in altitude, are not available, so that their application in Northern Canada is limited. Incorporating real-world conditions, e.g. changes in ground surface temperature, snow cover changes, can only be included by numerical techniques. Numerical techniques require the definition of initial and boundary conditions. Most critical is the upper or

atmospheric boundary condition at the soil surface. Critical parameters at the local scale are solar radiation, wind speed and air temperature (Mittaz et al. 2000). However, spatial permafrost modelling at the catchment scale requires a less site-specific approach to the energy balance, with short-wave radiation attenuated through the atmosphere, wind fields modified by local conditions based on satellite-derived leaf area indices, etc. (Chen et al. 2003, Riseborough et al. 2008).

Zhang et al. (2006) developed the Northern Ecosystem Soil Temperature (NEST) numeric model to simulate the evolution of the ground thermal regime of the Canadian landmass since the end of the Little Ice Age. The study considered the effects of vegetation, snow, forest floor or moss layers, peat layers, mineral soils, and bedrock. Results showed permafrost retreat in the southern edge of permafrost in Manitoba and the eastern parts towards the Hudson Bay. However, exact and local results are not available from that study due to the spatial resolution of half-degree latitude and longitude.

The arctic terrestrial simulator (ATS) model is a physically-based, integrated tool of the permafrost-related process model developed from the Amanzi code (Painter et al. 2016). It is an open-source model that couples the surface energy balance model (Atchley et al. 2015) and three-dimensional subsurface thermal hydrology model (Jan et al. 2020, Karra et al. 2014, Painter et al. 2016) allowing permafrost-affected regions multidimensional simulations. The ATS model simulate the snow process, such as snow insulation and snow thermal conduction (Painter et al. 2016). However, the ATS model has shortcomings in solving the convergence of nonlinear system around the transition between freezing and thawing and simulating topography change by subsurface ice melting that require movement of grid/mesh cells while maintaining the water and energy balance inside the moving grid (Bui et al. 2020, Dall'Amico et al. 2011).

CryoGrid 2 is a transient permafrost model that calculates ground temperature according to conductive heat transfer in soil and snowpack (Westermann et al. 2013). The change in internal energy is determined by Fourier's law of heat conduction. The model has been used in different permafrost-related studies (e.g., Westermann et al. (2013)). Angelopoulos et al. (2019) simulated coastline retreat and subsea permafrost evolution following successive stages of a thawing sequence at the Bykovsky Peninsula using CryoGrid 2. Their result indicated the freezing point depression produced salt diffusion preventing ice formation in sediment and enhancing permafrost degradation. They concluded that salt diffusion might facilitate the release of greenhouse gasses into the atmosphere and affecting designs of offshore and coastline infrastructure. Myhra et al. (2017) modelled the distribution and temporal evolution of permafrost in a steep rock wall along the latitudinal transect from the southern to northern Norway using CryoGrid 2D. Their result showed the existence, and thermal regime of the permafrost varies strongly depending on the snow and glacier cover on the plateau.

2.4 Hydrological models in cold regions

Hydrological model selection in cold regions should consider the models' ability to deal with unique processes of permafrost environment and applicability with moderate amounts of data (Bui et al. 2020). Such models are essential for understanding the arctic regions' complex hydrologic responses in a warming climate (Jan et al. 2020). Careful evaluation of hydrological models against observations helps to develop understanding and identifying modeling uncertainties (Jan et al. 2020, Pokorny et al. 2021, Unduche et al. 2018). The following part discusses some physically-based hydrological models that have been evaluated and effectively used for hydrologic studies in cold regions. These include HBV, ECOMAG, and WATFLOOD

2.4.1 HBV

The Hydrologiska Byråns Vattenbalansavdelning (HBV) model is a rainfall-runoff model developed by Lindström et al. (1997) at the Swedish Meteorological and Hydrological Institute. Subsequent improvements on the model gave significant confidence for different flood forecasting applications, inflow forecasting into hydropower reservoirs, and assessment of climate impact on water resources (Bui et al. 2020). The HBV model considers permafrost hydrology's critical processes such as snowmelt, snow routine, soil moisture, infiltration, and surface energy balance. The model simulates active layer thickness using an accumulated degree day coefficient, which is set up based on field measurement (Bruland and Killingtveit 2002, Bui et al. 2020). The HBV model requires the most basic input data such as daily precipitation and average daily air temperature, and computer facilities. It is suitable for studies with sparse data, such as the Arctic region and could be ideal tool for hydrological simulations in ungagged river basins. However, it is challenging in finding optimal parameters for HBV (Bergström 2006).

The HBV model has been used in several countries in the world. In Canada, the model is vastly used in flood forecasting operations by the Province of Manitoba. Unduche et al. (2018) evaluated the Canadian version of HBV model performance with three other hydrologic models. They indicated that the model could simulate flows accurately and can be used in operational flood forecasting. The HBV model has been used in different climate change studies (eg., Ahmad et al. (2020), Krysanova et al. (2017), Lestari and Dasanto (2019)); and the model performance gave the confidence to analyze and forecast projections under different emission scenarios.

Despite the HBV model's applicability in cold regions and capability of simulating active layer thickness dynamics (Osuch et al. 2019), the lack of the model ability to represent soil thermal

property and phase-changes of water during freezing and thawing processes in near-surface soil gives little confidence to apply it stand-alone in permafrost studies.

2.4.2 ECOMAG

The Ecological Model for Applied Geophysics (ECOMAG) is a physically-based, distributed hydrological model for simulated hydrological cycles and water quality transformation in catchments in cold climate regions (Motovilov 2013, Motovilov et al. 1999). It has hydrological and water quality sub-models. The model operates in a daily time step. The hydrologic sub-model incorporates several processes occurring in catchments, including surface runoff, evapotranspiration, infiltration, soil moisture, and subsurface flow. The model is capable of simulating hydrothermal processes, including the formation of snow cover, snowmelt rate, active layer thickness dynamics, infiltration of snowmelt into the unfrozen and frozen soil by integrating the governing equations of basic hydrodynamic and thermodynamic of water, vertical heat transfer, horizontal water flow, etc. (Motovilov 2013, Motovilov et al. 1999).

The ECOMAG model was tested for hydrological simulation in several river basins in cold climate regions such as Canada, Norway, and Russia. In a study conducted at the Lena River basin in Russia, Motovilov (2017) used the model to simulate hydrological parameters and compared the result with data from the hydrometric observations and concluded that the model performed well. In other studies conducted to investigate climate change impacts on twelve river basins in Africa, Asia, Australia, Europe, and North America, the ECOMAG model was used with eight other hydrological models (Krysanova et al. 2017). The model was applied on Lena and Mackenzie basins (Gelfan et al. 2017, Motovilov et al. 2017) with the other models; they assessed the model's ability and reliability to reproduce the historical streamflow series and analyzed projections using

climate change scenarios, and the model showed adequate performance. Coupling the ECOMAG model with a meteorological model was done by Churiulin et al. (2019) for the Sukhano River at Velikiy Ustyung, Russia. A similar study was conducted on the Ussuri River by Bugaets et al. (2018). Coupling the models in both studies allowed quantitative assessment of flood characteristics with a lack of data from hydrometeorological stations. The study recommended that the model could be used as a component of operational flood forecasting.

2.4.3 WATFLOOD

The WATFLOOD model is a distributed, partially physically-based hydrological model. It is widely used for flood forecasting and long-term hydrological simulation using distributed precipitation data from weather radar numerical weather models (Kouwen 2016). WATFLOOD implements a grouped response unit (GRU) approach and subdivides segments according to the similarity of hydrological responses. The runoff response from each unit with an individual land-cover make-up and topography (elevation) is calculated and routed downstream. The interception, infiltration, evaporation, snow accumulation and ablation, interflow, recharge, baseflow, and overland and channel routing are processes modeled (Kouwen 2016).

Numerous applications of WATFLOOD, especially in Canadian basins, are found in different studies. Notable recent applications including modeling climate change impacts (Toth 2006), estimating glacier wastage and seasonal melt contribution (Comeau et al. 2009), surface water quality (Jenkinson 2009), groundwater separation studies (Stadnyk et al. 2005), and operational flood forecasting (Unduche et al. 2018). Jing and Chen (2011) tested the performance of WATFLOOD in subarctic wetlands in the Deer River watershed located in the northern Hudson Bay Lowlands, Manitoba. They compared the model’s performance with another hydrologic model (SLURP). They concluded that the WATFLOOD model's inability to consider the existence

of permafrost and numerous seasonal ponds resulted in spring peak flows underestimation. They suggested modifications on the snowmelt algorithm, permafrost layer, and wetland routing would improve the model performance and reduce uncertainties. The WATFLOOD model was used to synthesize runoff hydrograph in Duffins Creek drainage basin in southern Ontario (Cranmer et al. 2001). They concluded that the model accurately captured rainfall-runoff processes for increasing rainfall intensities for peak flow, basin lag, and time to peak flow and indicated the model's suitability for flood forecasting and flood studies. They pointed out that uncertainty in computing peak flow magnitude might arise from rainfall and base-flow separation for the unit hydrograph method.

2.5 Modeling heat transport

Heat is the energy in transit due to temperature differences. There are three modes of heat transport, namely, conduction, convection, and radiation, in the shallow subsurface. Conduction occurs in a stationary material as a result of colliding molecules exchange energy by atomic vibrations (Zohuri 2017). Conduction is a thermally homogenizing force that induces heat transfer from a higher to lower temperature gradient until equilibrium is achieved. It is governed by Fourier's law, which is used to quantify heat transfer processes in terms of appropriate rate equations. Convection is a mode of heat transfer associated with two mechanisms; energy transfer due to random molecular motion (diffusion) and energy transferred by the bulk, or macroscopic, motion of the fluid (Bergman et al. 2011). This mode of heat transfer can be classified according to the nature of the flow, forced and free or natural convection. In the forced convection, flow is caused by external means, such as a fan, pump, or atmospheric wind. Whereas, in free or natural convection, the flow is induced by buoyancy forces, which are due to density differences caused

by temperature variations in the fluid (Bergman et al. 2011). Thermal radiation is energy emitted by matter that is at a nonzero temperature. The emission may be attributed to changes in the electron configurations of the constituent atoms or molecules (Bergman et al. 2011). This mode of heat transfer involves no direct contact, and it is in the form of electromagnetic energy waves and the absence of a suitable medium (Bergman et al. 2011).

In cold regions, consideration of phase change in heat transport modelling enhances the representation of the soil thermal process. Hansson et al. (2004) presented a new method that accounts for phase changes in a fully implicit numerical model for coupled heat transport and variably saturated water flow in both above and below zero temperature. It was based on the Richardson equation. Their approach enabled numerically stable mass and energy conservative solution. They evaluated the model by comparing predictions with data from the laboratory-based freezing experiment. They proposed a new function to better describe thermal conductivity dependency on ices and water content of frozen soil. Even though they only used one year of data and were subjected to change frequently due to snow ploughing operation, the numerical simulations have demonstrated the ability of codes to cope with rapidly changing boundary conditions. In other study benchmarking the numerical freeze/thaw model was done by Rühaak et al. (2015) using the INTERFROST consortium. They modeled the two benchmarks using Cast3M, SMOKER, SUTRA-ICE and FEFLOW and compared the results. One benchmark was analytical solution purely thermal simulation of frost penetration into a porous soil which was developed by Lunardini (1988) and the other was melting of a frozen inclusion that artificially simulates the thermo-hydraulically coupled thawing process. Their results exhibited good qualitative similarity for all codes.

Dacquay et al. (2020) used a finite element solver COMSOL Multiphysics to investigate conductive heat transfer in soil by considering the effects of pore water phase change coupled with convective heat transfer through pipe flow. Their research focussed on the long-term efficiency of a ground heat exchanger that extracts heat from the surrounding soil and sewage within the pipe in a cold climate. Their model resulted in 0.1℃ over 25 years maximum temperature change in the surrounding soil adjacent to the heat extraction during the heating season in Winnipeg, Manitoba. Gheysari et al. (2021) conducted similar studies to investigate the short-term and long-term performance and effectiveness of closed-loop horizontal GHP systems in a cold region. The resulting output was processed into extraction power, thermal output, and carbon emissions. Their result suggested that attaining stable heat extraction possible by placing the exchanger below the depths that are not affected by seasonal variation. The system was resilient to major climate pathways, and the system has less carbon footprint in Canada. Saaly et al. (2020) also had investigated the energy performance of below-grade envelops of institutional buildings in cold regions by considering pore water phase change on thermal properties and heat exchange between the basement structure and surrounding soils, developed 3D and 2D numerical analysis. They are also investigating the importance of insulation systems, and their result suggested applying this insulation helped reduce heat loss by 60%. Their result comparison between the 3D and 2D models suggest that the 2D model predicted a 22% higher heat flux than the 3D model. Bridger and Allen (2010) developed a 3D heat transport model to evaluate the influence of aquifer heterogeneity that used for thermal energy storage. Their result indicated that heat and cold energy moved preferentially in discrete zones within the aquifer over discrete interval. It was corroborated with monitored data from the stations in Agassiz, British Colombia, Canada.

3 Physically-Based Numerical Modelling to Identify Permafrost Degradation due to Climate Change

Abstract

The impact of climate change is global. In cold regions, climate change has contributed to an increased glacier ice melt rate and permafrost degradation. The effects of future climate change are usually studied by running numerical models with data from GCMs. In this study, the physically-based numerical models, HYDRUS-1D and Hansson's module were used to analyze the potential changes in ground temperature and the active layer at location about 60 km downstream of Gillam near the shore of Lower Nelson River, Manitoba, Canada. Model calibration and validation were using soil temperature data for the 2014-2015 and 2011-2012 period respectively. Correlation results showed that simulated soil temperature was in agreement with observed for Hansson's module for all season but HYDRUS-1D model showed significant variation for winter season. To analyze the potential change in active layer thickness and the stability of permafrost due to climate change, the calibrated model was run with two Global Circulation Models, CanESM2 (Canadian Center for Climate Modelling Second Generation Earth System Model) and MIROC5 (Model for Interdisciplinary Research on Climate) under two scenarios (RCP8.5 and RCP4.5). The results showed that permafrost would stay stable in sites with peat layers and the active layer increment up to 5 meters was observed for both GCMs under high emission scenarios by 2080's.

3.1 Introduction

Approximately one-quarter of the continental northern hemisphere's exposed land is covered by permafrost (Zhang et al. 1999). This occurrence has fundamental control over these regions' water cycle characteristics (Zhang et al. 2017a), and permafrost distribution can significantly impact subsurface pathways and fluxes (Walvoord and Kurylyk 2016). Climate change is expected to have a profound effect on the hydrological processes in cold regions through alterations in the spatial and temporal distribution of frozen ground (Ye et al. 2003). The development of Global climate models (GCMs) and run based on different emission scenarios had given better perspective and played instrumental role to project the extent of impacts of climate change (IPCC 2007). Biskaborn et al. (2019) reported permafrost temperature increase by 0.29 ± 0.12°C from 2007 to 2016 global level and an increase of temperature by 0.39 ± 0.15°C and 0.20 ± 0.10°C in continuous and discontinuous permafrost zones were observed, respectively. In Canada, different studies indicated the impacts of this climate warming on permafrost based on investigation of geothermal records (Gray et al. 2017), numerical computed hydraulic variations (Booshehrian et al. 2019), analytical models (Smith and Riseborough 1996) etc.

Permafrost degradation, triggered by global warming, is manifested in reduced permafrost extent and increased active layer thickness (Beck et al. 2015, Sannel et al. 2016). Predictive permafrost models forced with various climatic scenarios to see the impact on active-layer thickness (Dyke and Sladen 2010, Fagan and Nelson 2017, Lewkowicz et al. 2016) have indicated significant increase in the active-layer thickness in the future.

A critical aspect in permafrost degradation is the hydrological processes' changes, which results from free-flowing water, such as soil water and groundwater, and their associated flow paths. Freezing and thawing of water and soil have substantial impacts on a variety of hydrological

and geotechnical aspects. Snowmelt is a critical factor behind flooding and permafrost degradation and impacts the hydrological regime. Currently, it is not adequately represented in many hydrological models, and that the numerical modeler often has considerable difficulties to accurately parametrize the process (Bormann et al. 2011, Holländer et al. 2009, Holländer et al. 2014).

Recently, efforts to incorporate permafrost models into hydrologic studies (Bense et al. 2012, Brunner and Simmons 2012, Carturan et al. 2016, Kurylyk et al. 2014, Zhang et al. 2000), geotechnical (Rudy et al. 2017), and ecosystem models (Rivkina et al. 2018, Way and Lewkowicz 2018) has been carried out and are continuing. Such coupled models are computationally expensive (Anisimov and Reneva 2006). In addition to the required ensemble of modeling for the climate forecast, different scenarios regarding additional hydrological processes, freezing and thawing, need to be considered. Incorporating pore water phase change in energy and heat transfer models helped better representation of the processes in cold regions (Dacquay et al. 2020, Gheysari et al. 2021). Examples of potential changes in hydrological processes and their impact on hydrological modeling can be found in Abolt et al. (2017) and in Holländer et al. (2009) where changes in soil crusting resulted in inaccurate forecasts of discharge from an experimental catchment.

Most studies regarding permafrost degradation covers regional extent and do less likely represent detailed hydrological and physical processes at local scale. This is due to high computational demand and due to the limited data availability in the northern hemisphere and results in a limited understanding of local aspects of climate change and its impact in the region.

This research aims to understand and identify the potential impacts of permafrost thawing on the hydrological regime in Northern Manitoba due to climate change by evaluating permafrost

degradation. Two vadose-zone physically based numerical models were used in this research, HYDRUS-1D (v4.17) and Hansson Module. The specific objectives include 1) evaluation of soil temperature data to identify permafrost zones and active layer thickness and 2) numerical investigation of the effects of climate change on permafrost degradation under different emission scenarios at a local scale.

3.2 Study area

The study site is located in Northern Manitoba in the Hudson Plains Ecozone's polar/boreal wet ecoregion and is located near the lower Nelson River, approximately 775 km north of Winnipeg (Figure 1). The site lies within the regional transition zone between the discontinuous and continuous permafrost zone of northern Canada.

The Hudson Plains Ecozone climate is generally subarctic and is characterized by short cool summers and frigid winters. Based on the last climate normal for the period of (1981-2010) at Gillam, Manitoba, the temperature ranges from -10°C to +32°C during summer months (May - September) and from -45°C to +15°C in the winter (October - April). The coldest months are usually January and February. The annual average precipitation is about 452.5 mm with winter snowfall accounting for approximately 40% of the total precipitation amounts (Environment Canada, 2019). The vegetation ground cover is mostly mature jack pine with sparse green alder, predominantly lichen ground cover.

The study area's geology comprises different stratigraphic layers of peat, clay, sand, gravel, and limestone. Stratigraphic information retrieved from four boreholes on the site showed the following soil layers: 1.5 - 3 m peat, 5 - 30 m clay, 0.5 - 3 m sand, 0 - 11 m silt, 0 - 5 m gravel. These soil layers overly on a deep formation of limestone.

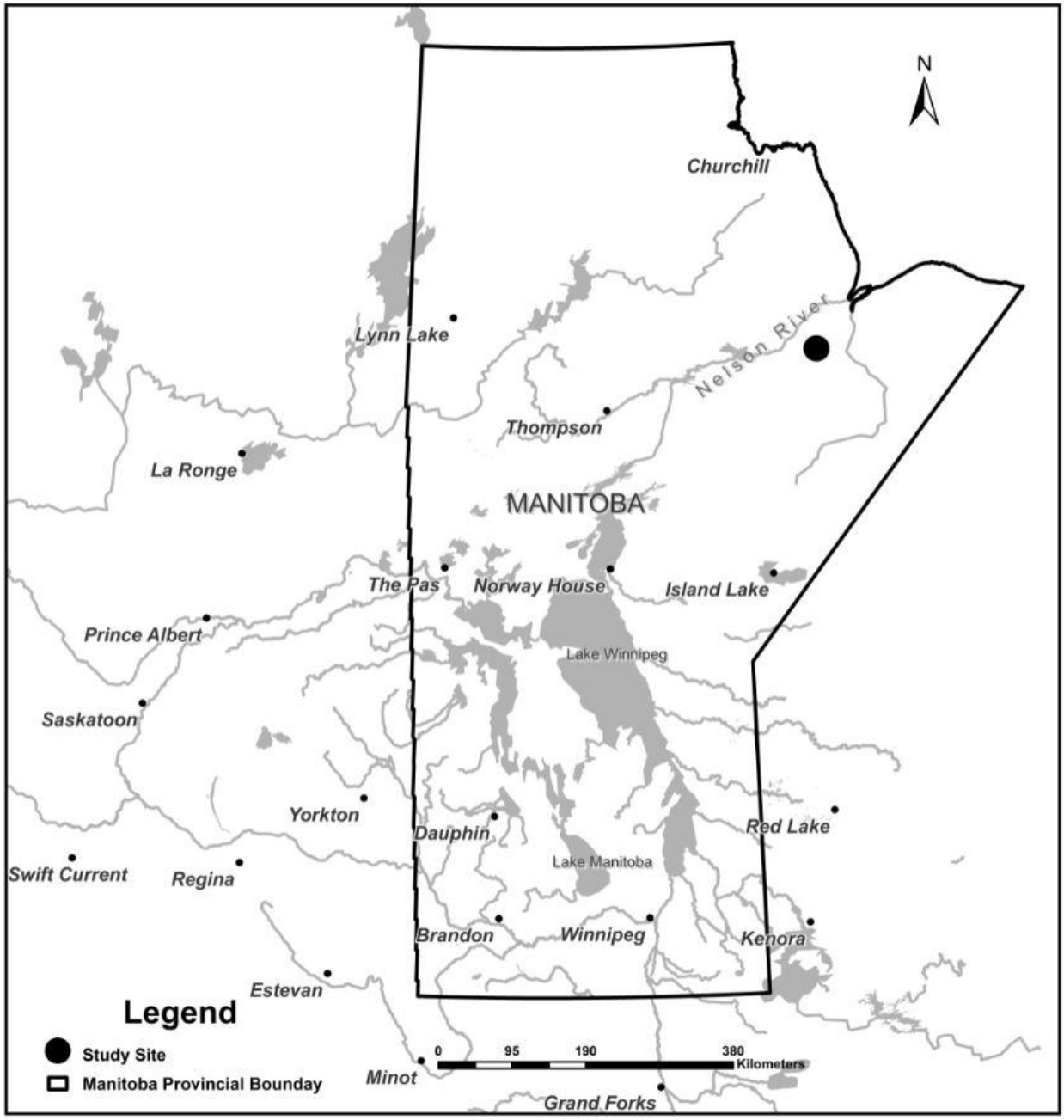

Figure 1. Study site

3.3 Data and methods

Continuous time series of both air temperature and soil temperature of the study site for the periods of 2011-2012 and 2014-2015 were obtained from Environment Canada (Environment Canada 2019) and Manitoba Hydro, respectively. Subsurface temperature from thermocouple and thermistors for 27 boreholes were retrieved from Manitoba Hydro's record. Both kind of sensors were installed at the same depth for verifiability and different life expectancy. Data quality was checked in terms of completeness, instrument recording error susceptibility, and permafrost indication, which is a temperature record of less than 0°C for at least two consecutive years (Dobinski 2011, Walvoord and Kurylyk 2016). Instrument recording error susceptibility was checked by regression analysis between thermocouple and thermistor temperature records. Daily average soil temperature record for boreholes exhibiting permafrost was used for numerical model calibration period (2014-2015) and validation period (2011-2012). For each selected borehole, the minimum, average, and maximum temperatures over two years were calculated for respective sensors' depth and used to create a temperature envelope with depth as an approach to define the permafrost. Future projections in the study site were derived from the station Gillam. The Gillam meteorological station was used because it offers a higher quality, longer term record and exhibits similar climate patterns as short-term metrological records located in closer proximity to the study personal communication with Vieira (2018). Due to significant gaps in the soil temperature data, depths with the most consistent long-term series were used for model calibration and validation in the study site.

3.3.1 Climate Change Projections

Two GCMs (Global Circulation Models) were used to analyze permafrost's potential changes due to climate change in the future. GCMs are numeric models that compute energy and mass balances based on physical equations and are used to translate future atmospheric, forcing scenarios into consistent physical effects on climate (Manitoba Hydro 2020). The GCM projections for temperature, precipitation, evaporation, runoff and wind speed for watershed located in Northern Manitoba has been evaluated and are in agreement that provide confidence (Manitoba Hydro 2020). The selected models were CanESM2 (Canadian Center for Climate Modelling Second Generation Earth System Model) and MIROC5 (Model for Interdisciplinary Research on Climate).

The second-generation Canadian Earth System Model (CanESM2) has evolved from the first generation Canadian earth system model (CanESM1) (Arora and Matthews 2009, Christian et al. 2010) of the Canadian Climate Modelling and Analysis (CCCma) (Arora et al. 2011). The model couples together an atmosphere-ocean general circulation model, a land-vegetation model, and a terrestrial and oceanic interactive carbon cycle (Arora et al. 2011). It is a global model developed to simulate historical climate change and variability, make centennial scale projections of future climate, and produce initialized seasonal and decadal predictions. (Arora et al. 2011, Swart et al. 2019).

Model for Interdisciplinary Research on Climate (MIROC5) is developed jointly at the Center for Climate System Research (CCSR), University of Tokyo; National Institute for Environmental Studies (NIES); and Japan Agency for Marine-Earth Science and Technology. By modifying and replacing most parts except for the atmospheric dynamical core of the previous

version, MIROC3.2 (Hasumi and Emori 2004), MIROC5 overcame deficiencies in the natural variability and climate sensitivity (Watanabe et al. 2010).

This study selected a moderate and high climate warming scenario (see section 2.1) following the representative concentration pathways (RCP4.5 and RCP8.5), and was used to analyze the impact on the permafrost. Bias corrected data was retrieved from (Canadian Centre for Climate Services (CCCS); Ouranos and the Pacific Climate Impacts Consortium (PCIC) 2019), climatedata.ca. The time horizon for the GCM calculation was the year 2100. For Gillam, the annual average temperature for the period of 1951-1980 was -4.6℃; for 1981-2010, it was -3.5℃. Under a high emission scenario, the projected annual average temperatures are -1.5, 0.9, and 2.9℃ for GCM-driven periods of 2021-2050, 2051-2080, and the last 30 years of the century respectively.

3.3.2 HYDRUS-1D model

The HYDRUS model numerically solves the Richards equation for variability saturated water flow and advection-dispersion type equations for heat and solute transport (Simunek et al. 2013). The heat transport equation considers heat transport due to conduction and convection.

The governing heat transport equation without considering the transfer of latent heat by vapor movement and as described with a conduction-dispersion equation by the Simunek et al. (2013) is as follows:

$$\frac{\partial C_p(\theta)T}{\partial t} = \frac{\partial}{\partial x}\left[\lambda(\theta)\frac{\partial T}{\partial x}\right] - C_w\frac{\partial qT}{\partial x} - C_w ST \qquad (1)$$

where, $C_p(\theta)$ and C_w were volumetric heat capacities [$ML^{-1}T^{-2}K^{-1}$] of the porous medium and the liquid phase, respectively, $\lambda(\theta)$ was the coefficient of the apparent thermal conductivity of soil [$MLT^{-3}K^{-1}$]. The first two terms of the above equation, on the right-hand side, represented

the heat flow due to conduction and the heat transported by the flowing water. The third term on the right-hand side of equation (1) stood for energy uptake by plant roots associated with root water uptake (Simunek et al. 2013).

Volumetric heat capacity was described by De Vries (1963) as follows:

$$C_p(\theta) = C_n\theta_n + C_o\theta_o + C_w\theta + C_a a_v \quad (2)$$

$$\approx (1.92\theta_n + 2.51\theta_0 + 4.18\theta) * 10^6 \ (ML^{-1}T^{-2}K^{-1})$$

In the above equation, the subscripts n, o, and w are representing solid phase, organic matter, gas phase, and liquid phase, respectively. The thermal conductivity was expressed using the equation:

$$\lambda_0(\theta) = b_1 + b_2\theta + b_3\theta^{0.5} \quad (3)$$

where b_1, b_2 and b_3 are empirical parameters [-], which were determined by Chung and Horton (1987) based on the soil texture.

3.3.3 Hansson's module

Hansson et al. (2004) presented a method that used and implemented a code designed for accounting phase change in water by coupling equations of governing heat transport and variably saturated flow in both positive and negative temperatures. This approach was successfully applied to simulate the soil temperature and showed a better fit with observed data than the standard HYDRUS code with the consideration of latent heat at different depths of the soil column during phase change of the water. The general governing equation in this model for heat transport in porous media was:

$$\frac{\partial C_p T}{\partial t} - L_{f\rho}\frac{\partial \theta_i}{\partial t} + L_0(T)\frac{\theta_v(T)}{\partial t} = \frac{\partial}{\partial x}\left[\lambda(\theta)\frac{\partial T}{\partial x}\right] - Cw\frac{\partial q_l T}{\partial x} - Cv\frac{\partial q_v T}{\partial x} - L_0(T)\frac{\partial q_v}{\partial x} - C_w ST \quad (4)$$

where, L_f is the latent heat of freezing ($L^2\ T^{-2}$) (approximately $3.34 \times 10^5\ L^2\ T^{-2}$), L_0 is the volumetric latent heat of the water ($M\ L^{-1}\ T^{-2}$). It is determined by $L_0 = L_w \rho_w$ where L_w is the latent heat of vaporization of water ($=2.501 \times 10^6 - 2.369.2\ T\ [°C]$) (Hansson et al. 2004).

In the above equation, the first term on the left side represents the change in energy content, while the second and third terms represent changes in the latent heat of the frozen and vapor phases, respectively. The terms on the right-hand side represent soil heat flow by conduction, convection of sensible heat flow with flowing water, transfer of sensible heat by diffusion of water vapor, transfer of latent heat due to diffusion of water vapor, and energy uptake associated with root water uptake, respectively (Hansson et al. 2004). In the above equation, the volumetric heat capacity of the soil, which was denoted by C_p($M\ L^{-1}\ T^{-2}\ K^{-1}$) was expressed by the following equation which was basically the sum of volumetric heat capacities of the solid (C_n), liquid (C_w), vapor (C_v) and ice (C_i), multiplied by their volumetric fractions θ (Hansson et al. 2004):

$$C_p = C_n\theta_n + C_w\theta w + C_v\theta_v + C_i\theta_i \qquad (5)$$

The heat flow equation in (4) was further simplified to avoid model uncertainties and stability that comes with lack of reliable and recorded data for soil moisture content and rate of downward flux of water. Therefore, the change in energy was evaluated using the soil heat flow by conduction and changes in latent heat of frozen phase (6) on MATLAB (R2016a). A finite implicit code was written using and the simplified equation was discretized along the borehole depth using the finite differences method and subsequently solved.

$$\frac{\partial C_p T}{\partial t} = \frac{\partial}{\partial x}\left[\lambda(\theta)\frac{\partial T}{\partial x}\right] + L_{f\rho}\frac{\partial \theta_i}{\partial t} \qquad (6)$$

3.3.4 Discretization

The basis of this research is predicting temperature evolution versus time, T(x,t) with accounting phase change in equation 4. A spatial grid was established with a discretization of 0.5 m, accounting for a depth of 100 m, and defined a 1D heat conduction equation with finite difference approximation. A time step of one day was considered during the simulation.

3.3.5 Boundary and initial conditions

Ground surface temperature is one of the most crucial boundary conditions needed in modeling permafrost degradation or evolution. Considering the interaction of air temperature and ground surface temperature is ideal in this perspective.

The ground surface temperature prediction for several studies in the northern climate was carried using n-factor (Dyke and Sladen 2010), which is valid to be applied at most North American sites. They are frequently used in different studies associated with permafrost degradation and evaluation, (e.g., Etzelmüller et al. (2011) Antonellini et al. (2014), Bonnaventure and Lewkowicz (2011), Lewkowicz et al. (2012)). The n-factor approach predicts the ground surface temperature by applying an adjustment to air temperature. Air temperature is multiplied by a factor for freezing and thawing seasons.

For studies where near surface temperature is not recorded (e.g., Yi et al. (2009)), it is common to consider the surface temperature and air temperature to be equal in a controlled volume as an alternative to evaluate ground temperature changes. For this study, air temperature measurements are directly used for the upper boundary condition, it is a good approximation of the surface temperature on time scales longer than the diurnal cycle (Beermann et al. 2017b). The lower boundary condition was defined based on extrapolation of measured soil temperature with

depth using linear regression equation. A value of 2℃ was used at 100 m depth. To overcome model instability and reduce uncertainty that come from less data availability, an assumption was made to use the soil water content as saturated and static so that moisture changes due to precipitations, snowmelt, or the general groundwater level are neglected.

The initial condition was based on the observed data (air temperature and soil temperature). The temperature data was plotted against depth. A regression equation was developed correlating nodal temperature values with depth at the first-time step (t = 0).

3.3.6 Parametrization

The material composition of the soil layers at each borehole was set based on specific ground composition for each site for B04, B05, B08, and B09, and it was interpolated for the rest of the boreholes using the Thiessen polygon method on ArcGIS and characteristics was allocated for the nearest borehole.

Soil thermal properties depend on the fraction of solid soil content, including organic matter content, mineral composition, the water content in the soil, and the porosity filled with air (Mikail et al. 2019). Soil thermal variables such as thermal conductivity and heat capacity, principally control soil temperature, and soil heat flow. The thermal properties of the soil material in this study was based on different literature publications, as shown in Table 2.

Table 2. Soil thermal parameters [a]

Type of Material	Thermal Conductivity (W/m*°C)	Specific Heat Capacity (J/kg*°C)
Peat	0-1.5	3650
Clay	0-1	920
Gravel	0-3.5	835
Limestone	0-3.5	910
Sand	0-3.5	1480
Silt	0-1	890

[a] Values compiled from (Bense et al. 2009, Bense et al. 2012, Chung and Horton 1987, Hansson et al. 2004, Langer et al. 2011, Simunek et al. 2013)

3.3.7 Model Calibration

The numerical model was calibrated against recorded soil temperature data. The numerical calibration started in 2014 with a corresponding ground temperature profile defined above in the initial condition. The permafrost's low hydraulic and thermal conductivity strongly affects the movement, storage, and exchange of surface and subsurface water and heat fluxes (Walvoord and Kurylyk 2016). The modeling of the soil column in different freezing and thawing condition were conducted for both models in two stages.

In the first stage, all models were calibrated and validated using historic soil temperature data. First, the HYDRUS-1D (v4.17) model was built. The observed data set was used for inverse calibration using the global optimization tool PA-DDS (Asadzadeh et al. 2014). Coupling between HYDRUS-1D and PA-DDS was carried out using MATLAB (R2016a). Second,

Hansson's model was set up and was calibrated and validated for the study period. Calibration used the observed data from 2014 to 2015 and Validation data from 2011 to 2012.

In the second stage, climate change impact on permafrost was evaluated using temperature data from CanESM2 and MIROC5. Bias-corrected and statistically downscaled data was retrieved from (Canadian Centre for Climate Services (CCCS); Ouranos and the Pacific Climate Impacts Consortium (PCIC) 2019) for both models. This data was used to analyze potential changes due to climate change in the future. Two emission scenarios, RCP8.5 and RCP4.5, were selected to predict the future impact on the soil temperature and permafrost's stability. The prediction horizon was until 2100. Recorded and simulated data were plotted on the same scale to help direct visualization and comparison of simulated-recorded data set and evaluate the model performance.

The calibration performance was evaluated using error metrics (root mean square error (RMSE) and mean absolute error (MAE)) to quantify the goodness-of-fit (correlation) of the model results with observed ground temperature values at different depths of each borehole.

The root mean square error (RMSE) approach adapted for this study is widely used in hydrology, groundwater, and climate research and is considered as a standard method for measuring model performance (Jackson et al. 2019). It is considered as a standard metric for model errors. The RMSE was calculated using the following formula:

$$RMSE = \left(\frac{1}{n}\sum_{i=1}^{n}|S_i - O_i|^2\right)^{\frac{1}{2}} \quad (9)$$

where n is the total number of observations [-], n_i is the i^{th} observation [-], S_i is the simulated values on the i^{th} day, and O_i is the observed values on an i^{th} day. RMSE values range between 0 and ∞, while smaller RMSE show a better fit (Jackson et al. 2019).

The second performance criteria were the mean absolute error (MAE), another useful measure that is widely used. It gave an idea of how close the predicted values were to the observed values (Jackson et al. 2019):

$$MAE = \frac{1}{n}\sum_{i=1}^{n}|S_i - O_i| \quad (10)$$

where n is the total number of observations [-], n_i is the ith observation [-], S_i is the simulated values on the ith day, and O_i is the observed values on an ith day. Close to zero MAE value indicates better performance, prediction values were the same as the observed values (Jackson et al. 2019).

3.3.8 Sensitivity Analysis

The general approach used was altering one parameter and keeping the other parameters the same to evaluate the simulation results' effects. This approach was determined to be feasible, and the method was proven to work for different studies, e.g., Holländer *et al.* (2016). The calibrated result and parameter values used were considered as a baseline. The thermal conductivity and heat capacity values were altered by ±10% and ±30 %.

3.4 Results

Temperature records obtained from Manitoba Hydro were evaluated to identify permafrost presence. Based on a time-series plot of soil temperatures less than 0°C for two consecutive years (Dobinski 2011, Walvoord and Kurylyk 2016), 13 boreholes exhibited permafrost out of the investigated 27 boreholes. A plot of the two-year observed averaged soil temperature versus depth helped to identify the approximate active layer thickness (ALT) and permafrost extent below the ground surface (Figure 2).

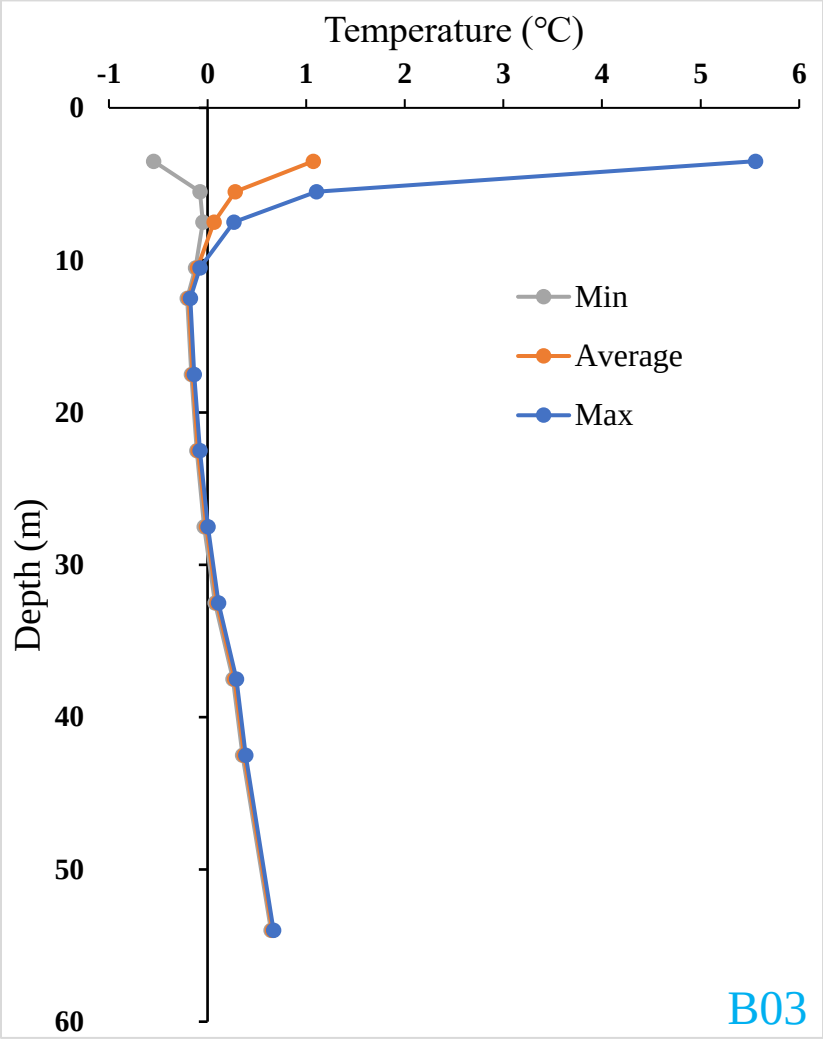

Figure 2. Observed soil temperature vs. depth envelope for borehole B03 (2014-2015)

A regression analysis was used to correlate the temperature readings between thermocouple and thermistor records. A strong correlation with R^2 value of 0.99 was observed. But due to the susceptibility of thermocouple temperature data to noise pollution (Abdalla et al. 2019, Abdelaziz 2012, Radajewski et al. 2019), this study considered the thermistor temperature records.

3.4.1 Model calibration and validation results

The HYDRUS-1D model captured summer season in the model calibration but simulated colder soil temperature for the winter season in all boreholes during the calibration period (2014-2015). Calibration with the Hansson module, on the other hand, captured both summer and winter seasons quite well for all boreholes. For example, simulated temperature at 4 m depth for borehole B01 (Figure 3) and at 1 m depth for borehole B07 (Figure 4) showed that the Hansson module matched well with the observed data while the HYDRUS-1D models greatly deviated for winter season.

Hansson's module also had better error metrics than that of HYDRUS-1D for all boreholes (Table 3 and Table 4). Due to Hansson module's better performance than the HYDRUS-1D model, subsequent model validation and sensitivity analyses results were based on it. The observed soil temperature data for 2011 - 2012 period was used to validate the Hansson module.

Results of the calibrated soil temperature from Hansson's module relative to observed data for boreholes B01 and B07 at different depths are shown in Figure 5 and Figure 6, respectively.

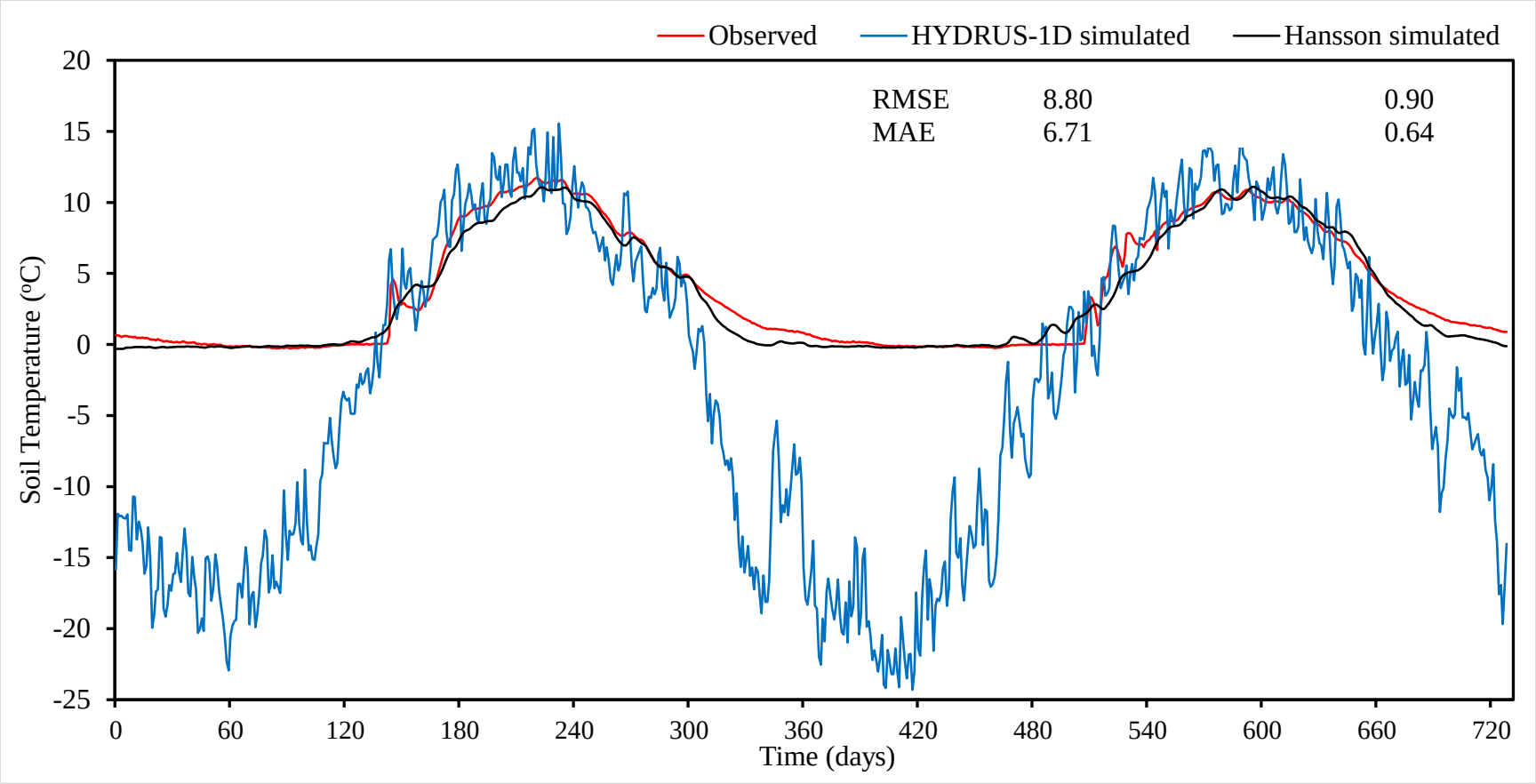

Figure 3. Two years of observed versus simulated (HYDRUS-1D) and simulated (Hansson) soil temperature data for B01 at 4 m depth

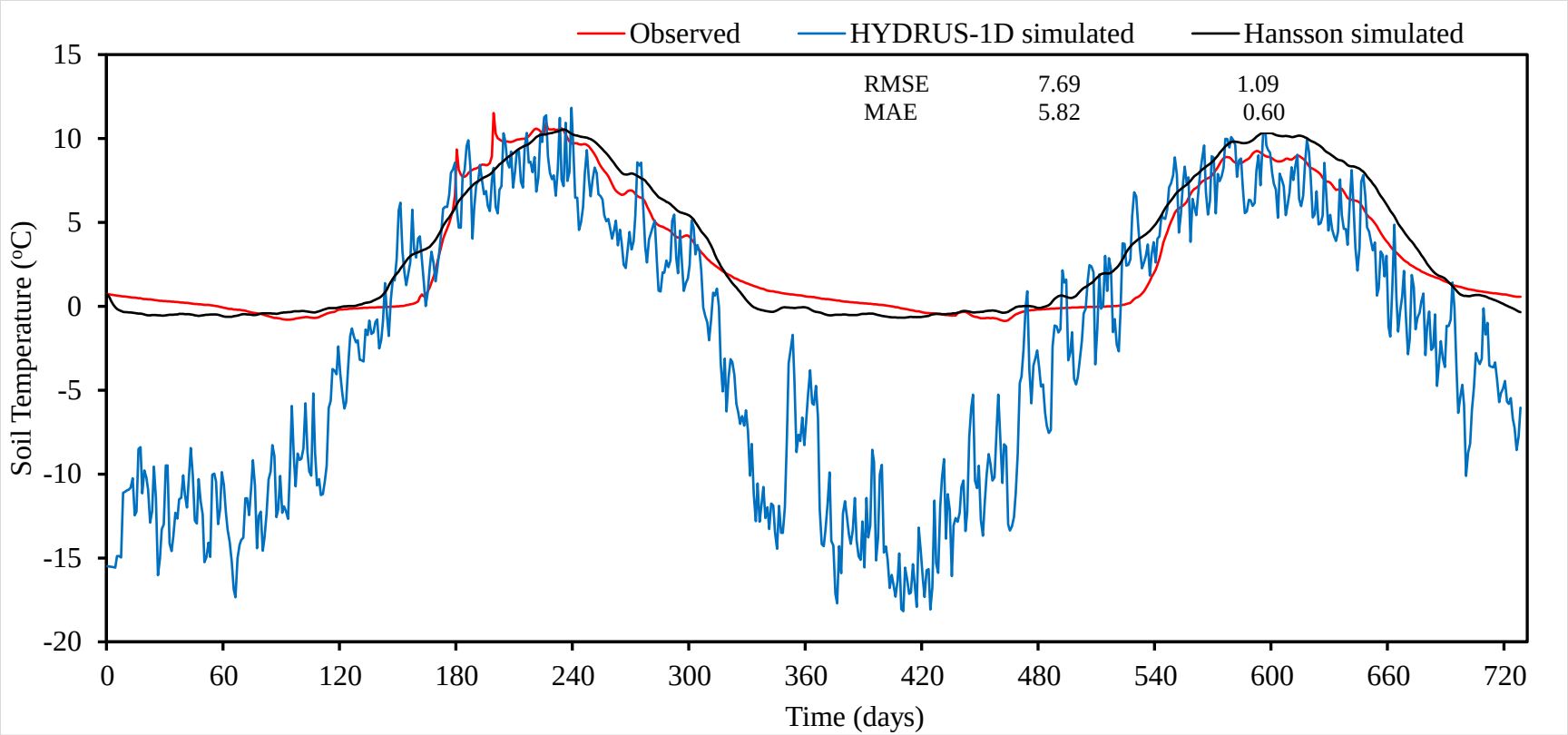

Figure 4. Two years of observed versus simulated (HYDRUS-1D) and simulated (Hansson) soil temperature data for B07 at 1 m depth

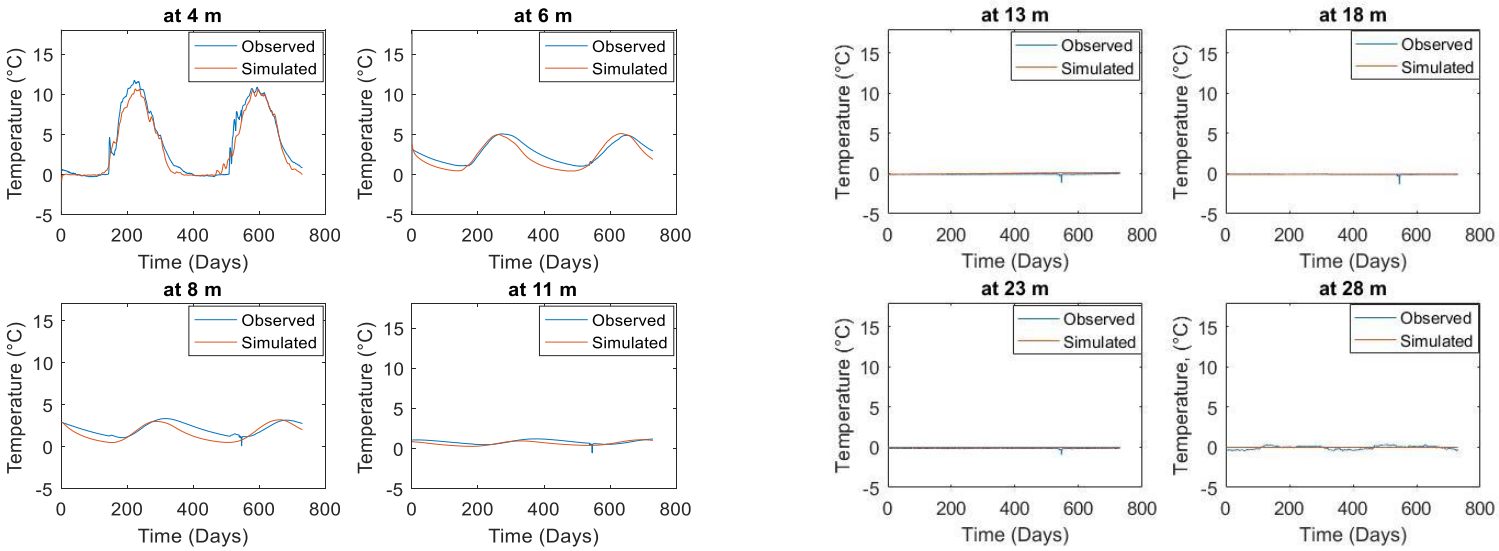

Figure 5. Two years of simulated (Hansson's module) versus observed soil temperature data for B01 at different depths

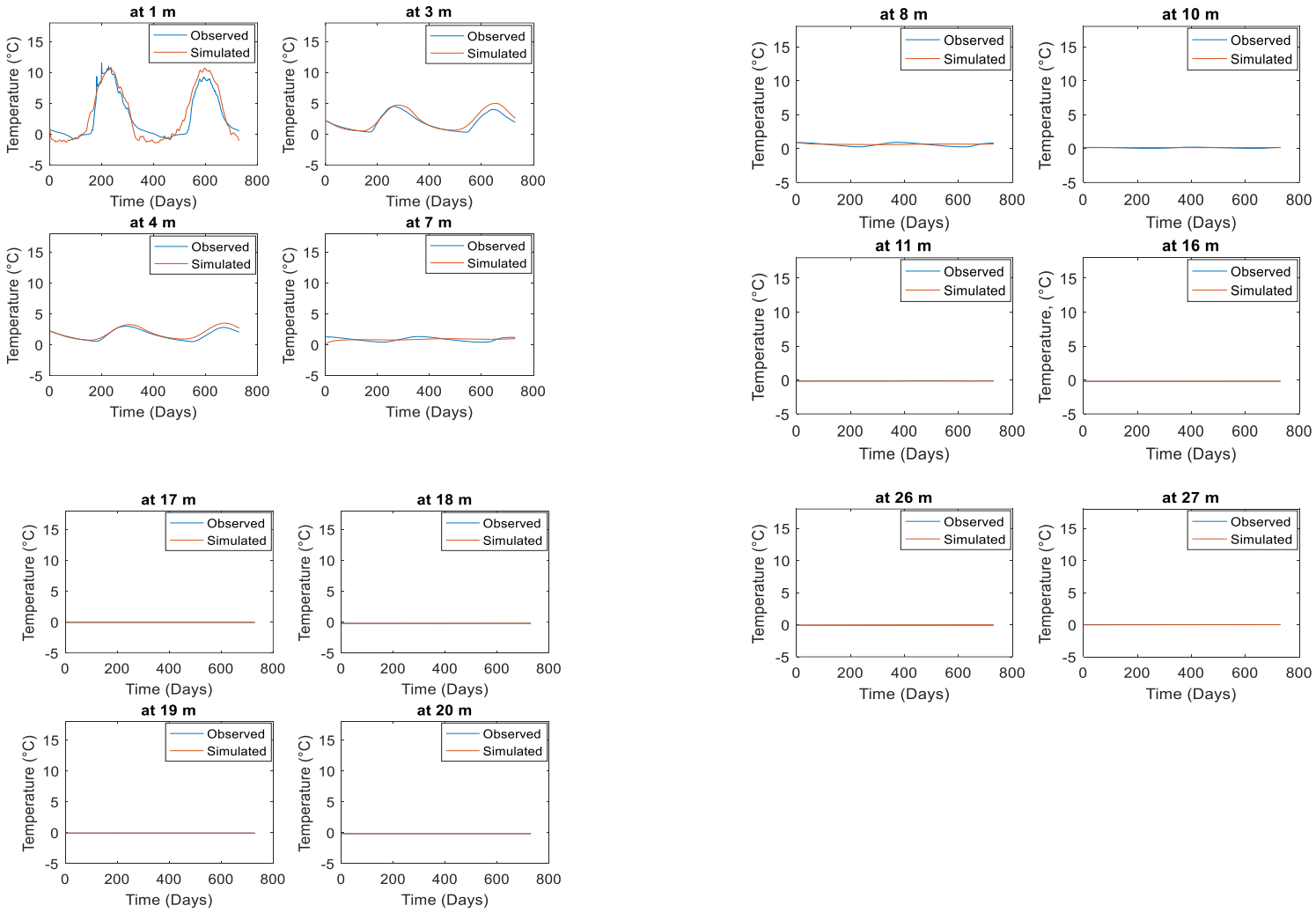

Figure 6. Two years of simulated Hansson's module versus observed soil temperature data for B07 at different depths

Table 3. Errors between calibrated and observed soil temperature values for borehole B01 at different depths

B01	HYDRUS-1D calibration		Hansson's module calibration		Hansson's module validation	
Depth (m)	RMSE (°C)	MAE (°C)	RMSE (°C)	MAE (°C)	RMSE (°C)	MAE (°C)
4	8.80	6.71	0.90	0.64	1.13	0.87
6	6.50	5.03	1.04	0.92	0.98	0.87
8	3.20	2.86	0.77	0.70	0.68	0.62
11	0.79	0.63	0.31	0.28	0.35	0.28
13	0.26	0.24	0.05	0.02	0.13	0.09
18	0.09	0.06	0.06	0.03	0.09	0.05
23	0.05	0.03	0.08	0.07	0.14	0.10
28	0.37	0.31	0.22	0.19	0.24	0.22

Table 4. Errors between calibrated and observed soil temperature values for borehole B07 at different depths

B07	HYDRUS-1D calibration		Hansson's module calibration		Hansson's module validation	
Depth (m)	RMSE (°C)	MAE (°C)	RMSE (°C)	MAE (°C)	RMSE (°C)	MAE (°C)
1	7.69	5.82	1.09	0.60	1.36	1.07
3	2.71	2.52	0.56	0.36	0.70	0.54
4	1.86	1.71	0.29	0.25	0.55	0.46
7	0.61	0.49	0.15	0.13	0.45	0.40
8	0.37	0.31	0.08	0.07	0.34	0.30
10	0.32	0.27	0.03	0.02	0.14	0.13
11	0.49	0.44	0.03	0.03	0.03	0.02
16	0.21	0.20	0.10	0.10	0.01	0.01
17	0.06	0.06	0.05	0.05	0.01	0.01
18	0.17	0.16	0.12	0.12	0.01	0.01
19	0.04	0.04	0.07	0.07	0.01	0.01
20	0.09	0.08	0.02	0.02	0.01	0.01
26	0.05	0.04	0.01	0.01	0.06	0.06
27	0.02	0.02	0.01	0.01	0.02	0.02

3.4.2 Sensitivity analysis results

The sensitivity of thermal conductivity and heat capacity were evaluated during the sensitivity analysis. Both parameters have minimal impact during the warm season. Altering these parameters with -10% and +10% have a negligible effect on the simulation results as compared to the results obtained by altering both parameters by -30% and +30% during the cold season. The simulation results for sensitivity analysis showed that increasing the thermal conductivity by +30% resulted in lower (colder) temperature while decreasing it by -30% gave higher temperature for the cold season (Figure 7), vice-versa was observed for altering the heat capacity by similar magnitude for the cold season (Figure 8).

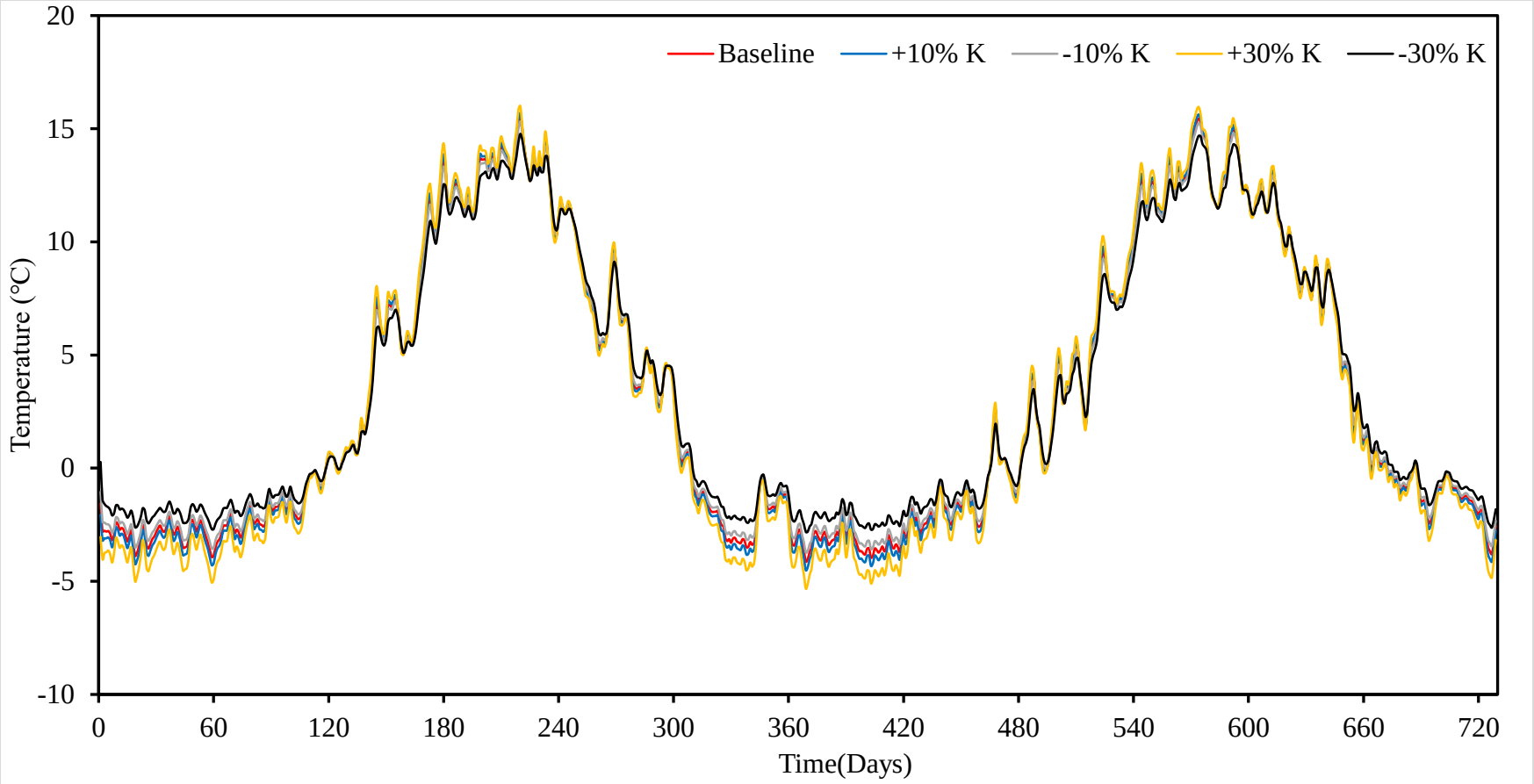

Figure 7. Sensitivity of heat conductivity to soil temperature at 4m depth for borehole B01

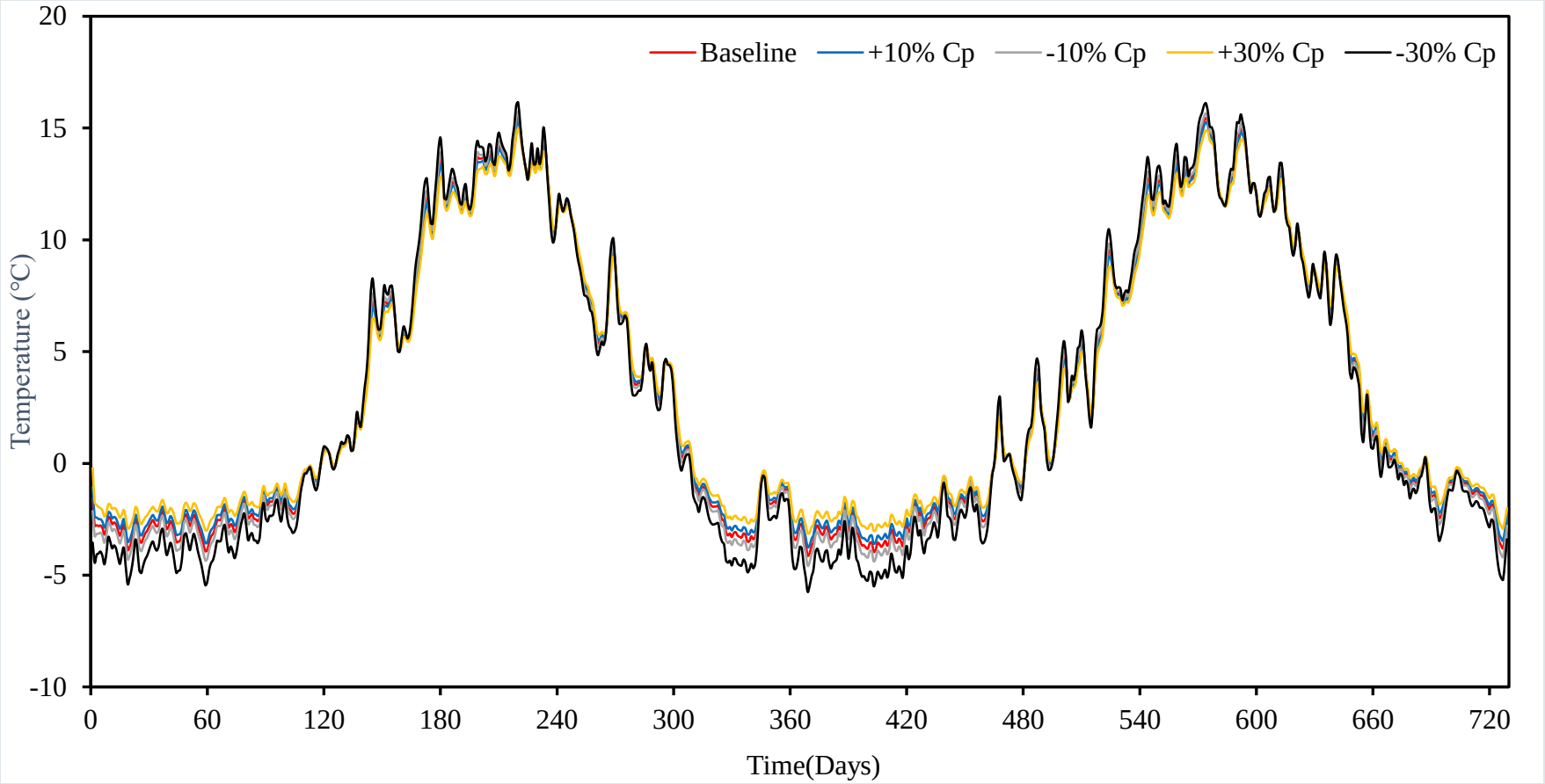

Figure 8. Sensitivity of heat capacity to soil temperature at 4 m depth for B01

3.4.3 Modelling permafrost degradation

Using the calibrated Hansson's module, the effect of climate change on permafrost was investigated with CanESM2 and MIROC5 considering moderate (RCP4.5) and extreme (RCP8.5) emission scenarios. Results from the GCMs and emission scenarios were based on different 30-year periods namely; historic (1950 – 1979), baseline (1980 – 2009), 2020's (2010 – 2039), 2050's (2040 – 2069), and 2080's (2070 – 2099). The GCM simulations helped to identify areas within different boreholes where permafrost was projected to degrade or remain stable through changes in the active layer thickness (ALT).

The evolution of the ALT under RCP4.5 and RCP8.5 climate-warming trends were simulated for all soil profiles for all eight boreholes. Table 5 summarized results of boreholes that has exhibited degradation of permafrost (increased ALT). This change in ATL were generally observed in boreholes B01, B07, and B08. Both GCMs generally predicted stable ALT for all boreholes under current climate conditions (baseline) and 2020's. An example of such boreholes where both GCMs predicted changes in ALT under moderate (RCP4.5) and high (RCP8.5) emission scenarios is B07 (Figure 9 and Figure 10).

Table 5. Boreholes with predicted changes in active layer thickness according to CanESM2 and MIROC5 under RCP4.5 and RCP8.5 scenarios

		CanESM2		MIROC5	
		RCP4.5	RCP8.5	RCP4.5	RCP8.5
B01	Baseline	stable	stable	stable	stable
	2020's	stable	stable	stable	stable
	2050's	stable	stable	stable	stable
	2080's	~2m	~5m	~1m	~6m
B07	Baseline	stable	stable	stable	stable
	2020's	stable	~1m	stable	stable
	2050's	~1m	~2m	~1m	~2m
	2080's	~2m	~5m	~2m	~5m
B08	Baseline	stable	stable	stable	stable
	2020's	stable	stable	stable	stable
	2050's	stable	stable	stable	stable
	2080's	stable	~2m	stable	~1m

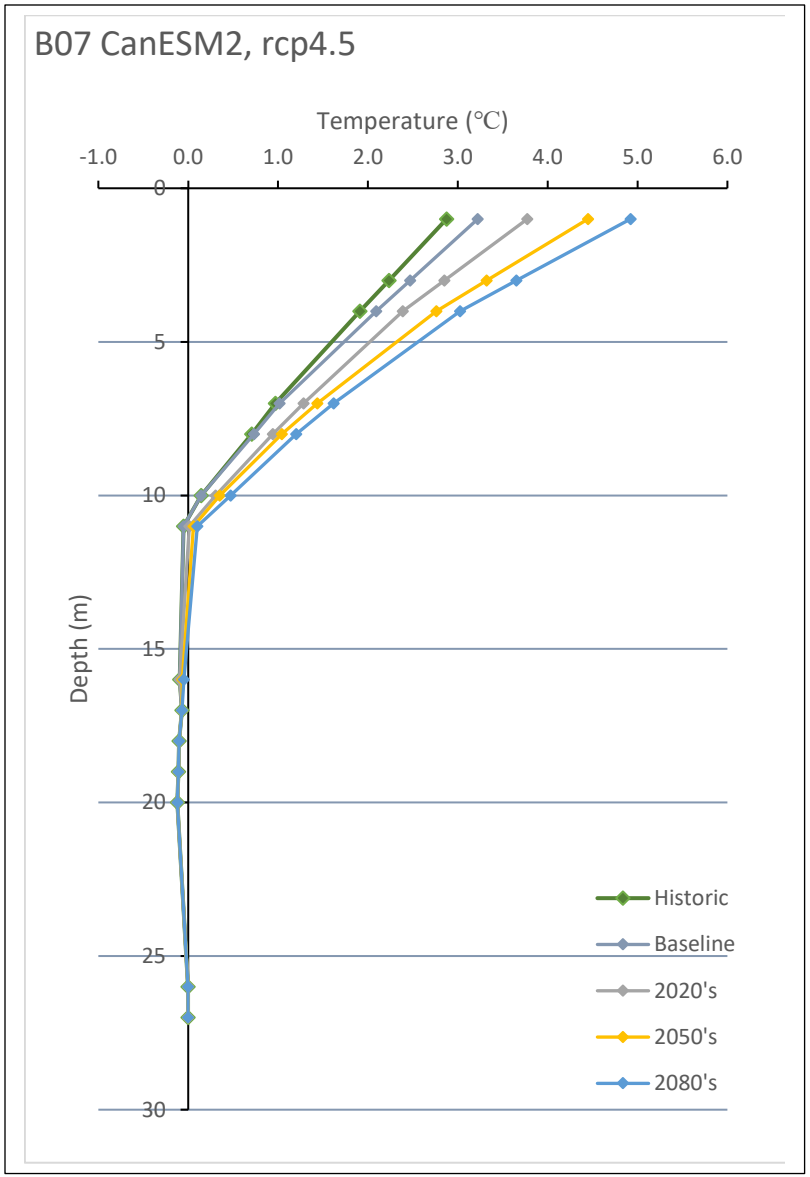

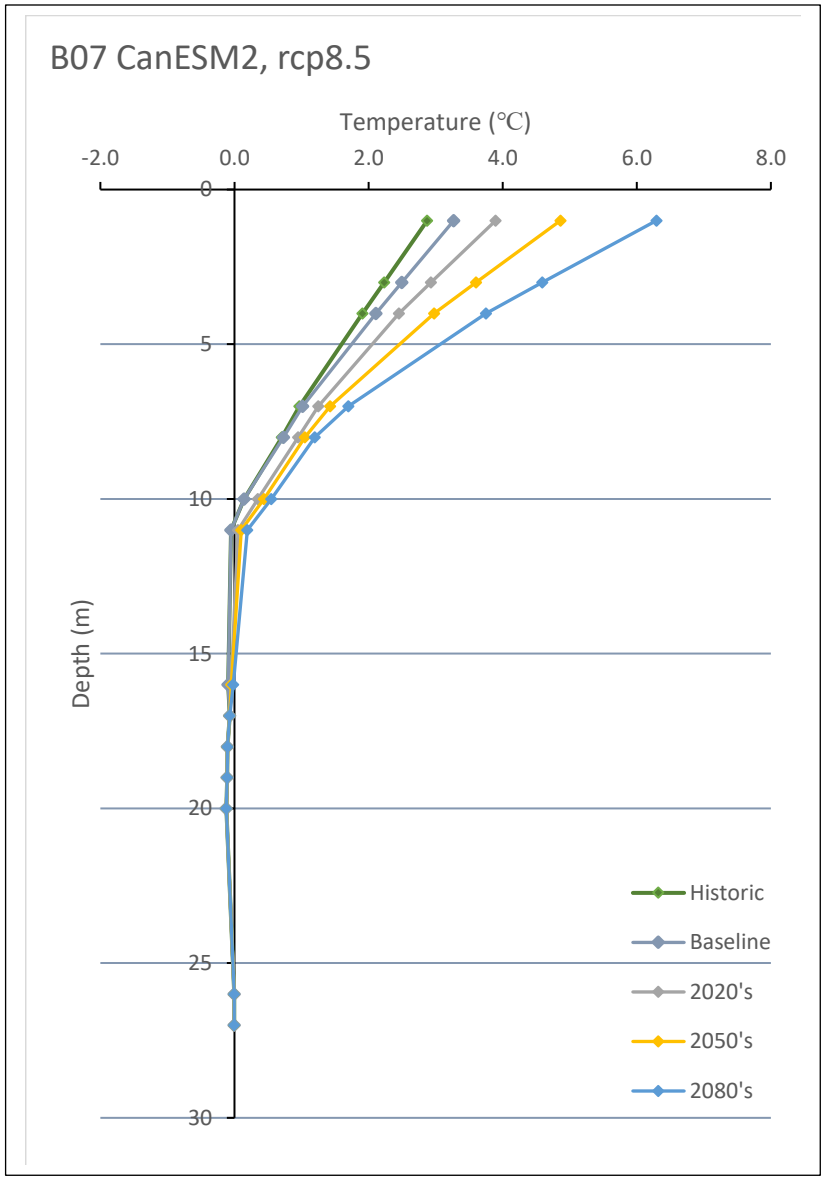

Figure 9. Changes in ALT in borehole B07 according to CanESM2 under rcp4.5 and rcp8.5 emission scenarios

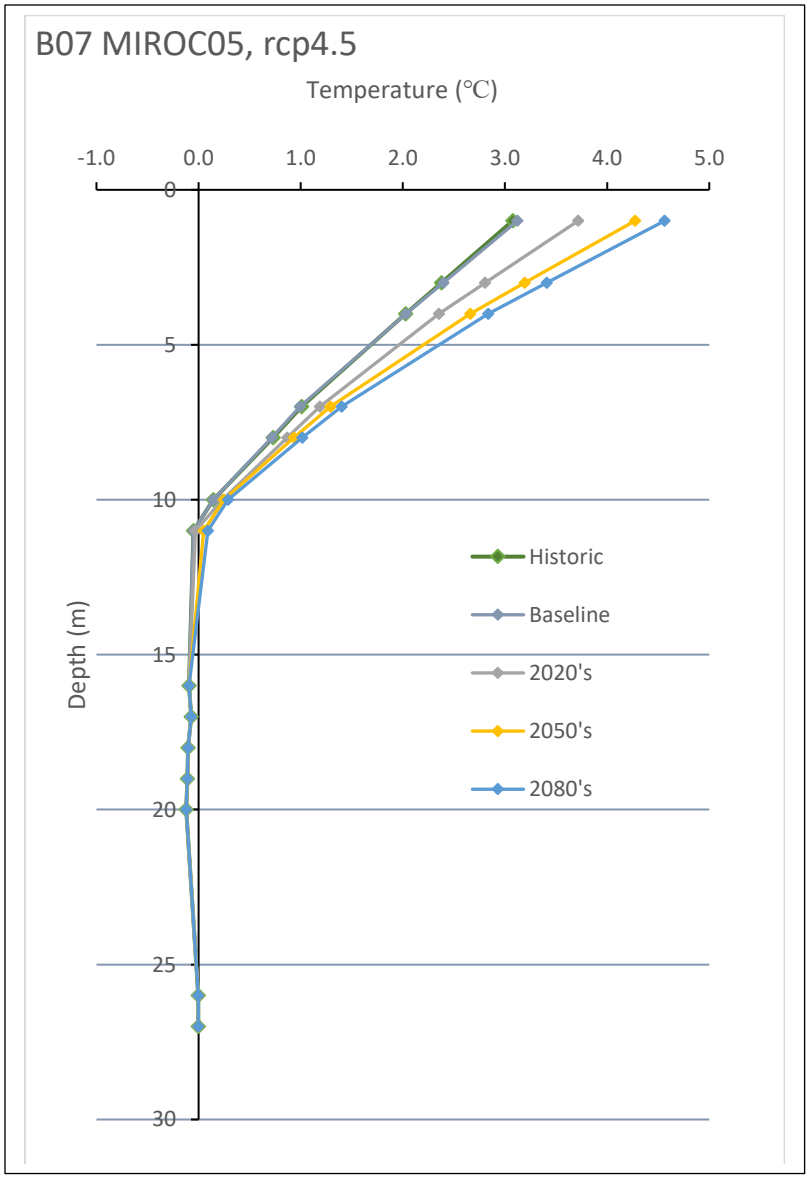

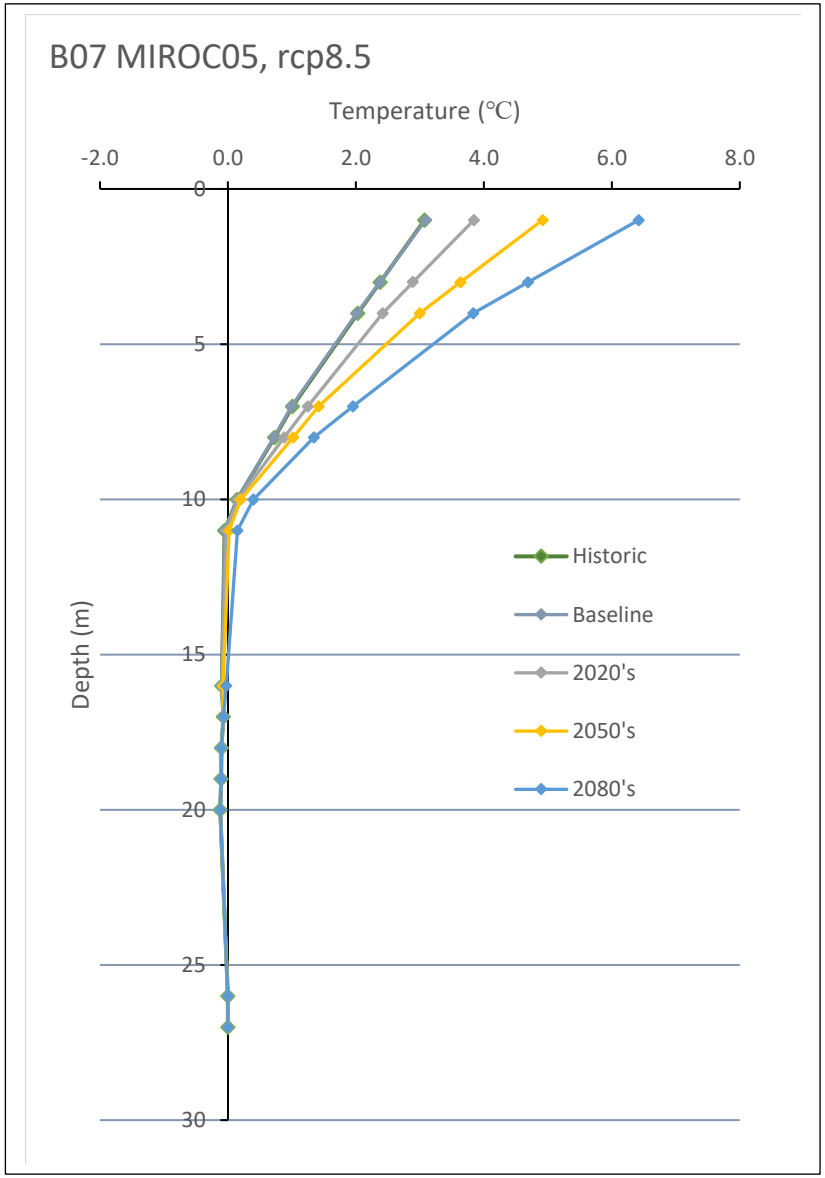

Figure 10. Changes in ALT in borehole B07 according to MIROC5 under rcp4.5 and rcp8.5 emission scenarios

3.5 Discussion

From the ground temperature records for the 27 boreholes retrieved to investigate the presence of permafrost, thirteen of the boreholes exhibited permafrost as their temperature records were less than 0℃ for two consecutive years. Permafrost thickness in the study site varied between approximately 4 m to 20 m in a discontinuous permafrost region (French and Egorov 1998). The region is considered “warm” permafrost site as it is close to its melting point of 0℃ and it is susceptible to near-term thaw as minimal sensible heat if required (Kurylyk et al. 2016).

All modeled boreholes in this study were calibrated to reproduce measured ground temperatures at respected depths closely. The model domain was 100 m discretized in a constant depth of 0.5 m. The simulated results from HYDRUS-1D (v4.17) were not able to depict the release of latent heat during the phase change of water during winter. Thus, winter season temperature simulations were profoundly propagating the events seen on the air temperature, which was used as the boundary condition. However, the model was able to capture the summer season effectively for all modeled boreholes.

The RMSE and MAE values for the very top nodes in all boreholes showed errors were even higher than the recorded average temperature for the calibration period; for example, B01 had an RMSE of 8.8℃ and an MAE of 6.7℃ at the top node, which is below 3.5 m from the ground surface. On the other hand, better simulation performance was observed during calibration with the Hansson's model, which is an extension of the HYDRUS-1D model and also accounts for the effect of latent heat energy (Hansson et al. 2004). Errors associated with calibration (error metrics) were less for the Hansson’s module in comparison with the HYDRUS-1D (v4.17) model. Model calibration was based on data from January 2014 to December 2015 and the calibrated model was validated for data spanning the 2011 - 2012 period. The observed soil temperature and

Hansson's model calibration results are plotted for all boreholes Appendix C. The Hansson's model showed way better agreement than the HYDRUS-1D (v4.17) model. For example, the RMSE and MAE for B02 were 0.9℃ and 0.6℃ for the calibration period 1.1℃ and 0.9℃ for the validation period, respectively. Error metrics results of both models for all boreholes, and each depth has been tabulated and presented in Appendix D.

Coarsely spaced sensors, lack of detailed knowledge of the ice content, other geophysical parameters, and some assumptions made during model establishment presented significant sources of uncertainties for this study. Parameters that significantly affected model results were investigated through sensitivity analyses. For this study, model sensitivity was evaluated by changing the calibrated thermal conductivity and heat capacity. The approach followed included varying one parameter by ±10% and ±30% while keeping the other same as the calibration. This analysis showed negligible change in the simulation result for varying both parameters by ±10% for all seasons and increasing both parameters by ±30% during the summer season. For the winter, Increasing the heat conductivity by +30% underestimated the winter temperature in reference to the calibrated temperature. A similar trend was observed when the heat capacity was altered by -30%. While reducing the heat conductivity by -30% has resulted in higher temperatures during winter, a similar trend was observed while altering the heat capacity by +30%.

Changes in permafrost conditions were assessed by tracking two key indicators: permafrost temperature and active layer thickness. Projections for future soil temperature were conducted by running the future climate data collected and used as a boundary condition for calibrated Hansson's module. In general, Hansson's model simulated the ALT realistically for all soil profiles under current climate conditions with the climate forcing datasets used. This gave confidence about future projections of ALT increases.

Future projections were made by using two GCMs; namely, CanESM2 and MIROC5 considering moderate (RCP4.5) and extreme (RCP8.5) emission scenarios. The average air temperature over the study site is expected to increase by 2.9℃ based on the last 30 years of the 21st century under high emission scenarios.

Simulation results indicated that sites with peat layers remained stable for both GCMs in all emission scenarios. Similar trends have been discussed in a study conducted by Burn (1998); they suggested that this could be due to the minimal snow cover on residential peat and latent heat in the ice-rich ground. Peat and ice act as thermal insulators.

Future projections on sites devoid of peat showed a significant impact on the fate of permafrost. For example, the results for B07 from both GCMs projected increase in active layer thickness will approximately 1 m and 2 m in the 2050's and 2080's period for moderate emission scenarios, respectively. This active layer thickness was profoundly observed on the high emission scenario indicating increment up to 2 m and 5 m similar periods, respectively.

3.6 Conclusion

This research investigated permafrost's presence using soil temperature data recorded by Manitoba hydro at the study site and identified ‘warm’ permafrost from 13 boreholes. Two vadose-zone models, namely Hansson’s module and HYDRUS-1D, models were calibrated. The Hansson’s module gave reasonable simulation results for all soil profiles in both summer and winter seasons. HYDRUS-1D model captures summer season effectively but resulted in colder soil temperature for the winter season since it doesn’t factor in the latent heat. This implies that factoring in heat transfer parameters into hydrological models provides reasonable predictions about the fates of degrading permafrost.

Two GCMs models with moderate and high emission rate scenarios were selected to evaluate climate change effects on the permafrost. Permafrost stays stable in sites with peat layers and degrades up to 5 meters for both GCMs under high emission scenarios. The accuracy of the model estimate can be increased by incorporating additional data, such as snow cover, vegetation cover, soil moisture content.

4 Conclusion and Recommendation

4.1 Conclusion

This study investigated permafrost using soil temperature data recorded by Manitoba hydro at a study site in Northern Manitoba and identified 'warm' permafrost from 13 boreholes. From the time-series plot of soil temperatures for two consecutive years, the thermistor records were considered more reliable and adopted for this study due to their less susceptibility to noise pollution and a strong correlation (R^2 = 0.99) from regression analyses as opposed to thermocouple temperature data.

Calibrated results from two vadose-zone models for conduction heat transfer namely, HYDRUS-1D and Hansson's module, showed that the latter better-predicted soil temperatures as summer and winter seasons were captured reasonably well. The former resulted in colder temperature for the winter season and was therefore not used in the investigation of permafrost. The different results from these two vadose-zone models underscore the importance of incorporating appropriate thermal properties and associated water phase changes in models to accurately characterize permafrost evolution.

With the huge impact of climate change on the hydroclimatic regime of permafrost zones, two GCMs (CanESM2 and MIROC5) with moderate (RCP4.5) and high emission rate (RCP8.5) scenarios were selected to evaluate climate change effect on permafrost. The investigation showed that permafrost will remain stable in sites with peat layers but could degrade up to 5 meters in areas without peat based on both GCMs under high emission scenarios by 2080s. This predicted thawing of permafrost in future years under high emission scenarios implies that water budgets of

catchments in permafrost zones are less likely to be accurately predicted by hydrological models calibrated under current climate conditions and need to be modified.

Degrading permafrost as shown in this work could have far-reaching consequences on the regional hydrology and climatology, water supply, ecosystem, carbon cycle, and infrastructural stability in northern communities. However, this would require long-term data collection and coupling numerical and watershed models. Across the globe, numerous studies using field observations and modeling have reported that decreasing permafrost have resulted in increased streamflow, groundwater recharge, winter discharge, alter in soil water storage, delay in the release of water in streams, ecosystem carbon release and storage, soil respiration, and collapse of infrastructures such as dam, buildings, etc. (Gao et al. 2021, Liu et al. 2018, Ma et al. 2020, Wang et al. 2017).

4.2 Recommendation for future work

Some limitation in this study comes with the lack of site-specific soil properties that would have helped improve modeling results. The Hansson calibrated model parameters should be verified with laboratory experiments with soil samples collected from the study site or artificially developed in the lab. Further investigation on the effect of peat would widen our scope of knowledge on the nature of atmospheric and ground temperature interaction and the impact of climate change.

Another limitation in this study is the lack of data for model inputs affecting permafrost, such as snow and vegetation cover, soil moisture content, near-surface ground temperature, etc. These should be incorporated into the existing physically based numerical model.

Long-term data enhances and boosts modelers' perspective to give more reliable and sensible results, identifying further unknowns. It also provides a sufficient warm-up period for the model to get initialized and reach equilibrium. Different studies have demonstrated this to improve modeling, and uncertainties associated with GCMs could be reduced by introducing more GCMs and creating ensembles.

Existing hydrological models should be coupled with the heat transfer models to determine the fates of melting permafrost. This approach will also help quantify the degradation of permafrost and assess its extent to investigate further if more mitigation measures are needed to avoid catastrophic structural damage, adept new reservoir management scheme.

5 Bibliography

Abdalla, M., Pannir, S. and Elqurashi, E. (2019) Temperature Measurement and Calibration Setup (TH1).

Abdelaziz, Y. (2012).

Abolt, C., Young, M. and Caldwell, T. (2017) Numerical Modelling of Ice-Wedge Polygon Geomorphic Transition. Permafrost and Periglacial Processes 28(1), 347-355.

Adane, Z., Zlotnik, V.A., Rossman, N.R., Wang, T. and Nasta, P. (2019) Sensitivity of potential groundwater recharge to projected climate change scenarios: A site-specific study in the Nebraska Sand Hills, USA. Water (Switzerland) 11(5), <xocs:firstpage xmlns:xocs=""/>.

Ahmad, B., Usman, M., Syed, A., Khan, M. and Malik, K. (2020) Prognosis of Hydro-Meteorological Attributes based on Simulation and Projection of Streamflow in a High-Altitude Basin using Hydrologiska Byråns Vattenbalansavdelning (HBV) Model. 4, ep20015.

Angelopoulos, M., Westermann, S., Overduin, P., Faguet, A., Olenchenko, V., Grosse, G. and Grigoriev, M.N. (2019) Heat and Salt Flow in Subsea Permafrost Modeled with CryoGRID2. Journal of geophysical research. Earth surface 124(4), 920-937.

Anisimov, O. and Reneva, S. (2006) Permafrost and changing climate: the Russian perspective. Ambio 35(4), 169-175.

Anisimov, O.A., Shiklomanov, N.I. and Nelson, F.E. (2002) Variability of seasonal thaw depth in permafrost regions: a stochastic modeling approach. Ecological Modelling 153(3), 217-227.

Antonellini, M., Dentinho, T., Khattabi, A., Masson, E., Mollema, P., Silva, V. and Silveira, P. (2014) An integrated methodology to assess future water resources under land use and climate change: an application to the Tahadart drainage basin (Morocco). Environmental Earth Sciences 71(4), 1839-1853.

Arenson, L., Kääb, A. and O'Sullivan, A. (2016) Detection and Analysis of Ground Deformation in Permafrost Environments. Permafrost and Periglacial Processes 27(4), 339-351.

Arora, V. and Matthews, H.D. (2009) Characterizing uncertainty in modeling primary terrestrial ecosystem processes. Global Biogeochemical Cycles - GLOBAL BIOGEOCHEM CYCLE 23.

Arora, V., Scinocca, J., Boer, G., Christian, J., Denman, K., Flato, G., Kharin, V., Lee, W. and Merryfield, W. (2011) Carbon emission limits required to satisfy future representative concentration pathways of greenhouse gases. Geophysical Research Letters - GEOPHYS RES LETT 38.

Asadzadeh, M., Tolson, B.A. and Burn, D.H. (2014) A new selection metric for multiobjective hydrologic model calibration. Water Resources Research 50(9), 7082-7099.

Atchley, A., Painter, S., Harp, D., Coon, E., Wilson, C., Liljedahl, A. and Romanovsky, V. (2015) Using field observations to inform thermal hydrology models of permafrost dynamics with ATS (v0.83). Geoscientific Model Development Discussions 8, 3235-3292.

Ballantyne, C.K. (2008) The periglacial environment. Third Edition. Hugh M. French. John Wiley and Sons Ltd, Chichester, UK, 2007. xviii + 458 pp. ISBN-13: 978-0-470-86588-0 (HB), 978-0-470-86589-7 (PB, pp. 101-104, John Wiley & Sons, Ltd., Chichester, UK.

Bao, T., Liu, Z. and Bland, J. (2019) A multivariate freezing-thawing depth prediction model for spring load restriction. Cold Regions Science and Technology 167, <xocs:firstpage xmlns:xocs=""/>.

Beck, I., Ludwig, R., Bernier, M., Levesque, E. and Boike, J. (2015) Assessing Permafrost Degradation and Land Cover Changes (1986-2009) using Remote Sensing Data over Umiujaq, Sub-Arctic Québec. Permafrost and Periglacial Processes 26(2), 129-141.

Beermann, F., Langer, M., Wetterich, S., Strauss, J., Boike, J., Fiencke, C., Schirrmeister, L., Pfeiffer, E.-M. and Kutzbach, L. (2017a) Permafrost Thaw and Liberation of Inorganic Nitrogen in Eastern Siberia. Permafrost and Periglacial Processes 28(4), 605-618.

Beermann, F., Langer, M., Wetterich, S., Strauss, J., Boike, J., Fiencke, C., Schirrmeister, L., Pfeiffer, E.M. and Kutzbach, L. (2017b) Permafrost Thaw and Liberation of Inorganic Nitrogen in Eastern Siberia. Permafrost and Periglacial Processes 28(4), 605-618.

Beilman, D.W., Vitt, D.H. and Halsey, L.A. (2001) Localized Permafrost Peatlands in Western Canada: Definition, Distributions, and Degradation. Arctic, Antarctic, and Alpine Research 33(1), 70-77.

Bense, V.F., Ferguson, G. and Kooi, H. (2009) Evolution of shallow groundwater flow systems in areas of degrading permafrost. Geophysical Research Letters 36(L22401), urn:issn:0094-8276.

Bense, V.F., Kooi, H., Ferguson, G. and Read, T. (2012) Permafrost degradation as a control on hydrogeological regime shifts in a warming climate. Journal of Geophysical Research: Earth Surface 117(F3), n/a-n/a.

Bergman, T.L., Lavine, A.S. and Incropera, F.P. (2011) Fundamentals of Heat and Mass Transfer, 7th Edition, John Wiley & Sons, Incorporated.

Bergström, S. (2006) Experience from applications of the HBV hydrological model from the perspective of prediction in ungauged basins. IAHS-AISH Publication, 97-107.

Biskaborn, B., Smith, S., Noetzli, J., Matthes, H., Vieira, G., Streletskiy, D., Schoeneich, P., Romanovsky, V., Lewkowicz, A., Abramov, A., Allard, M., Boike, J., Cable, W., Christiansen, H., Delaloye, R., Diekmann, B., Drozdov, D., Etzelmüller, B., Grosse, G. and Lantuit, H. (2019) Permafrost is warming at a global scale. Nature Communications 10.

Boike, J., Nitzbon, J., Anders, K., Grigoriev, M., Bolshiyanov, D.Y., Langer, M., Lange, S., Bornemann, N., Morgenstern, A., Schreiber, P., Wille, C., Chadburn, S., Gouttevin, I., Burke, E. and Kutzbach, L. (2019) A 16-year record (2002-2017) of permafrost, active-layer, and meteorological conditions at the Samoylov Island Arctic permafrost research site, Lena River delta, northern Siberia: An opportunity to validate remote-sensing data and land surface, snow, and permafrost models. Earth System Science Data 11, 261-299.

Bonnaventure, P. and Lewkowicz, A. (2011) Modelling climate change effects on the spatial distribution of mountain permafrost at three sites in northwest Canada. Climatic Change 105(1), 293-312.

Bonnaventure, P.P. and Lewkowicz, A.G. (2013) Impacts of mean annual air temperature change on a regional permafrost probability model for the southern Yukon and northern British Columbia, Canada. Cryosphere 7(3), 935-946.

Booshehrian, A., Wan, R. and Su, X. (2019) Hydraulic variations in permafrost due to open-pit mining and climate change: a case study in the Canadian Arctic. Acta Geotechnica.

Bormann, H., Hollaender, H.M., Blume, T., Buytaert, W., Chirico, G.B., Exbrayat, J.F., Gustafsson, D., Hoelzel, H., Kraft, P., Krausse, T., Nazemi, A., Stamm, C., Stoll, S., Bloeschl, G. and Fluehler, H. (2011) Comparative discharge prediction from a small artificial catchment without model calibration; representation of initial hydrological catchment development. Die Bodenkultur (Wien) 62(1), 23-29.

Boucher-Brossard, G., Bernatchez, P., Corriveau, M. and Jolivet, Y. (2017) Calculating Lateral Frost Front Penetration in a Rapidly Retreating Cliff of Fine Sediments. Permafrost and Periglacial Processes 28(1), 32-41.

Bridger, D.W. and Allen, D.M. (2010) Heat transport simulations in a heterogeneous aquifer used for aquifer thermal energy storage (ATES). Canadian Geotechnical Journal 47(1), 96-115.

Brown, R.J.E. (1970) Permafrost in Canada; its influence on northern development. Univ. Toronto Press; (Canadian Building Series 4).

Brown, R.J.E. (1974) Permafrost terminology, National Research Council of Canada, Ottawa.

Bruland, O. and Killingtveit, Å. (2002) APPLICATION OF THE HBV-MODEL IN ARCTIC CATCHMENTS – SOME RESULTS FROM SVALBARD.

Brunner, P. and Simmons, C.T. (2012) HydroGeoSphere: A Fully Integrated, Physically Based Hydrological Model. Ground Water 50(2), 170-176.

Bugaets, A., Gartsman, B., Gelfan, A., Motovilov, Y., Sokolov, O., Gonchukov, L., Kalugin, A., Moreido, V., Suchilina, Z. and Fingert, E. (2018) The integrated system of hydrological forecasting in the Ussuri River basin based on the ECOMAG model. Geosciences (Basel) 8(1), 5.

Bui, M.T., Lu, J. and Nie, L. (2020) A Review of Hydrological Models Applied in the Permafrost-Dominated Arctic Region. Geosciences (Basel) 10(401), 401.

Burn, C. (1998) Field investigations of permafrost and climatic change in north - west North America. Collect. Nordicana 57.

Bush, E., Lemmen, D.S. and editors (2019) Canada's Changing Climate Report : Executive Summary, Environment and Climate Change Canada, Ottawa, QC, CA.

Byun, E., Yang, J.-W., Kim, Y. and Ahn, J. (2017) Trapped Greenhouse Gases in the Permafrost Active Layer: Preliminary Results for Methane Peaks in Vertical Profiles of Frozen Alaskan Soil Cores. Permafrost and Periglacial Processes 28(2), 477-484.

Camill, P. (2005) Permafrost thaw accelerates in boreal peatlands during late-20th century climate warming. Climatic Change 68(1-2), 135-152.

Canadian Centre for Climate Services (CCCS); Ouranos and the Pacific Climate Impacts Consortium (PCIC) (2019) Climate data for resilient canada.

Carturan, L., Zuecco, G., Seppi, R., Zanoner, T., Borga, M., Carton, A. and Dalla Fontana, G. (2016) Catchment-Scale Permafrost Mapping using Spring Water Characteristics. Permafrost and Periglacial Processes 27(3), 253-270.

Chadburn, S.E., Burke, E.J., Cox, P.M., Friedlingstein, P., Hugelius, G. and Westermann, S. (2017) An observation-based constraint on permafrost loss as a function of global warming. Nature climate change 7(5), 340-344.

Changwei, X. and Gough, W.A. (2013) A Simple Thaw-Freeze Algorithm for a Multi-Layered Soil using the Stefan Equation. Permafrost and Periglacial Processes 24(3), 252-260.

Chen, W., Zhang, Y., Cihlar, J., Smith, S. and Riseborough, D. (2003) Changes in soil temperature and active layer thickness during the twentieth century in a region in western Canada. Journal of Geophysical Research 108.

Cheng, G. and Jin, H. (2013) Permafrost and groundwater on the Qinghai-Tibet Plateau and in northeast China. Hydrogeology Journal 21(1), 5-23.

Christian, J., Arora, V., Boer, G., Curry, C., Zahariev, K., Denman, K., Flato, G., Lee, W., Merryfield, W., Roulet, N. and Scinocca, J. (2010) The global carbon cycle in the Canadian Earth system model (CanESM1): Preindustrial control simulation. Journal of Geophysical Research (Biogeosciences) 115.

Chung, S.-O. and Horton, R.J. (1987) Soil heat and water flow with a partial surface mulch. Water Resources Research 23(12), 2175-2186.

Churiulin, E.V., Krylenko, I.N., Frolova, N.L. and Belyaev, B.M. (2019) Research of opportunities of combined use of the runoff formation ECOMAG model and mesoscale atmosphere circulation COSMO-Ru model (on the example of floods on the Sukhona River at the Velikiy Ustyug). IOP Conference Series: Earth and Environmental Science 263, 012057.

Clarke, L., Edmonds, J., Jacoby, H., Pitcher, H., Reilly, J. and Richels, R. (2007) Scenarios of Greenhouse Gas Emissions and Atmospheric Concentrations.

Comeau, L.E.L., Pietroniro, A. and Demuth, M.N. (2009) Glacier contribution to the North and South Saskatchewan Rivers. Hydrological Processes 23(18), 2640-2653.

Connon, R.F., Quinton, W.L., Craig, J.R. and Hayashi, M. (2014) Changing hydrologic connectivity due to permafrost thaw in the lower Liard River valley, NWT, Canada. Hydrological Processes 28(14), 4163-4178.

Cranmer, A.J., Kouwen, N. and Mousavi, S.F. (2001) Proving WATFLOOD: modelling the nonlinearities of hydrologic response to storm intensities. Canadian journal of civil engineering 28(5), 837-855.

Dacquay, C., Holländer, H.M., Kavgic, M., Maghoul, P., Liu, H. and Fujii, H. (2020) Evaluation of an integrated sewage pipe with ground heat exchanger for long-term efficiency estimation. Geothermics 86, 101796.

Dall'Amico, M., Endrizzi, S., Gruber, S. and Rigon, R. (2011) A robust and energy-conserving model of freezing variably-saturated soil. The Cryosphere 5(2), 469.

Davies, M.C.R., Hamza, O. and Harris, C. (2001) The effect of rise in mean annual temperature on the stability of rock slopes containing ice-filled discontinuities. Permafrost and Periglacial Processes 12(1), 137-144.

Derksen, C., Burgess, D., Duguay, C., Howell, S., Murdryk, L., Smith, S., Thackeray, C. and Kirchmele-Young, M. (2018) Canada's changing climate report, Environment and Climate Change Canada = Environnement et changement climatique Canada, Gatineau, QC.

Dobinski, W. (2011) Permafrost. Earth-Science Reviews 108(3), 158-169.

Draebing, D., Haberkorn, A., Krautblatter, M., Kenner, R. and Phillips, M. (2017) Thermal and Mechanical Responses Resulting From Spatial and Temporal Snow Cover Variability in Permafrost Rock Slopes, Steintaelli, Swiss Alps. Permafrost and Periglacial Processes 28(1), 140-157.

Duan, L., Man, X., Kurylyk, B. and Cai, T. (2017) Increasing Winter Baseflow in Response to Permafrost Thaw and Precipitation Regime Shifts in Northeastern China. Water 9(1), 25.

Dyke, L.D. and Sladen, W.E. (2010) Permafrost and peatland evolution in the northern Hudson Bay lowland, Manitoba.(Report). Arctic 63(4), 429.

Environment Canada (2019) Historical climate data.

Etzelmüller, B., Schuler, T., Isaksen, K., Christiansen, H., Farbrot, H. and Benestad, R. (2011) Modeling the temperature evolution of Svalbard permafrost during the 20th and 21st century. The Cryosphere 5.

Fagan, J. and Nelson, F. (2017) Spatial Sampling Design in the Circumpolar Active Layer Monitoring Programme. Permafrost and Periglacial Processes 28(1), 42-51.

French, H.M. and Egorov, I.E. (1998) 20th Century Variations in the southern limit of permafrost near Thompson, Northern Manitoba, Canada, Collection Nordicana No. 55, University of Laval, Quebec, p. 297-304, Yellowknife Canada, June 1998.

Fujino, J., Nair, R., Kainuma, M., Masui , T. and Matsuoka, Y. (2006) Multi-Gas Mitigation Analysis on Stabilization Scenarios Using AIM Global Model. The Energy Journal Multi-Greenhouse Gas Mitigation and Climate Policy, 343-354.

Gao, H., Wang, J., Yang, Y., Pan, X., Ding, Y. and Duan, Z. (2021) Permafrost Hydrology of the Qinghai-Tibet Plateau: A Review of Processes and Modeling. Frontiers in Earth Science 8(535).

Gelfan, A., Gelfan, A., Gustafsson, D., Gustafsson, D., Motovilov, Y., Motovilov, Y., Arheimer, B., Arheimer, B., Kalugin, A., Kalugin, A., Krylenko, I., Krylenko, I., Lavrenov, A. and Lavrenov, A. (2017) Climate change impact on the water regime of two great Arctic rivers: modeling and uncertainty issues. Climatic Change 141(3), 499-515.

Gheysari, A.F., Holländer, H.M., Maghoul, P. and Shalaby, A. (2021) Sustainability, climate resiliency, and mitigation capacity of geothermal heat pump systems in cold regions. Geothermics 91, 101979.

Gray, J., Davesne, G., Fortier, D. and Godin, E. (2017) The Thermal Regime of Mountain Permafrost at the Summit of Mont Jacques-Cartier in the Gaspé Peninsula, Québec, Canada: A 37 Year Record of Fluctuations showing an Overall Warming Trend. Permafrost and Periglacial Processes 28(1), 266-274.

Guo, D., Wang, H. and Li, D. (2012) A projection of permafrost degradation on the Tibetan Plateau during the 21st century. Journal of Geophysical Research Atmospheres.

Hällberg, P. (2018) Permafrost Modelling and Climate Change Simulations in Northern Sweden.

Hansson, K., Simunek, J., Mizoguchi, M., Lundin, L.-C. and Van Genuchten, M. (2004) Water Flow and Heat Transport in Frozen Soil -- Numerical Solution and Freeze-Thaw Applications. Vadose Zone Journal 3(2), 693-704.

Hasumi, H. and Emori, S. (2004) K-1 Coupled GCM (Miroc Description)1.

Haynes, K., Connon, R. and Quinton, W. (2019) Hydrometeorological measurements in peatland-dominated, discontinuous permafrost at Scotty Creek, Northwest Territories, Canada. Geoscience Data Journal 6.

Hijioka, Y., Matsuoka, Y., Nishimoto, H., Masui, T. and Kainuma, M. (2008) Global GHG emission scenarios under GHG concentration stabilization targets. Journal of Global Environment Engineering 13, 97-108.

Hinzman, L.D., Kane, D.L., Gieck, R.E. and Everett, K.R. (1991) Hydrologic and thermal properties of the active layer in the Alaskan Arctic. Cold Regions Science and Technology 19(2), 95-110.

Hoelzle, M. and Haeberli, W. (1995) Simulating the effects of mean annual air temperature changes on permafrost distribution and glacier size. An example from the Upper Engadin, Swiss Alps. Annals of Glaciology 21, 399-405.

Holländer, H., Blume, T., Bormann, H., Buytaert, W., Chirico, G.B., Exbrayat, J.F., Gustafsson, D., Hölzel, H., Kraft, P., Stamm, C., Stoll, S., Blöschl, G. and Flühler, H. (2009) Comparative predictions of discharge from an artificial catchment (Chicken Creek) using sparse data. Hydrology and Earth System Sciences 13(11), 2069.

Holländer, H.M., Bormann, H., Blume, T., Buytaert, W., Chirico, G.B., Exbrayat, J.F., Gustafsson, D., xF, lzel, H., Krau, xC, x9F, e, T., Kraft, P., Stoll, S., Bl, xF, schl, G., Fl, xFc and hler, H. (2014) Impact of modellers' decisions on hydrological a priori predictions. Hydrology and Earth System Sciences 18(6), 2065.

IPCC (2007) Report of the 26th session of the IPCC, Bangkok. April 30–May 4 2007. Intergovernmental Panel on Climate Change, Geneva, Switzerland.

IPCC (2018) Global Warming of 1.5°C. An IPCC Special Report on the impacts of global warming of 1.5°C above pre-industrial levels and related global greenhouse gas emission pathways, in the context of strengthening the global response to the threat of climate change, sustainable development, and efforts to eradicate poverty [Masson-Delmotte, V., P. Zhai, H.-O. Pörtner, D. Roberts, J. Skea, P.R. Shukla, A. Pirani, W. Moufouma-Okia, C. Péan, R. Pidcock, S. Connors, J.B.R. Matthews, Y. Chen, X. Zhou, M.I. Gomis, E. Lonnoy, T. Maycock,

M. Tignor, and T. Waterfield (eds.)]. In Press. Library journal (1976) 144(4), 40.

Ishikawa, M., Jamvaljav, Y., Dashtseren, A., Sharkhuu, N., Davaa, G., Iijima, Y., Baatarbileg, N. and Yoshikawa, K. (2018) Thermal states, responsiveness and degradation of marginal permafrost in Mongolia. Permafrost and Periglacial Processes 29(4), 271-282.

Jackson, E.K., Roberts, W., Nelsen, B., Williams, G.P., Nelson, E.J. and Ames, D.P. (2019) Introductory overview: Error metrics for hydrologic modelling – A review of common practices and an open source library to facilitate use and adoption. Environmental Modelling and Software 119, 32-48.

Jan, A., Coon, E. and Painter, S. (2020) Evaluating integrated surface/subsurface permafrost thermal hydrology models in ATS (v0.88) against observations from a polygonal tundra site. Geoscientific Model Development 13, 2259-2276.

Jenkinson, R.W. (2009) Surface water quality modelling considering riparian wetlands, ProQuest Dissertations Publishing.

Jing, L. and Chen, B. (2011) Hydrological modeling of subartic wetlands: Comparison between SLURP and WATFLOOD. Environmental Engineering Science 28, 521-533.

Karra, S., Painter, S. and Lichtner, P. (2014) Three-phase numerical model for subsurface hydrology in permafrost-affected regions (PFLOTRAN-ICE v1.0). The Cryosphere 8.

Kouwen (2016) WATFLOOD™/CHARM Canadian hydrological and routing model, University of Waterloo, Waterloo.

Koven, C., Riley, W. and Stern, A. (2013) Analysis of Permafrost Thermal Dynamics and Response to Climate Change in the CMIP5 Earth System Models. Journal of Climate 26, 1877-1900.

Krysanova, V., Vetter, T., Eisner, S., Huang, S., Pechlivanidis, I., Strauch, M., Gelfan, A., Kumar, R., Aich, V., Arheimer, B., Chamorro, A., van Griensven, A., Kundu, D., Lobanova, A., Mishra, V., Plötner, S., Reinhardt, J., Seidou, O., Wang, X., Wortmann, M., Zeng, X. and Hattermann, F.F. (2017) Intercomparison of regional-scale hydrological models and climate change impacts projected for 12 large river basins worldwide—a synthesis. Environmental Research Letters 12(10), 105002.

Kujala, K., Seppälä, M. and Holappa, T. (2008) Physical properties of peat and palsa formation. Cold Regions Science and Technology 52(3), 408-414.

Kundzewicz, Z.W. and Somlyódy, L. (1997) Climatic change impact on water resources in a system perspective. Water Resour. Manag, 11, 407–435. [CrossRef].

Kurylyk, B., Hayashi, M., Quinton, W., McKenzie, J. and Voss, C. (2016) Influence of vertical and lateral heat transfer on permafrost thaw, peatland landscape transition, and groundwater flow. Water Resources Research.

Kurylyk, B.L., MacQuarrie, K.T.B. and McKenzie, J.M. (2014) Climate change impacts on groundwater and soil temperatures in cold and temperate regions: Implications, mathematical theory, and emerging simulation tools. Earth-Science Reviews 138, 313-334.

Lacelle, D., Bjornson, J. and Lauriol, B. (2010) Climatic and geomorphic factors affecting contemporary (1950–2004) activity of retrogressive thaw slumps on the Aklavik Plateau, Richardson Mountains, NWT, Canada. Permafrost and Periglacial Processes 21(1), 1-15.

Langer, M., Westermann, S., Muster, S., Piel, K. and Boike, J. (2011) The surface energy balance of a polygonal tundra site in northern Siberia – Part 2: Winter. The Cryosphere 5(2), 509-524.

Lestari, I. and Dasanto, B. (2019) Determination of Extreme Hydrological Index using HBV Model Simulation Results (Case Study : Upper Ciliwung Watershed). Agromet 33, 20-29.

Lewkowicz, A., Weege, S., Biskaborn, B., Streletskiy, D., Romanovsky, V. and Fortier, R. (2016) Report from the International Permafrost Association. Permafrost and Periglacial Processes 27(3), 316-319.

Lewkowicz, A.G., Bonnaventure, P.P., Smith, S.L. and Kuntz, Z. (2012) Spatial and thermal characteristics of mountain permafrost, northwest canada. Geografiska annaler. Series A, Physical geography 94(2), 195-213.

Lindström, G., Johansson, B., Persson, M., Gardelin, M. and Bergström, S. (1997) Development and test of the distributed HBV-96 hydrological model. Journal of hydrology (Amsterdam) 201(1), 272-288.

Liu, G., Zhao, L., Li, R., Wu, T., Jiao, K. and Ping, C. (2017) Permafrost Warming in the Context of Step-wise Climate Change in the Tien Shan Mountains, China. Permafrost and Periglacial Processes 28(1), 130-139.

Liu, W., Chen, S., Liang, J., Qin, X., Kang, S., Ren, J. and Qin, D. (2018) The effect of decreasing permafrost stability on ecosystem carbon in the northeastern margin of the Qinghai–Tibet Plateau. Scientific Reports 8(1), 4172.

Luedtke, B. and Howkins, A. (2012) Polarized climates: the distinctive histories of climate change and politics in the Arctic and Antarctica since the beginning of the Cold War, pp. 145-159, John Wiley & Sons, Inc., Hoboken, USA.

Lunardini, V.J. (1978) Theory of N-factors and correlation of data, pp. 40-46, National Council of Canada.

Lunardini, V.J. (1988) Freezing of soil with an unfrozen water content and variable thermal properties, US Army Corps of Engineers, Cold Regions Research & Engineering Laboratory, Hanover, NH.

Ma, Q., Jin, H., Bense, V., Luo, D., Marchenko, S., Harris, S. and Yong-Chao, L. (2020) Impacts of degrading permafrost on streamflow in the source area of Yellow River on the Qinghai-Tibet Plateau, China. Advances in Climate Change Research 10.

Manitoba Hydro (2020) Climate Change Report.

Masui, T., Matsumoto, K.i., Hijioka, Y., Kinoshita, T., Nozawa, T., Ishiwatari, S., Kato, E., Shukla, P., Yamagata, Y. and Kainuma, M. (2011) An Emission Pathway for Stabilization at 6Wm-2 Radiative Forcing. Climatic Change 109, 59-76.

McKenzie, J. and Voss, C. (2013) Permafrost thaw in a nested groundwater-flow system. Hydrogeology Journal 21.

Mikail, R., Hazar, E., Mikayilov, F. and Erdel, E. (2019) On the influence of boundary conditions at depth in modeling heat transfer in soil.

Mittaz, C., Hoelzle, M. and Haeberli, W. (2000) First results and interpretation of energy flux measurements of Alpine permafrost. Annals of Glaciology 31, 275-280.

Moss, R., Edmonds, J., Hibbard, K., Manning, M., Rose, S., Vuuren, D., Carter, T., Emori, S., Kainuma, M., Kram, T., Meehl, G., Mitchell, J., Nakicenovic, N., Riahi, K., Smith, S., Ronald, S., Thomson, A., Weyant, J. and Wilbanks, T. (2010) The Next Generation of Scenarios for Climate Change Research and Assessment. Nature 463, 747-756.

Motovilov, Y. (2013) ECOMAG: A distributed model of runoff formation and pollution transformation in river basins. IAHS-AISH Proceedings and Reports 361, 227-234.

Motovilov, Y., Kalugin, A. and Gelfan, A. (2017) An ECOMAG-based Regional Hydrological Model for the Mackenzie River basin, p. 8064.

Motovilov, Y.G. (2017) Modeling fields of river runoff (a case study for the Lena River basin). Russian meteorology and hydrology 42(2), 121-128.

Motovilov, Y.G., Gottschalk, L., Engeland, K. and Belokurov, A. (1999) ECOMAG—Regional Model of Hydrological Cycle. Application to the NOPEX Region; , Department of Geophysics, University of Oslo, Oslo, Norway.

Myhra, K.S., Westermann, S. and Etzelmüller, B. (2017) Modelled Distribution and Temporal Evolution of Permafrost in Steep Rock Walls Along a Latitudinal Transect in Norway by CryoGrid 2D. Permafrost and Periglacial Processes 28(1), 172-182.

Oleson, K., Lawrence, D., B, G., Flanner, M., Kluzek, E., Lawrence, P., Levis, S., Swenson, S., Thornton, E., Feddema, J., Heald, C., Lamarque, J.-F., Niu, G.-Y., Qian, T., Running, S., Sakaguchi, K., Yang, Z.-L., Zeng, X. and Zeng, X. (2010) Technical Description of version 4.0 of the Community Land Model (CLM).

Osuch, M., Wawrzyniak, T. and Nawrot, A. (2019) Diagnosis of the hydrology of a small Arctic permafrost catchment using HBV conceptual rainfall-runoff model. Hydrology Research 50.

Painter, S., Coon, E., Atchley, A., Berndt, M., Garimella, R., Moulton, J., Svyatskiy, D. and Wilson, C. (2016) Integrated surface/subsurface permafrost thermal hydrology: Model formulation and proof-of-concept simulations. Water Resources Research 52.

Palmer, M.J., Burn, C.R. and Kokelj, S.V. (2012) Factors influencing permafrost temperatures across tree line in the uplands east of the Mackenzie Delta, 2004–2010 1, 2 1 This article is one of a series of papers published in this CJES Special Issue on the theme of Fundamental and applied research on permafrost in Canada . 2 Polar Continental Shelf Contribution 03611. Canadian Journal Of Earth Sciences 49(8), 877-894.

Plaza, C., Pegoraro, E., Bracho, R., Celis, G., Crummer, K., Hutchings, J., Hicks Pries, C., Mauritz, M., Natali, S., Salmon, V., Schädel, C., Webb, E. and Schuur, E. (2019) Direct observation of permafrost degradation and rapid soil carbon loss in tundra. Nature Geoscience 12, 1.

Pokorny, S., Stadnyk, T., Ali, G., Lilhare, R., Déry, S. and Koenig, K. (2021) Cumulative Effects of Uncertainty on Simulated Streamflow in a Hydrologic Modeling Environment. Elementa: Science of the Anthropocene 9.

Press, W., Teukolsky, S., Vetterling, W. and Flannery, B. (1992), pp. 394,425.

Quinton, W., Braverman, M., Carpino, O., Chasmer, L., Connon, R., Devoie, É., Haynes, K., Pietroniro, A., Rezanezhad, F., Schincariol, R. and Sonnentag, O. (2019) A synthesis of three decades of hydrological research at Scotty Creek, NWT, Canada. Hydrology and Earth System Sciences 23(4), 2015-2039.

Radajewski, M., Decker, S. and Krüger, L. (2019) Direct temperature measurement via thermocouples within an SPS/FAST graphite tool. Measurement 147, 106863.

Riahi, K., Grubler, A. and Nakicenovic, N. (2007) Scenarios of long-term socio-economic and environmental development under climate stabilization. Technological Forecasting and Social Change 74, 887-935.

Riahi, K., Rao, S., Krey, V., Cho, C., Chirkov, V., Fischer, G., Kindermann, G., Nakicenovic, N. and Rafaj, P. (2011) RCP 8.5—A scenario of comparatively high greenhouse gas emissions. Climatic Change 109(1), 33.

Riseborough, D., Shiklomanov, N., Etzelmüller, B., Gruber, S. and Marchenko, S. (2008) Recent Advances in Permafrost Modeling. Permafrost and Periglacial Processes 19, 137-156.

Rivkina, E., Abramov, A., Spirina, E., Petrovskaya, L., Shatilovich, A., Shmakova, L., Scherbakova, V. and Vishnivetskaya, T. (2018) Earth's perennially frozen environments as a model of cryogenic planet ecosystems. Permafrost and Periglacial Processes 29(4), 246-256.

Rudy, A.A., Lamoureux, S., Treitz, P., Ewijk, K., Bonnaventure, P. and Budkewitsch, P. (2017) Terrain Controls and Landscape-Scale Susceptibility Modelling of Active-Layer Detachments, Sabine Peninsula, Melville Island, Nunavut. Permafrost and Periglacial Processes 28(1), 79-91.

Rühaak, W., Anbergen, H., Grenier, C., McKenzie, J., Kurylyk, B.L., Molson, J., Roux, N. and Sass, I. (2015) Benchmarking Numerical Freeze/Thaw Models. Energy Procedia 76, 301-310.

Saaly, M., Bobko, K., Maghoul, P., Kavgic, M. and Holländer, H. (2020) Energy performance of below-grade envelope of an institutional building in cold regions. Journal of Building Engineering 27, 100911.

Salem, G.S.A., Kazama, S., Shahid, S. and Dey, N.C. (2018) Impacts of climate change on groundwater level and irrigation cost in a groundwater dependent irrigated region. Agricultural water management 208, 33-42.

Sannel, A.B.K., Hugelius, G., Jansson, P. and Kuhry, P. (2016) Permafrost Warming in a Subarctic Peatland – Which Meteorological Controls are Most Important? Permafrost and Periglacial Processes 27(2), 177-188.

Shmelev, D., Veremeeva, A., Kraev, G., Kholodov, A., Spencer, R.M., Walker, W. and Rivkina, E. (2017) Estimation and Sensitivity of Carbon Storage in Permafrost of North-Eastern Yakutia. Permafrost and Periglacial Processes 28(2), 379-390.

Shojae Ghias, M., Therrien, R., Molson, J. and Lemieux, J.-M. (2019) Numerical simulations of shallow groundwater flow and heat transport in continuous permafrost setting under impact of climate warming. Canadian Geotechnical Journal 56(3), 436-448.

Simunek, J.J., Šejna, M., Saito, H., Sakai, M. and Van Genuchten, M. (2013) The Hydrus-1D Software Package for Simulating the Movement of Water, Heat, and Multiple Solutes in Variably Saturated Media, Version 4.17, HYDRUS Software Series 3, Department of Environmental Sciences, University of California Riverside, Riverside, California. USA.

Smith, M.W. and Riseborough, D. (1996) Ground temperature monitoring and detection of climate change. Permafrost and Periglacial Processes 16, 313-335.

Smith, S. and Wigley, T.M.L. (2006) Multi-Gas Forcing Stabilization with the MiniCAM. The Energy Journal Multi-Greenhouse Gas Mitigation and Climate Policy, 373-392.

Stadnyk, T., Amour, N., Kouwen, N., Edwards, T., Pietroniro, A. and Gibson, J. (2005) A groundwater separation study in boreal wetland terrain: The WATFLOOD hydrological model compared with stable isotope tracers. Isotopes in Environmental and Health Studies 41, 49-68.

Stone, L.E., Fang, X., Haynes, K.M., Helbig, M., Pomeroy, J.W., Sonnentag, O. and Quinton, W.L. (2019) Modelling the effects of permafrost loss on discharge from a wetland-dominated, discontinuous permafrost basin. Hydrological Processes 33(20), 2607-2626.

Streletskiy, D., Shiklomanov, N., Little, J., Nelson, F., Brown, J., Nyland, K. and Klene, A. (2017) Thaw Subsidence in Undisturbed Tundra Landscapes, Barrow, Alaska, 1962-2015. Permafrost and Periglacial Processes 28(3), 566-572.

Swart, N., Cole, J., Kharin, V., Lazare, M., Scinocca, J., Gillett, N., Anstey, J., Arora, V., Christian, J., Hanna, S., Jiao, Y., Lee, W., Majaess, F., Saenko, O., Seiler, C., Seinen, C., Shao, A., Solheim, L., von Salzen, K. and Winter, B. (2019) The Canadian Earth System Model version 5 (CanESM5.0.3). Geoscientific Model Development Discussions, 1-68.

Thomson, A.M., Calvin, K.V., Smith, S.J., Kyle, G.P., Volke, A., Patel, P., Delgado-Arias, S., Bond-Lamberty, B., Wise, M.A., Clarke, L.E. and Edmonds, J.A. (2011) RCP4.5: a pathway for stabilization of radiative forcing by 2100. Climatic Change 109(1), 77.

Toth, B., A. Pietroniro, F.M. Conley and N. Kouwen (2006) Modelling climate change impacts in the Peace and Athabasca catchment and delta I – hydrological model application. Hydrological Process.

Unduche, F., Tolossa, H., Senbeta, D. and Zhu, E. (2018) Evaluation of four hydrological models for operational flood forecasting in a Canadian Prairie watershed. Hydrological Sciences Journal 63.

van Vuuren, D.P., Edmonds, J., Kainuma, M., Riahi, K., Thomson, A., Hibbard, K., Hurtt, G.C., Kram, T., Krey, V., Lamarque, J.-F., Masui, T., Meinshausen, M., Nakicenovic, N., Smith, S.J. and Rose, S.K. (2011) The representative concentration pathways: an overview. Climatic Change 109(1), 5.

Vieira, M.J.F. (2018) Hydroclimatic Studies Engineer, Manitoba Hydro, Hydrology and Climate Section, Water Resources Department.

Vuuren, D., Eickhout, B., Lucas, P. and Elzen, M. (2006) Long-Term Multi-Gas Scenarios to Stabilise Radiative Forcing - Exploring Costs and Benefits Within an Integrated Assessment Framework. The Energy Journal Multi-Greenhouse Gas Mitigation and Climate Policy, 201-234.

Vuuren, D., Elzen, M., Lucas, P., Eickhout, B., Strengers, B., van Ruijven, B., Wonink, S. and Houdt, R. (2007) Stabilizing greenhouse gas concentrations at low levels: An assessment of reduction strategies and costs. Climatic Change 81, 119-159.

Vuuren, D., Stehfest, E., Elzen, M., Kram, T., Vliet, J., Deetman, S., Isaac, M., Klein Goldewijk, K., Hof, A., Mendoza Beltran, A., Oostenrijk, R. and van Ruijven, B. (2011) RCP2.6: Exploring the possibility to keep global mean temperature increase below 2°C. Climatic Change 109, 95-116.

Wagner, A., Lindsey, N., Dou, S., Gelvin, A., Saari, S., Williams, C., Ekblaw, I., Craig, U., Borglin, S., Morales, A. and Ajo-Franklin, J. (2018) Permafrost Degradation and Subsidence Observations during a Controlled Warming Experiment. Scientific Reports (Nature Publisher Group) 8(10908), 1-9.

Walvoord, M.A. and Kurylyk, B. (2016) Hydrologic Impacts of Thawing Permafrost-A Review. Vadose Zone Journal 15(6).

Wang, X., Rensheng, C. and Yang, Y. (2017) Effects of Permafrost Degradation on the Hydrological Regime in the Source Regions of the Yangtze and Yellow Rivers, China. Water 9, 897.

Watanabe, M., Suzuki, T., O'Ishi, R., Komuro, Y., Watanabe, S., Emori, S., Takemura, T., Chikira, M., Ogura, T., Sekiguchi, M., Takata, K., Yamazaki, D., Yokohata, T., Nozawa, T., Hasumi, H., Tatebe, H. and Kimoto, M. (2010) Improved Climate Simulation by MIROC5: Mean States, Variability, and Climate Sensitivity. Journal of Climate 23, 6312-6335.

Way, R. and Lewkowicz, A. (2018) Environmental controls on ground temperature and permafrost in Labrador, northeast Canada. Permafrost and Periglacial Processes 29(2), 73-85.

Westermann, S., Schuler, T.V., Gisnås, K. and Etzelmüller, B. (2013) Transient thermal modeling of permafrost conditions in Southern Norway. The Cryosphere 7(2), 719-739.

Willeit, M. and Ganopolski, A. (2015) Coupled Northern Hemisphere permafrost-ice-sheet evolution over the last glacial cycle. Climate of the Past 11(9), 1165-1180.

Wise, M., Calvin, K., Thomson, A., Clarke, L., Bond-Lamberty, B., Sands, R., Smith, S., Janetos, A. and Edmonds, J. (2009) Implications of Limiting CO2 Concentrations for Land Use and Energy. Science (New York, N.Y.) 324, 1183-1186.

Ye, B., Yang, D. and Kane, D.L. (2003) Changes in Lena River streamflow hydrology: Human impacts versus natural variations. Water Resources Research 39(7), n/a-n/a.

Yi, S., McGuire, A., Harden, J., Kasischke, E., Manies, K., Hinzman, L., Liljedahl, A., Randerson, J., Liu, H., Romanovsky, V., Marchenko, S. and Kim, Y. (2009) Interactions between soil thermal and hydrological dynamics in the response of Alaska ecosystems to fire disturbance. Journal of Geophysical Research.

Zhang, S., Du, H. and Harbor, J. (2017a) The Effect of Confining Pressure and Water Content on Compressive Strength and Deformation of Ice-Rich Silty Sand. Permafrost and Periglacial Processes 28(1), 298-305.

Zhang, T., Barry, R.G., Knowles, K., Heginbottom, J.A. and Brown, J. (1999) Statistics and characteristics of permafrost and ground-ice distribution in the Northern Hemisphere1. Polar Geography 23(2), 132-154.

Zhang, Y., Chen, W. and Riseborough, D. (2006) Temporal and spatial changes of permafrost in Canada since the end of the Little Ice Age. Journal of Geophysical Research 111.

Zhang, Y., Cheng, G., Li, X., Jin, H., Yang, D., Flerchinger, G., Chang, X., Bense, V., Han, X. and Liang, J. (2017b) Influences of Frozen Ground and Climate Change on Hydrological Processes in an Alpine Watershed: A Case Study in the Upstream Area of the Hei'he River, Northwest China. Permafrost and Periglacial Processes 28(2), 420-432.

Zhang, Z., Kane, D.L. and Hinzman, L. (2000) Development and application of a spatially-distributed Arctic hydrological and thermal process model (ARHYTHM). Hydrological Processes 14(6), 1017-+.

Zhao, S.-P., Nan, Z.-T., Huang, Y.-B. and Zhao, L. (2017) The Application and Evaluation of Simple Permafrost Distribution Models on the Qinghai-Tibet Plateau. Permafrost and Periglacial Processes 28(2), 391-404.

Zohuri, B. (2017).

6 Appendices

Appendix A: Borehole data

Table A - 1: Stratigraphic data of study area from boreholes

Boreholes	Layer Thickness (m)	Type of Material
B01, B08, B09	1.2	Sand
	5.5	Clay
	3	Sand
	11	Silt
	2	Sand
	5	Gravel
	72	Limestone
B02, B03, B04, B06	1	Peat
	5	Clay
	3	Gravel
	21	Clay
	1	Sand
	1	Boulder
	68	Limestone
B05	1.5	Peat
	1	Sand
	31	Clay
	1	Boulder/Sand
	4	Clay/Boulder
	63	Limestone

Appendix B: Two years (2014-2015) averaged, maximum, and minimum temperature vs depth envelopes

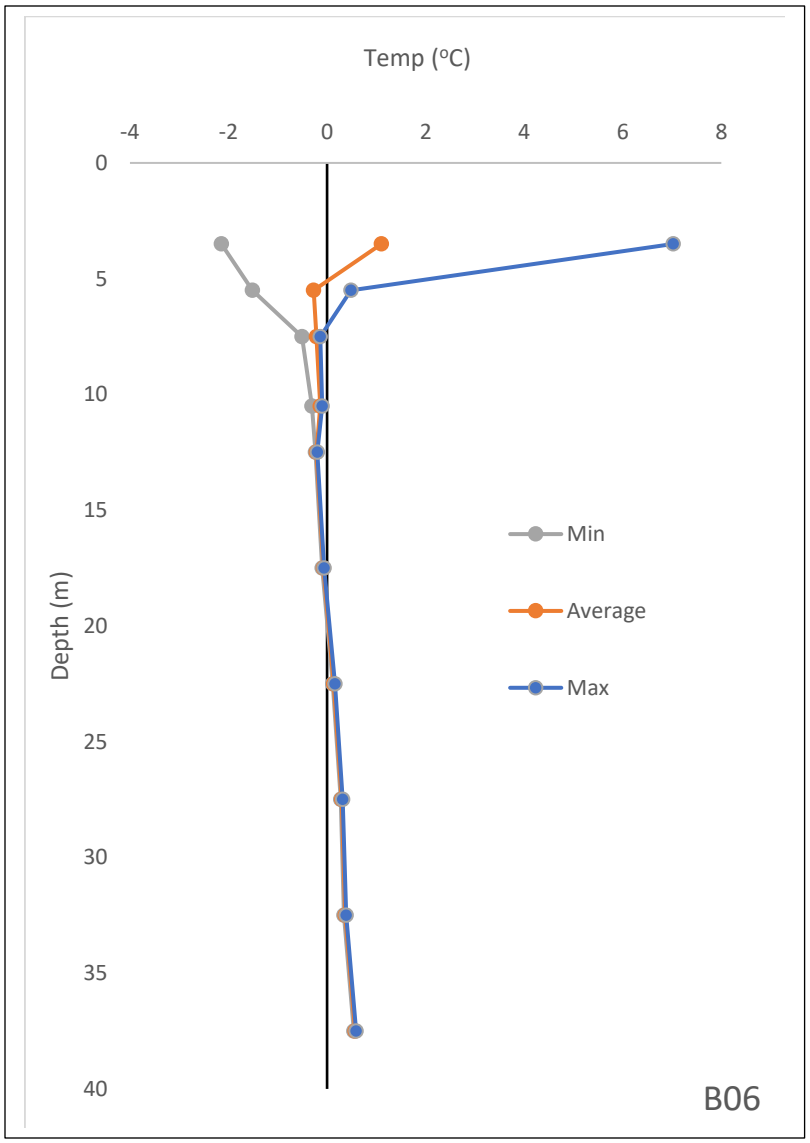

Figure B - 1: Temperature vs. depth envelope for borehole B06

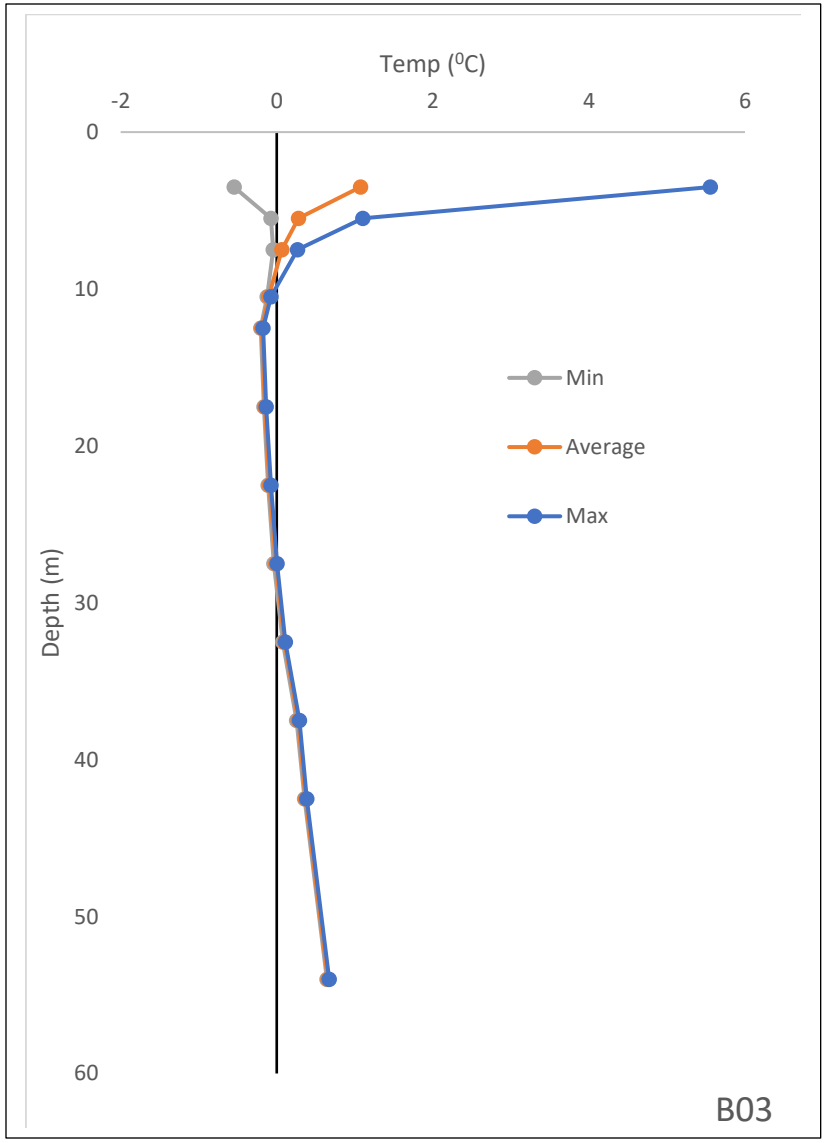

Figure B - 2: Temperature vs. depth envelope for borehole B03

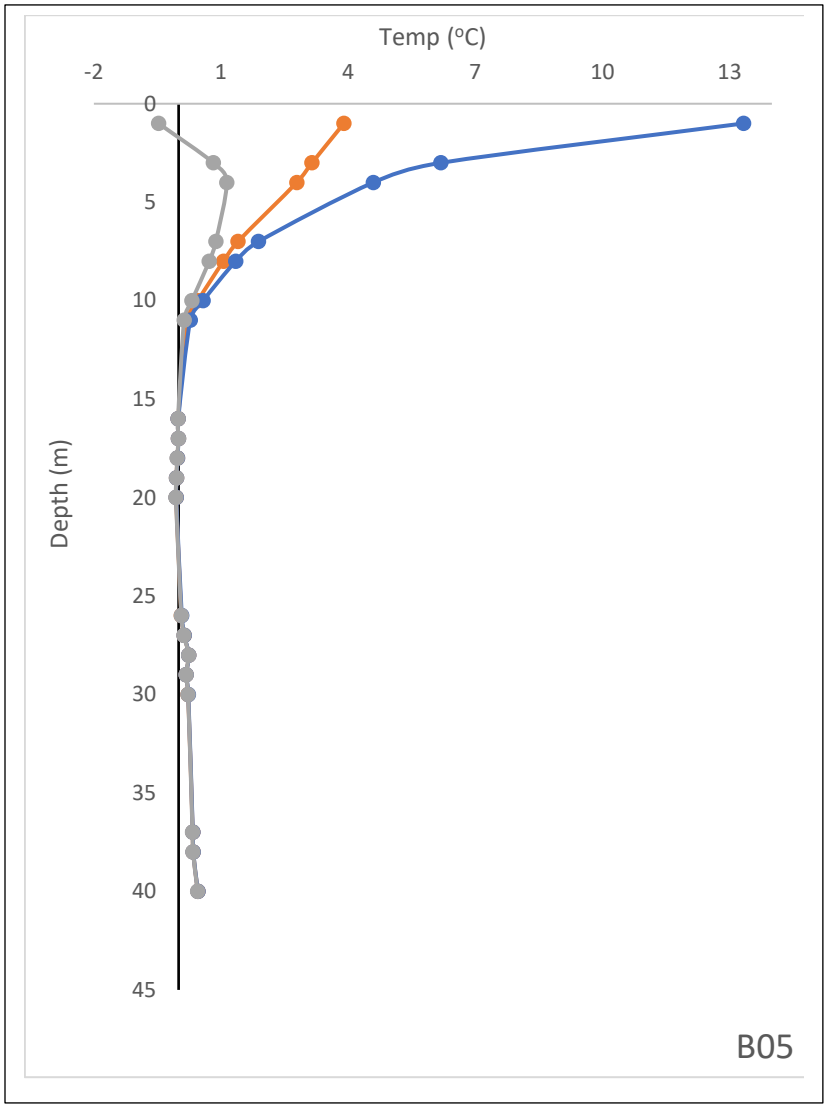

Figure B - 3: Temperature vs. depth envelope for borehole B05

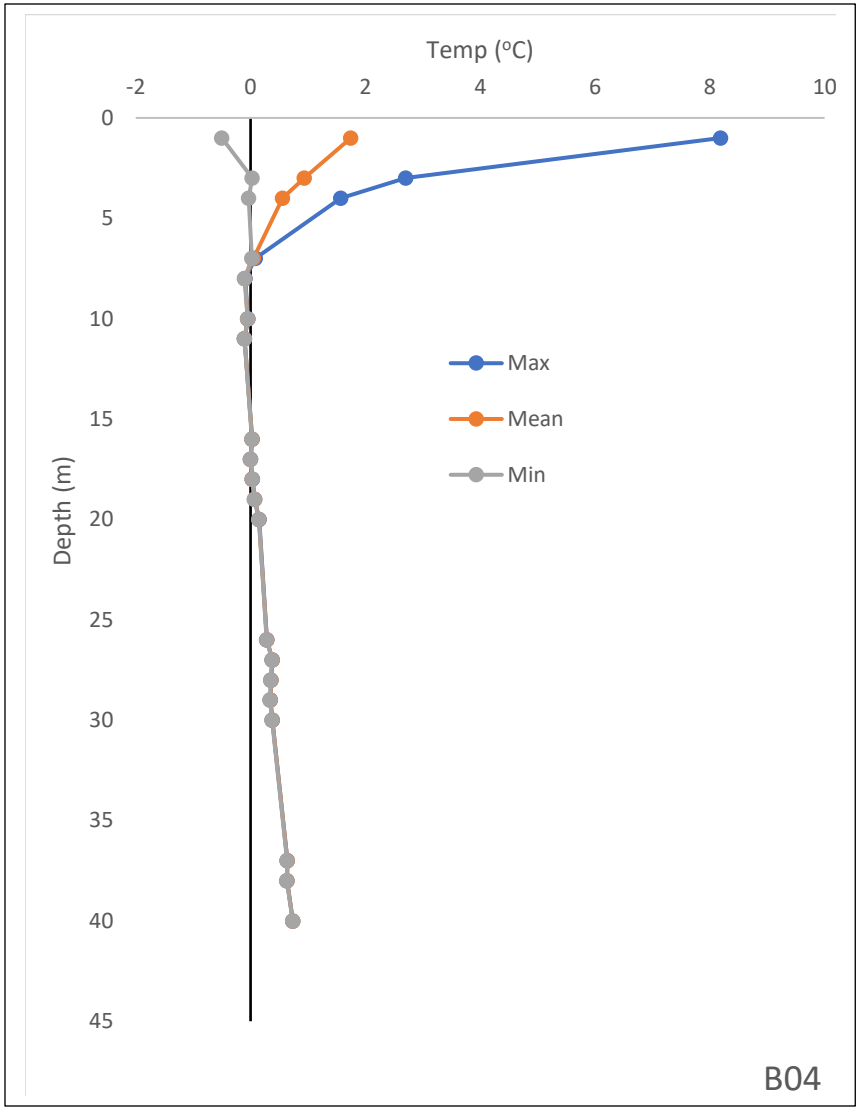

Figure B - 4: Temperature vs. depth envelope for borehole B04

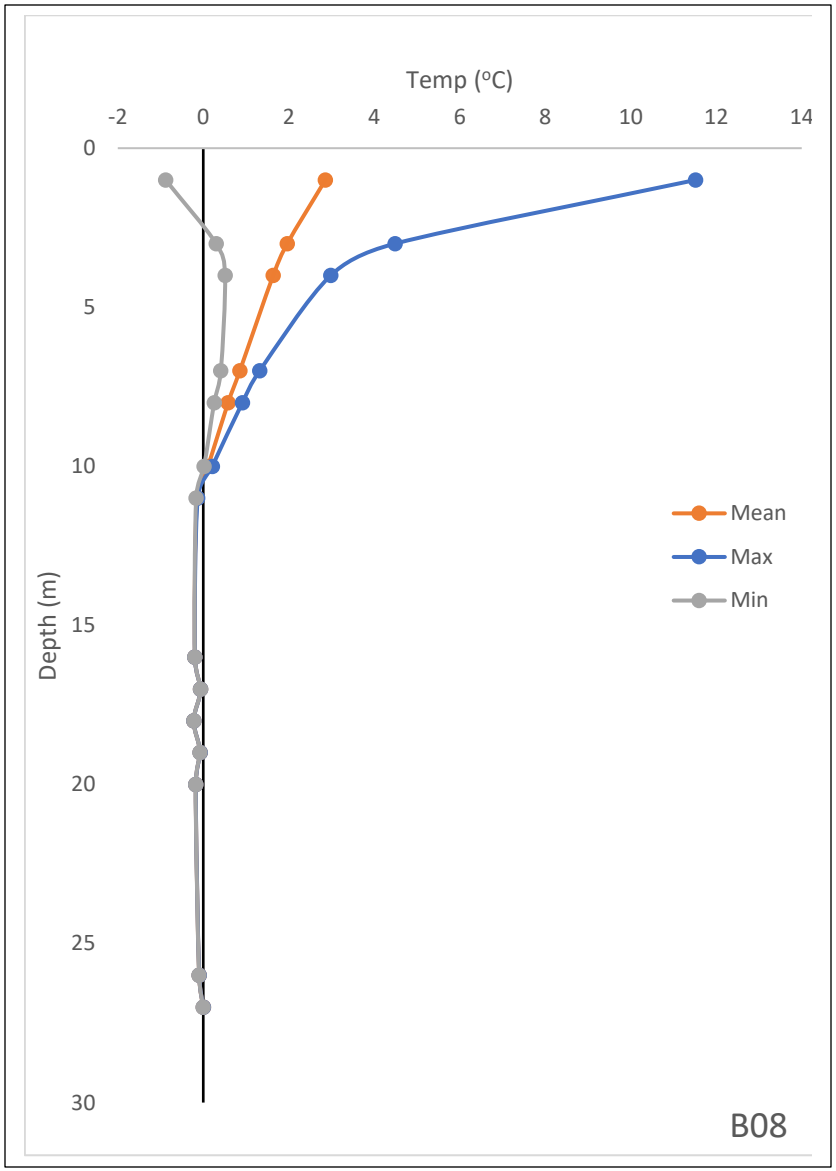

Figure B - 5: Temperature vs. depth envelope for borehole B08

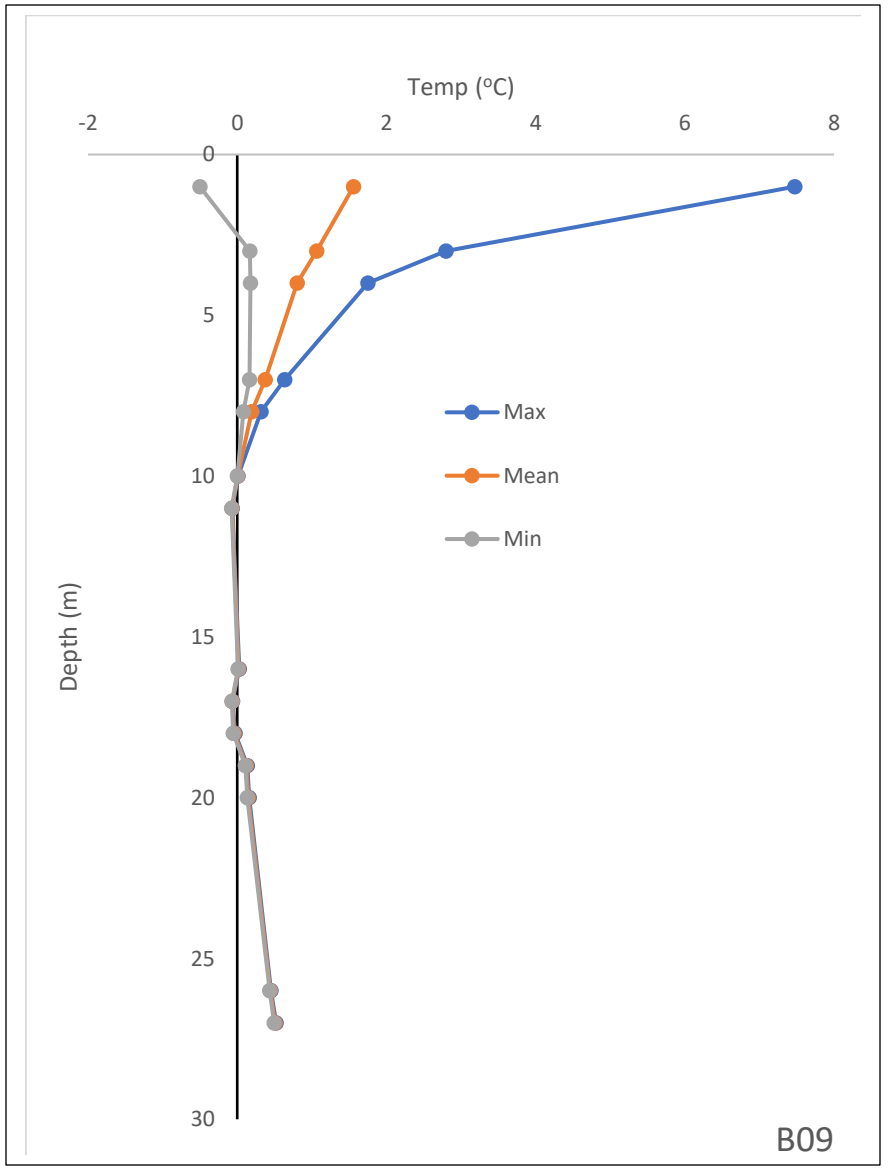

Figure B - 6: Temperature vs. depth envelope for borehole B09

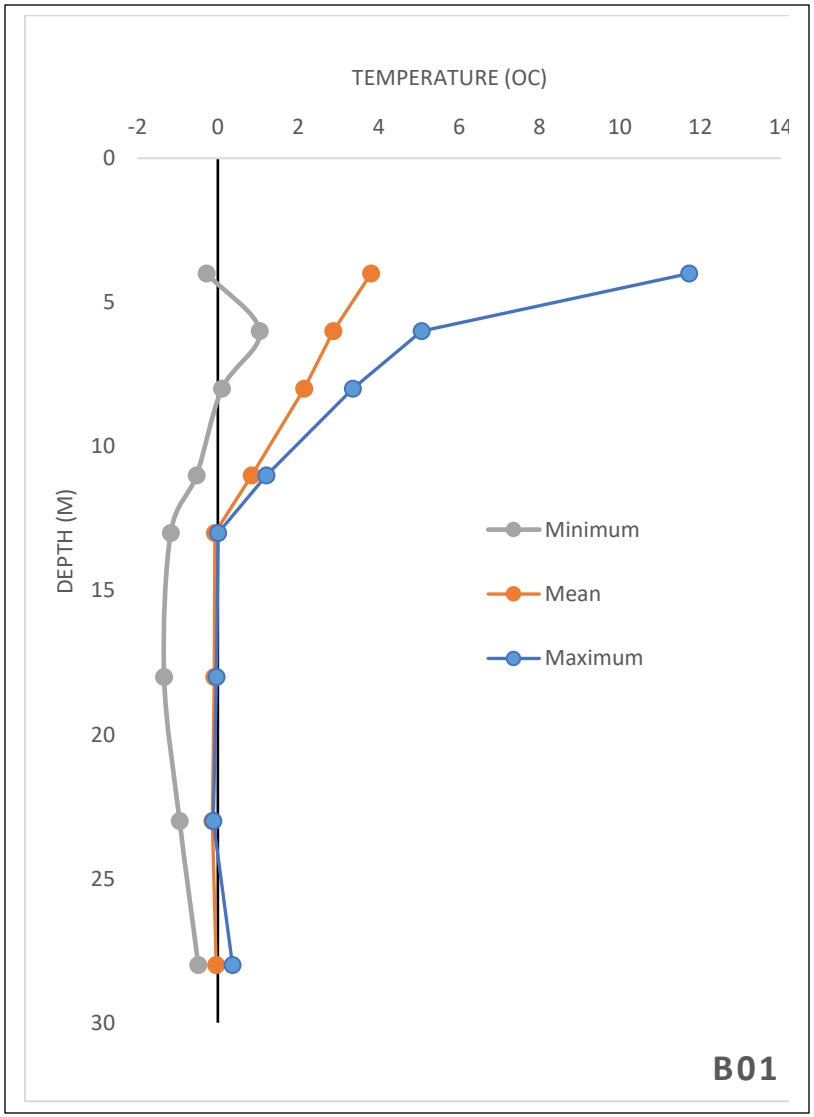

Figure B - 7: Temperature vs. depth envelope for borehole B01

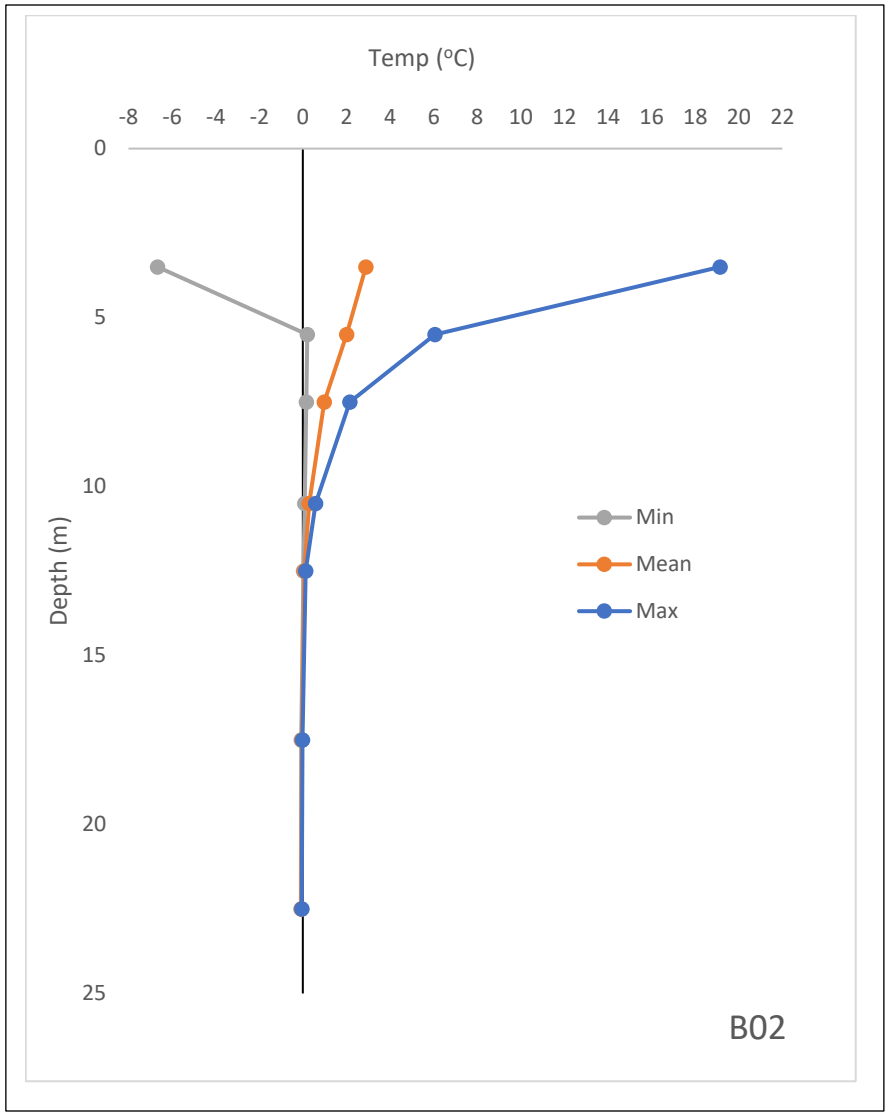

Figure B - 8: Temperature vs. depth envelope for borehole B02

Appendix C: Hansson's module calibration

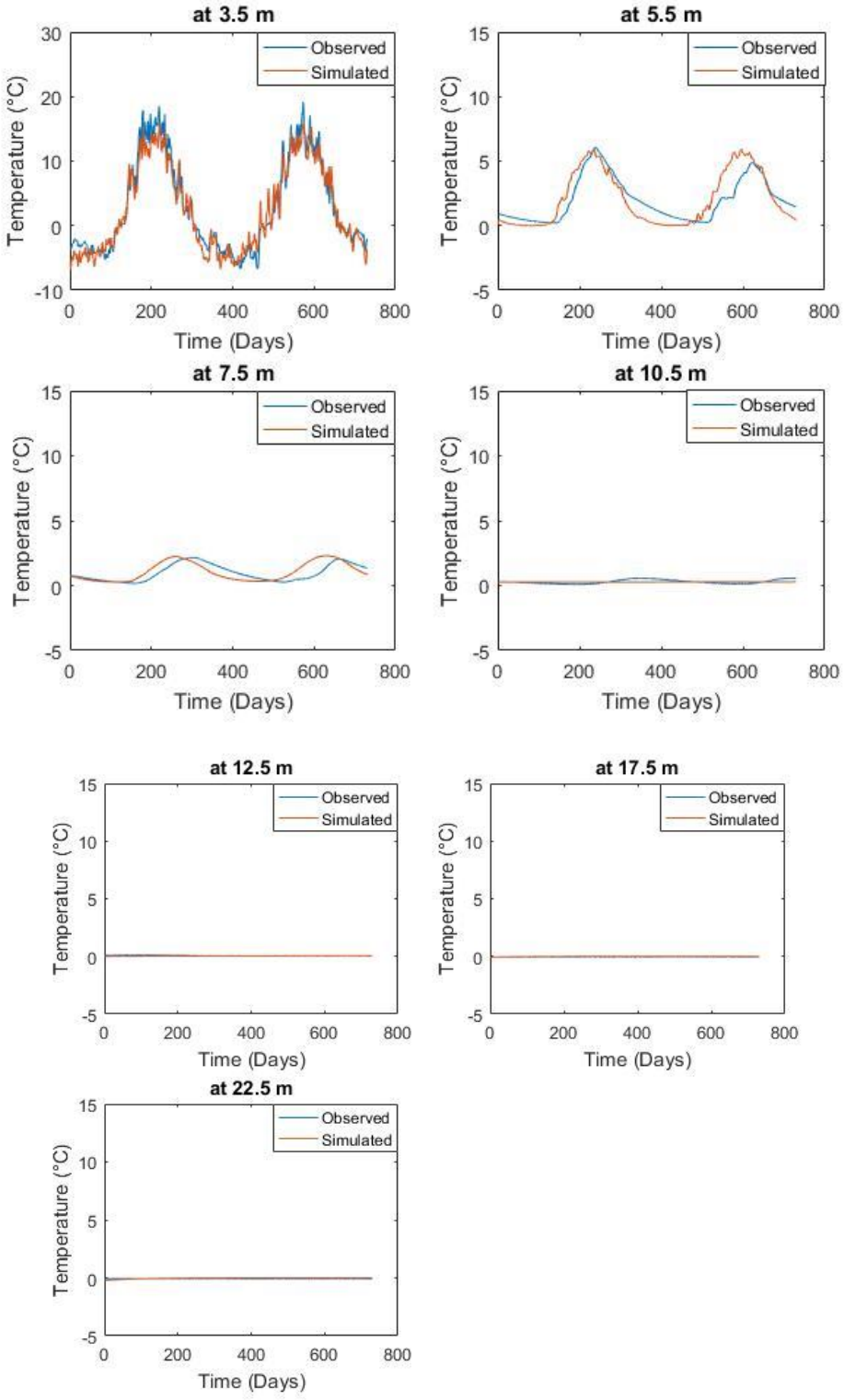

Figure C - 1: Two years of simulated and observed soil temperature data at different depths for B02

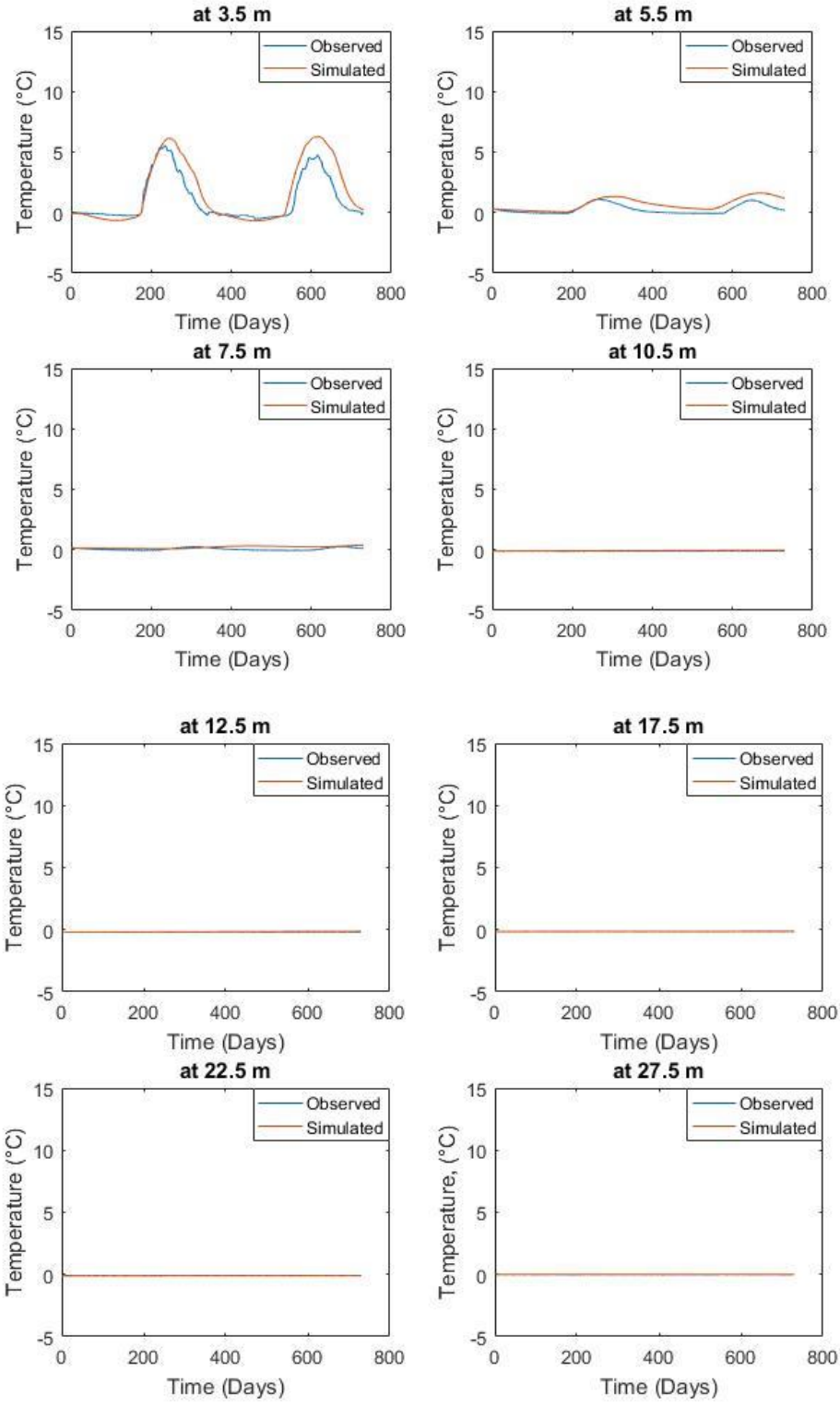
at 3.5 m
at 5.5 m
at 7.5 m
at 10.5 m
at 12.5 m
at 17.5 m
at 22.5 m
at 27.5 m
Observed
Simulated
Temperature (°C)
Temperature, (°C)
Time (Days)
15
10
5
0
-5
0
200
400
600
800

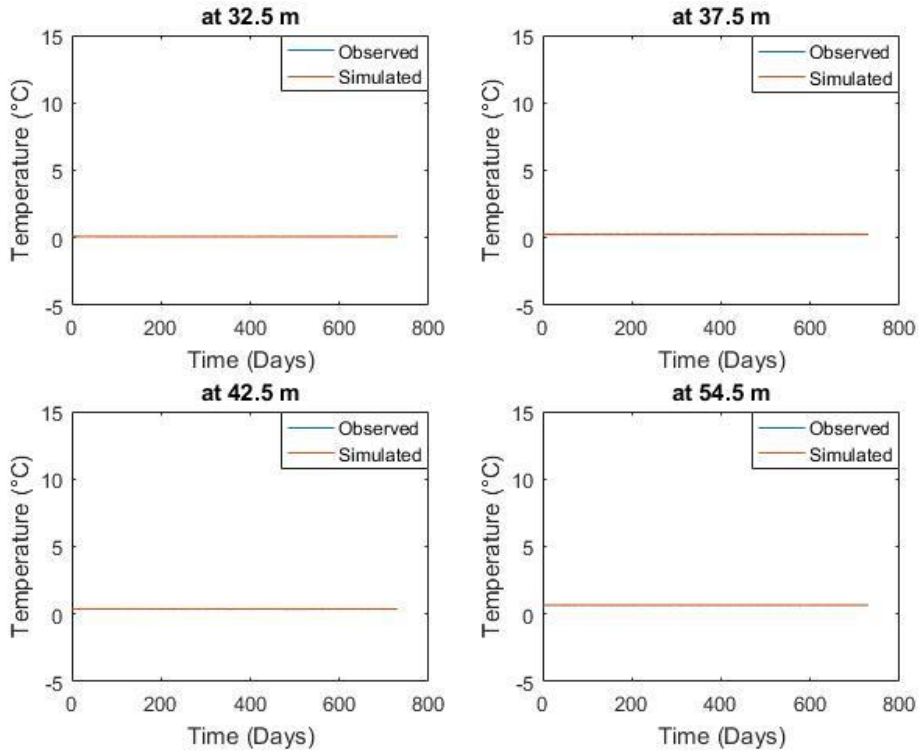

Figure C - 2: Two years of simulated and observed soil temperature data at different depths for B03

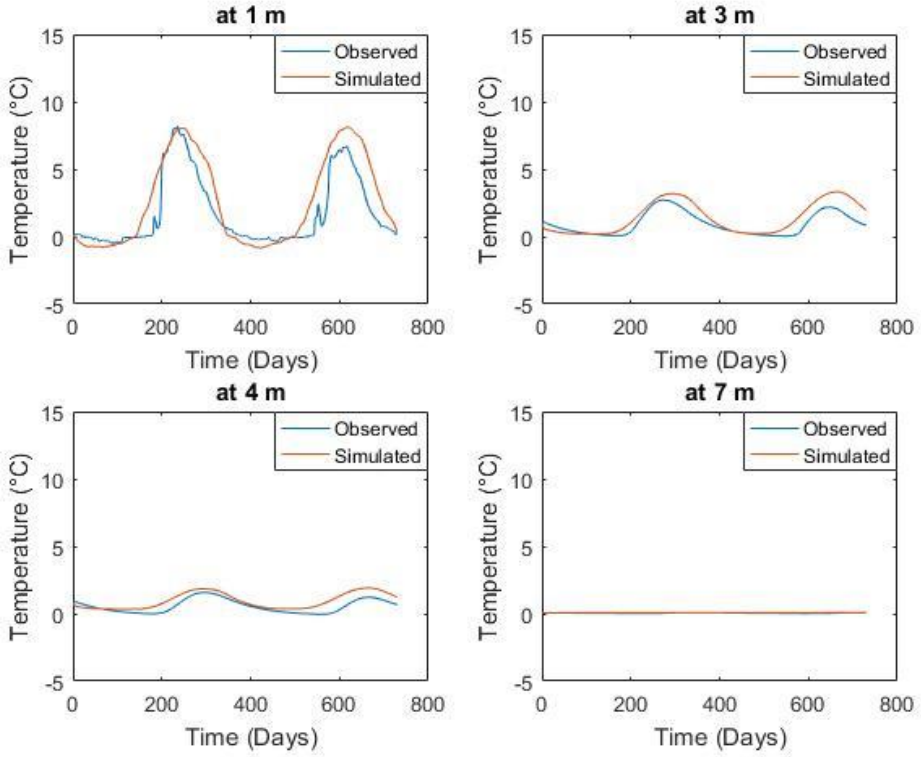
at 1 m
at 3 m
at 4 m
at 7 m
Observed
Simulated
Temperature (°C)
Time (Days)
15
10
5
0
-5
0
200
400
600
800

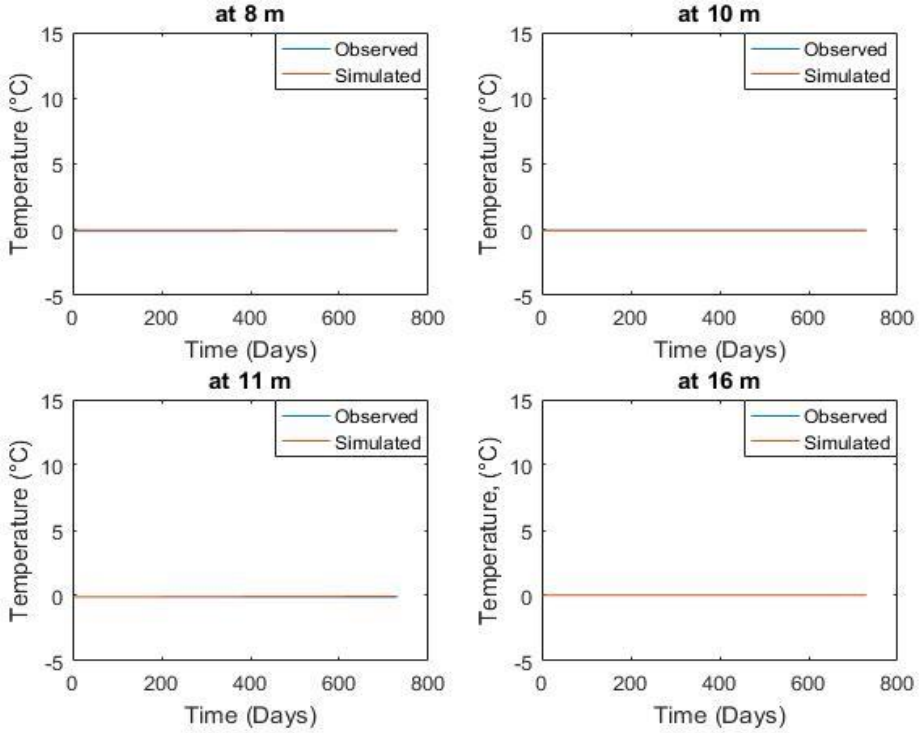
at 8 m
at 10 m
at 11 m
at 16 m
Observed
Simulated
Temperature (°C)
Temperature, (°C)
Time (Days)
15
10
5
0
-5
0
200
400
600
800

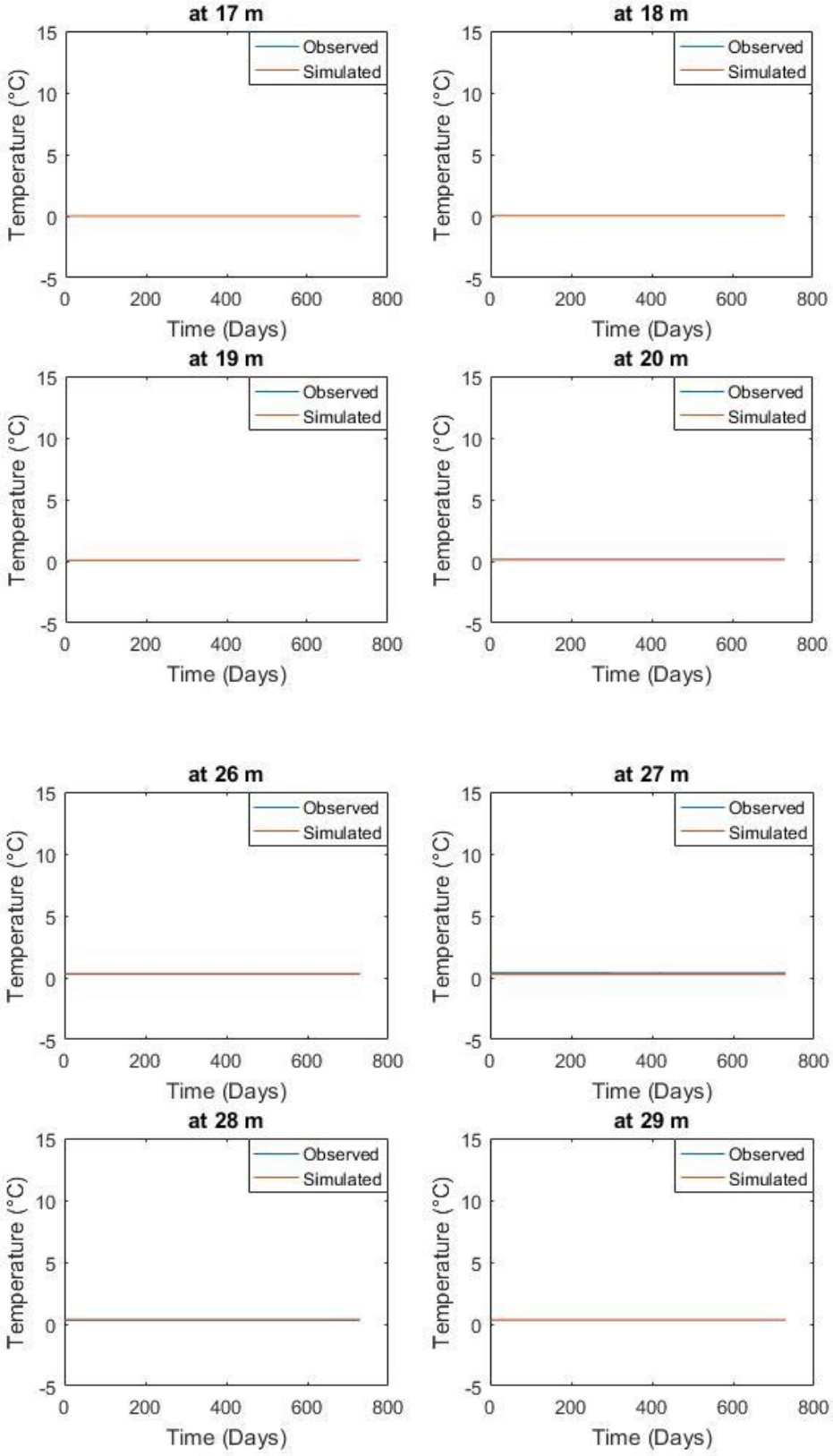
at 17 m
at 18 m
at 19 m
at 20 m
at 26 m
at 27 m
at 28 m
at 29 m
Observed
Simulated
Temperature (°C)
Time (Days)
15
10
5
0
-5
0
200
400
600
800

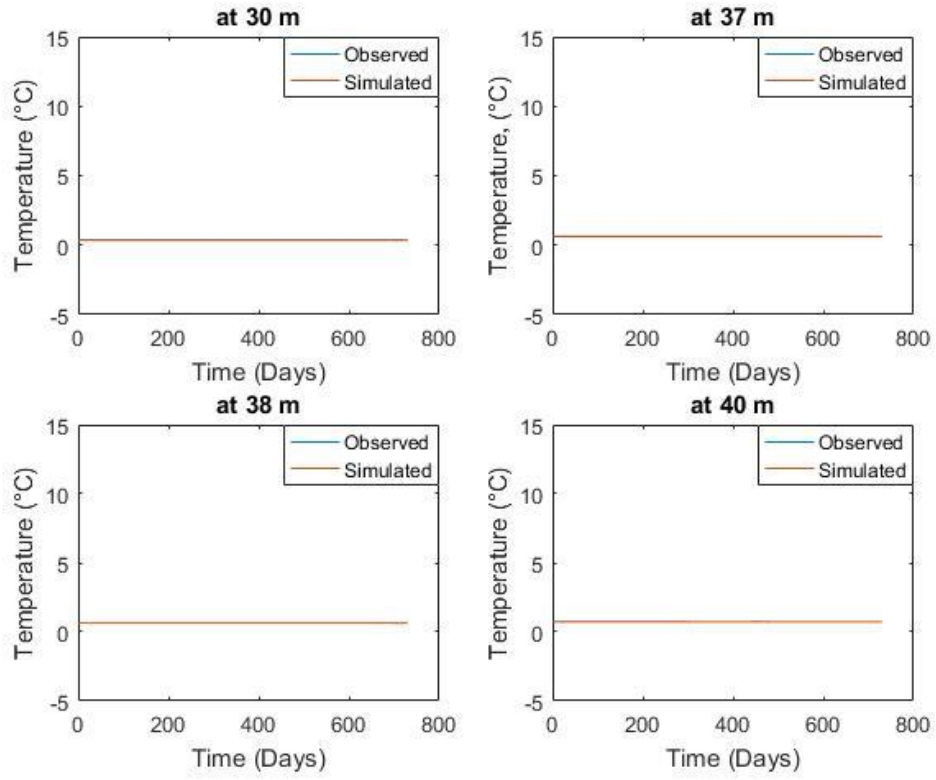

Figure C - 3: Two years of simulated and observed soil temperature data at different depths for B04

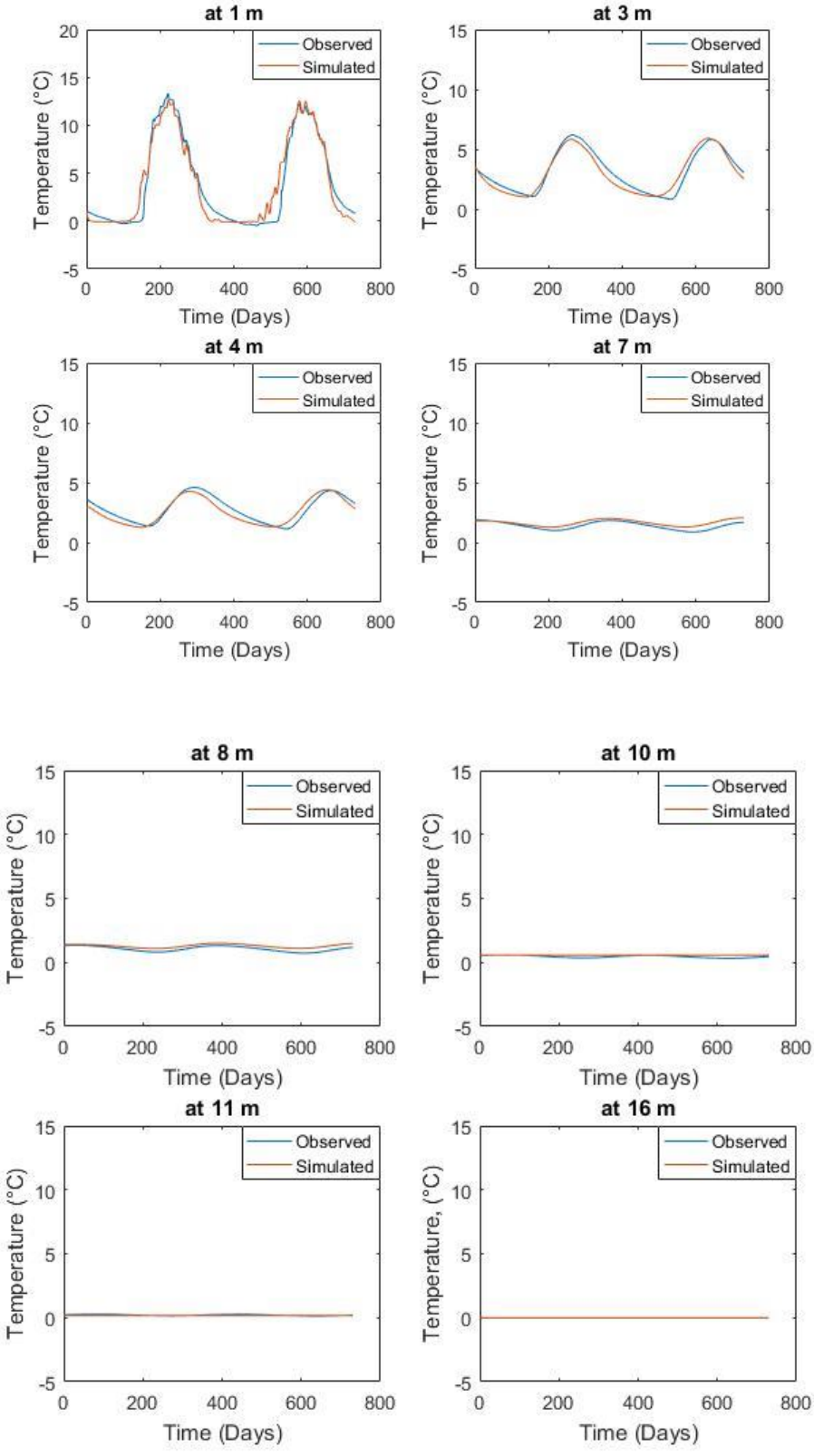
at 1 m
at 3 m
at 4 m
at 7 m
at 8 m
at 10 m
at 11 m
at 16 m
Observed
Simulated
Temperature (°C)
Temperature, (°C)
Time (Days)

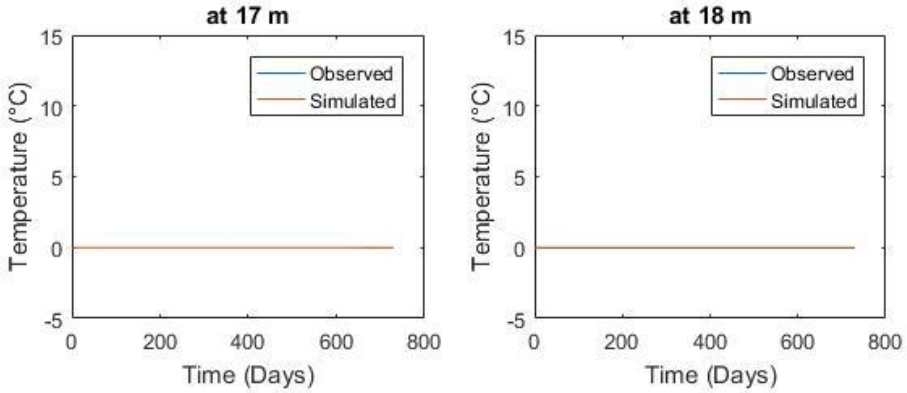
at 17 m
Observed
Simulated
Temperature (°C)
Time (Days)

at 18 m
Observed
Simulated
Temperature (°C)
Time (Days)

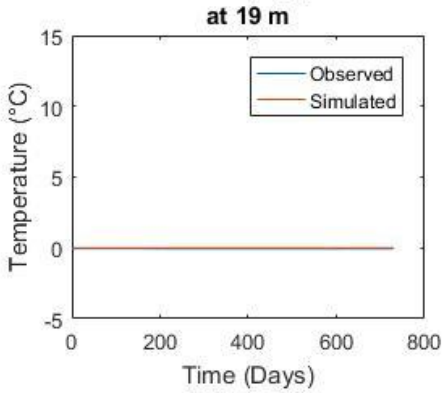
at 19 m
Observed
Simulated
Temperature (°C)
Time (Days)

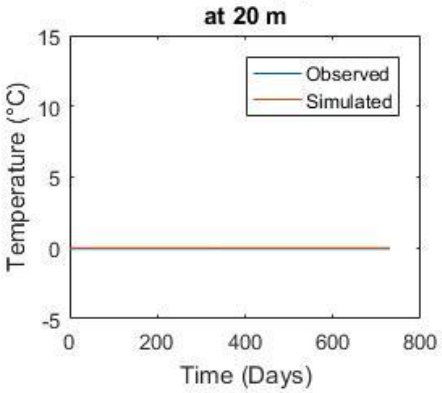
at 20 m
Observed
Simulated
Temperature (°C)
Time (Days)

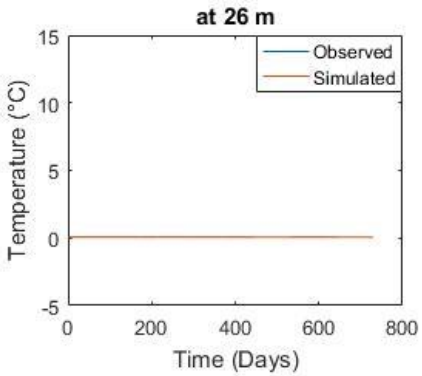
at 26 m
Observed
Simulated
Temperature (°C)
Time (Days)

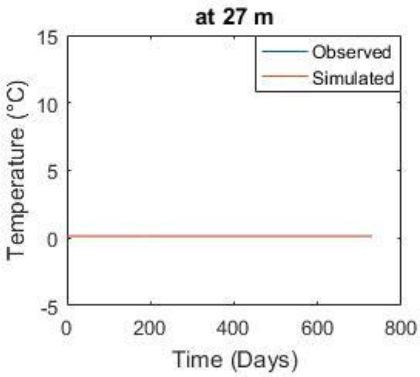
at 27 m
Observed
Simulated
Temperature (°C)
Time (Days)

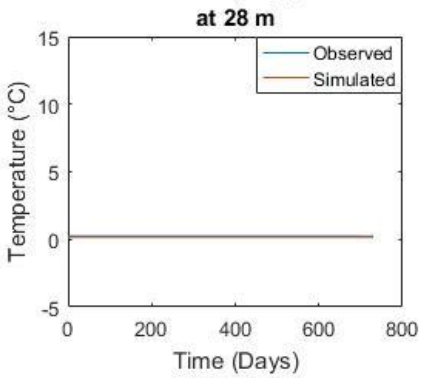
at 28 m
Observed
Simulated
Temperature (°C)
Time (Days)

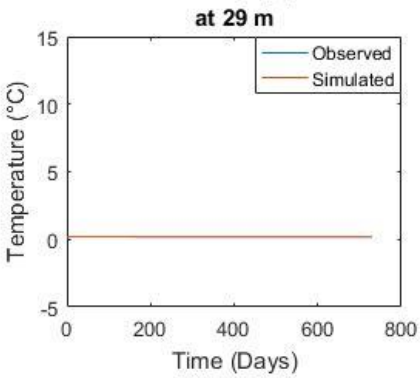
at 29 m
Observed
Simulated
Temperature (°C)
Time (Days)

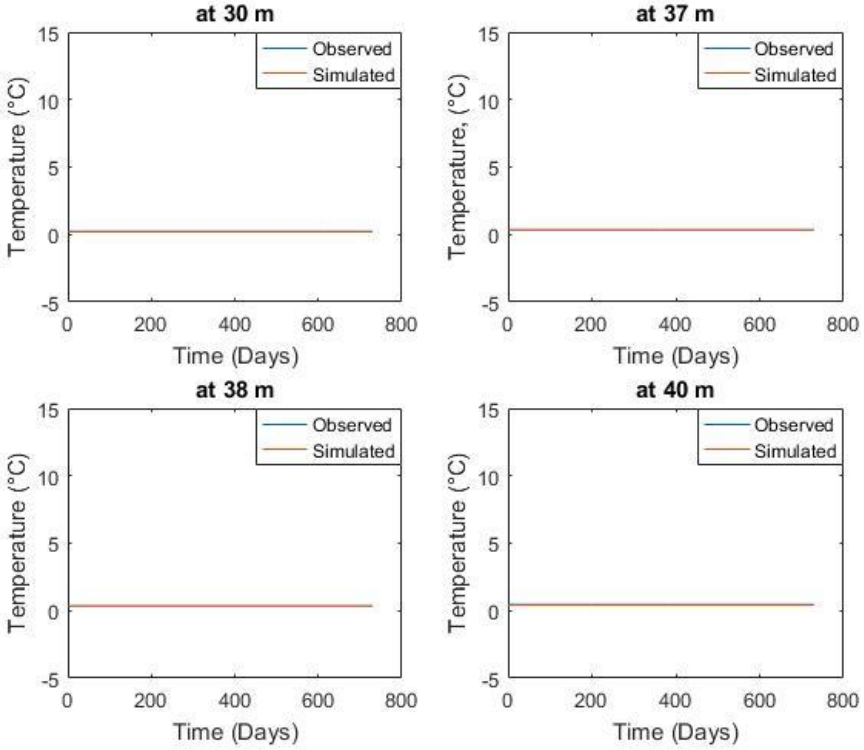

Figure C - 4: Two years of simulated and observed soil temperature data at different depth for B05

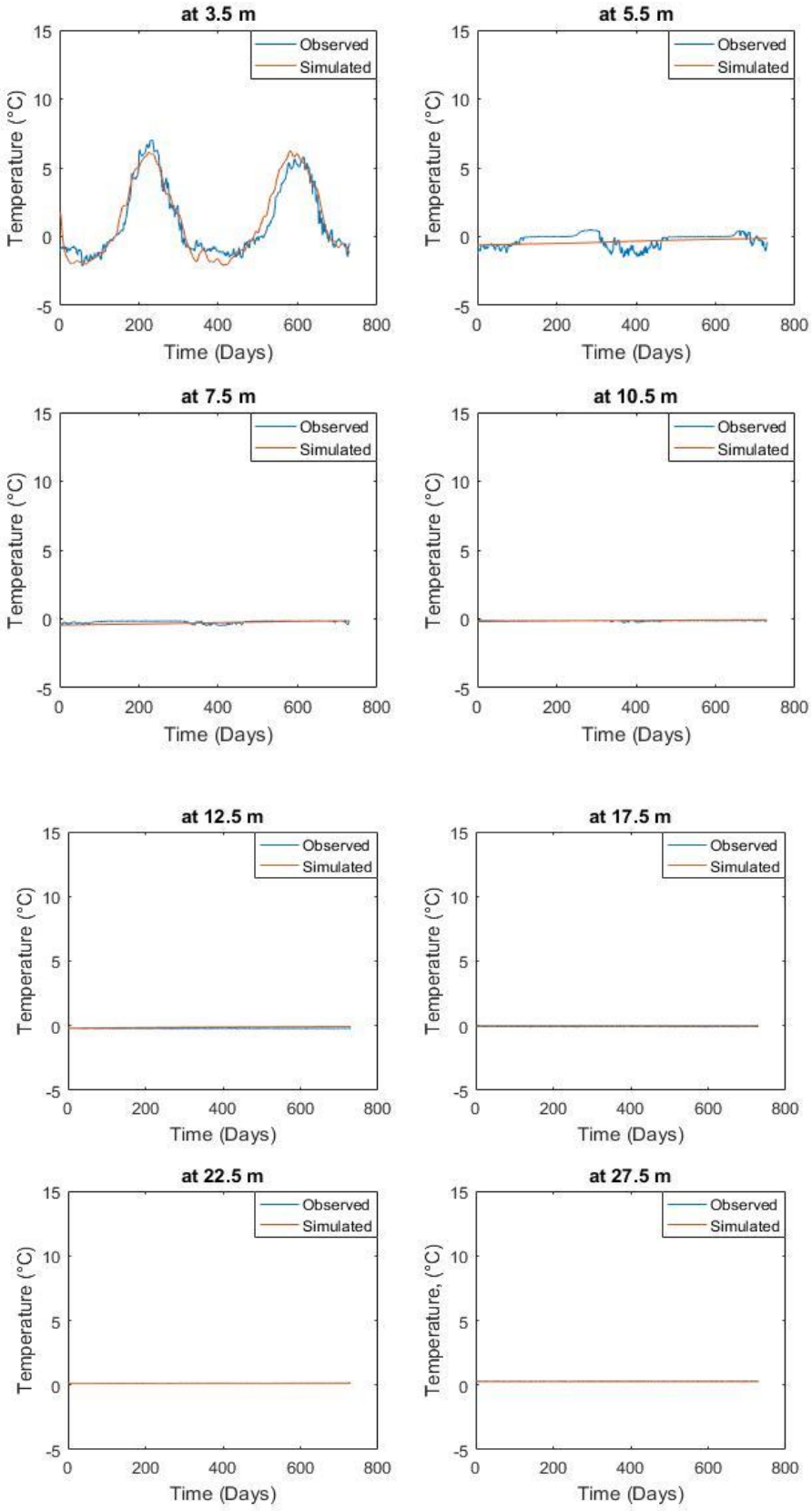
at 3.5 m
at 5.5 m
at 7.5 m
at 10.5 m
at 12.5 m
at 17.5 m
at 22.5 m
at 27.5 m
Observed
Simulated
Temperature (°C)
Temperature, (°C)
Time (Days)
15
10
5
0
-5
0
200
400
600
800

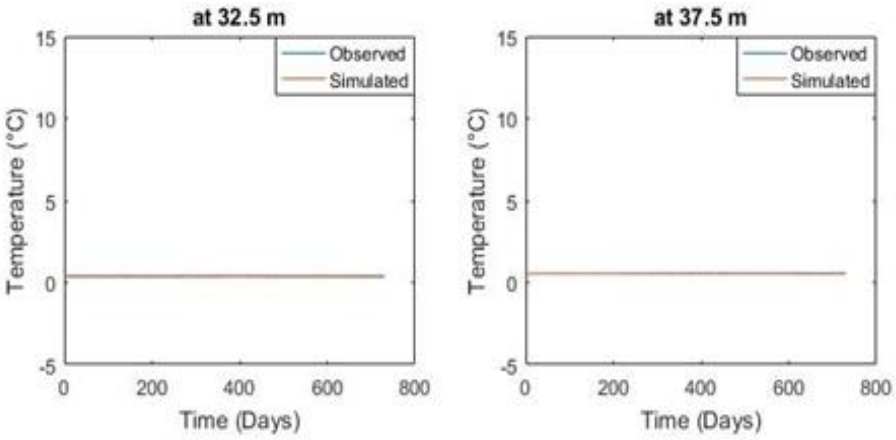

Figure C - 5: Two years of simulated and observed soil temperature data at different depths for B06

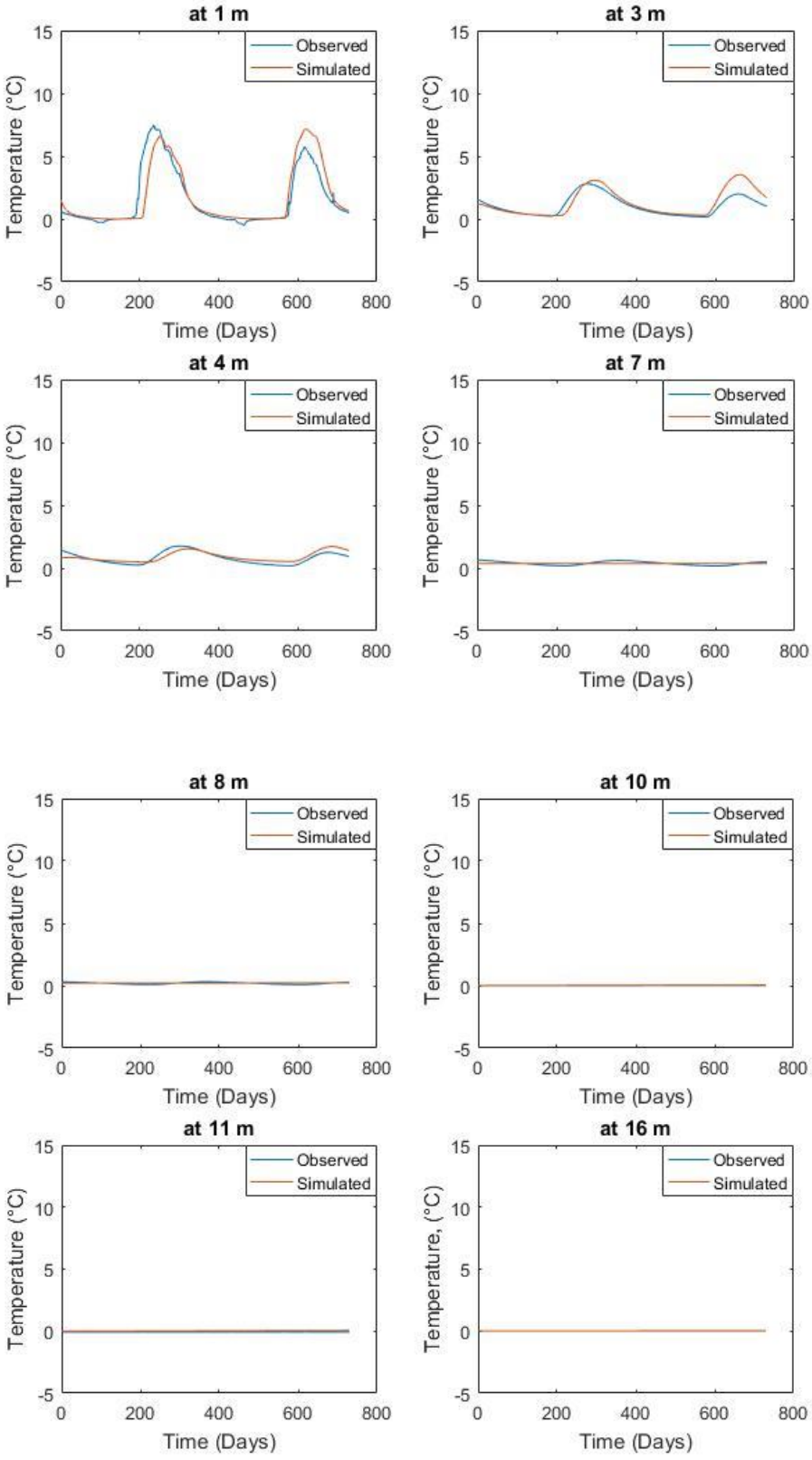
at 1 m
at 3 m
at 4 m
at 7 m
at 8 m
at 10 m
at 11 m
at 16 m
Observed
Simulated
Temperature (°C)
Temperature, (°C)
Time (Days)
15
10
5
0
-5
0
200
400
600
800

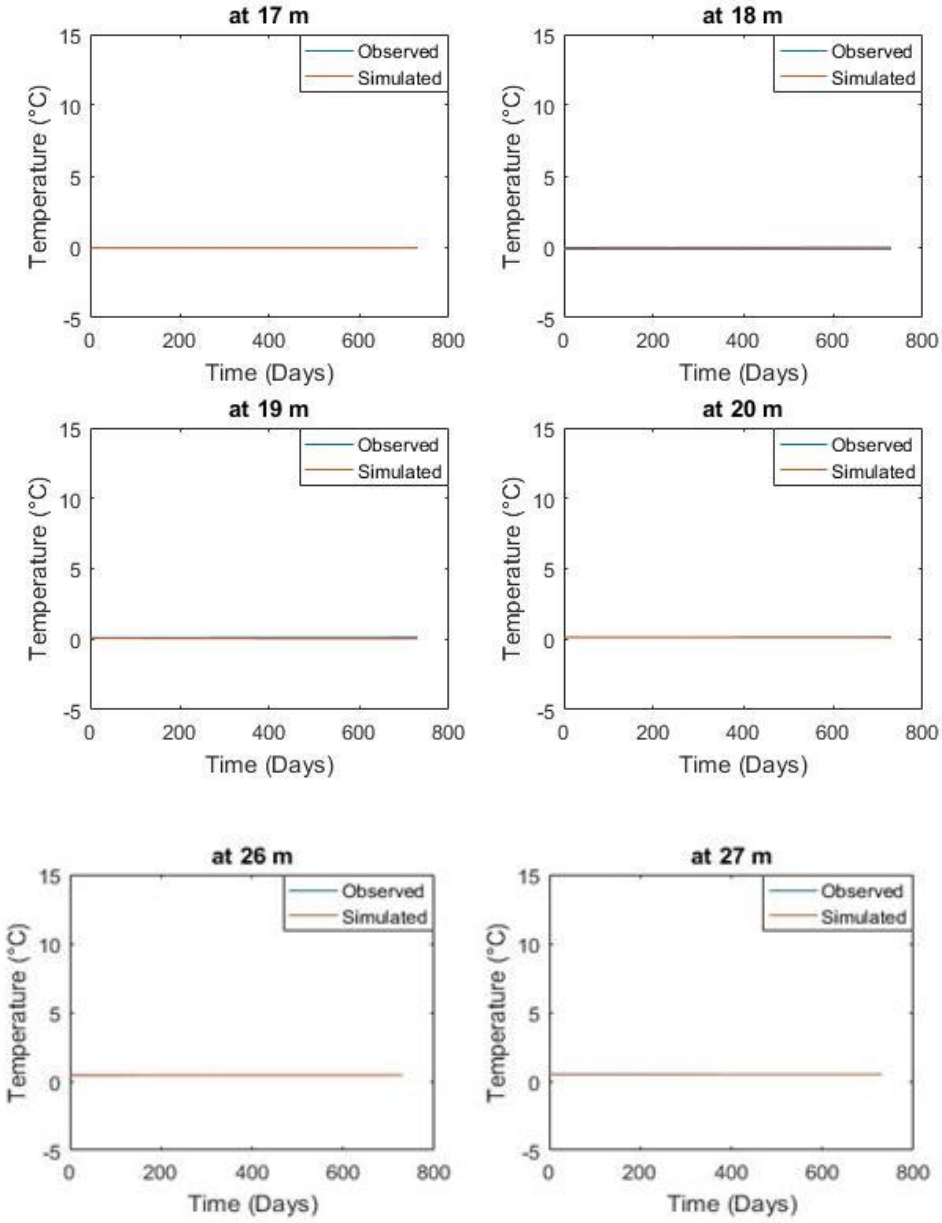

Figure C - 6:Two years of Simulated and Observed Soil Temperature at different depth for B08

Appendix D: Error Metrics

Table D - 1: Errors between calibrated and observed soil temperature values for borehole B02 at different depths

		Hydrus-1D		Hansson Calibration	
Borehole	Depth (m)	RMSE (°C)	MAE (°C)	RMSE (°C)	MAE (°C)
B02	3.5	10.58	7.67	1.75	1.40
	5.5	6.33	5.92	0.70	0.58
	7.5	4.80	4.72	0.54	0.43
	10.5	3.68	3.67	0.15	0.13
	12.5	3.24	3.24	0.05	0.03
	17.5	2.73	2.73	0.08	0.05
	22.5	2.38	2.38	0.11	0.08

Table D - 2: Errors between calibrated and observed soil temperature values for borehole B03 at different depths

		Hydrus-1D		Hansson Calibration	
Borehole	Depth (m)	RMSE (°C)	MAE (°C)	RMSE (°C)	MAE (°C)
B03	3.5	4.34	3.23	1.16	0.81
	5.5	4.01	3.39	0.50	0.41
	7.5	3.81	3.27	0.19	0.16
	10.5	3.37	2.84	0.04	0.03

	12.5	3.03	2.51	0.03	0.03
	17.5	2.49	1.94	0.01	0.01
	22.5	2.09	1.56	0.01	0.01
	27.5	1.54	1.09	0.01	0.01
	32.5	1.25	0.86	0.01	0.01
	37.5	1.28	0.93	0.03	0.03
	42.5	1.28	0.98	0.01	0.01
	54	0.95	0.75	0.01	0.01

Table D - 3: Errors between calibrated and observed soil temperature values for borehole B04 at different depths

		Hydrus-1D		Hansson Calibration	
Borehole	Depth (m)	RMSE (℃)	MAE (℃)	RMSE (℃)	MAE (℃)
B04	1	6.54	5.10	1.64	1.21
	3	3.74	3.01	0.69	0.54
	4	3.61	2.99	0.50	0.42
	7	3.13	2.66	0.03	0.03
	8	3.03	2.57	0.06	0.06
	10	2.80	2.32	0.03	0.03
	11	2.67	2.18	0.03	0.02
	16	2.30	1.78	0.00	0.00
	17	2.23	1.72	0.00	0.00
	18	2.19	1.67	0.00	0.00
	19	2.14	1.62	0.02	0.02
	20	2.10	1.58	0.02	0.02
	26	1.48	1.07	0.04	0.04
	27	1.44	1.04	0.11	0.11
	28	1.30	0.92	0.05	0.05
	29	1.21	0.84	0.01	0.01
	30	1.20	0.82	0.01	0.01
	37	1.29	0.96	0.05	0.05
	38	1.27	0.95	0.01	0.01
	40	1.33	1.01	0.05	0.05

Table D - 4: Errors between calibrated and observed soil temperature values for borehole B06 at different depths

		Hydrus-1D		Hansson Calibration	
Borehole	Depth (m)	RMSE (°C)	MAE (°C)	RMSE (°C)	MAE (°C)
B06	3.5	7.633	5.873	2.95	2.00
	5.5	5.859	4.969	0.46	0.39
	7.5	6.416	5.384	0.10	0.07
	10.5	6.679	5.478	0.05	0.04
	12.5	5.368	4.336	0.10	0.10
	17.5	3.358	2.612	0.21	0.21
	22.5	2.294	1.885	0.14	0.14
	27.5	1.580	1.353	0.12	0.12
	32.5	1.282	1.084	0.18	0.18
	37.5	0.966	0.797	0.57	0.57

Table D - 5: Errors between calibrated and observed soil temperature values for borehole B05 at different depths

		Hydrus-1D		Hansson Calibration	
Borehole	Depth (m)	RMSE (℃)	MAE (℃)	RMSE (℃)	MAE (℃)
B05	1	9.64	6.87	1.16	0.80
	3	4.89	4.37	0.87	0.75
	4	3.77	3.48	0.71	0.62
	7	1.43	1.24	0.29	0.25
	8	0.96	0.80	0.25	0.23
	10	0.30	0.24	0.15	0.12
	11	0.17	0.14	0.06	0.05
	16	0.11	0.10	0.01	0.01
	17	0.09	0.08	0.01	0.01
	18	0.10	0.08	0.03	0.03
	19	0.11	0.10	0.05	0.05
	20	0.12	0.11	0.06	0.06
	26	0.04	0.03	0.01	0.01
	27	0.02	0.02	0.02	0.02
	28	0.07	0.06	0.07	0.07
	29	0.02	0.02	0.01	0.01
	30	0.00	0.00	0.02	0.02
	37	0.06	0.06	0.02	0.02
	38	0.07	0.07	0.03	0.03
	40	0.03	0.03	0.04	0.04

Table D - 6: Errors between calibrated and observed soil temperature values for borehole B08 at different depths

		Hydrus-1D		Hansson Calibration	
Borehole	Depth (m)	RMSE (°C)	MAE (°C)	RMSE (°C)	MAE (°C)
B08	1	8.14	6.25	1.66	1.19
	3	2.36	2.07	0.74	0.57
	4	1.50	1.38	0.50	0.41
	7	0.51	0.46	0.28	0.25
	8	0.34	0.28	0.14	0.12
	10	0.20	0.15	0.01	0.01
	11	0.15	0.12	0.07	0.07
	16	0.03	0.03	0.04	0.03
	17	0.12	0.12	0.06	0.06
	18	0.12	0.11	0.08	0.08
	19	0.03	0.02	0.07	0.07
	20	0.03	0.03	0.07	0.07
	26	0.17	0.17	0.09	0.09
	27	0.17	0.17	0.13	0.13

Appendix E: Two Years averaged observed, simulated temperature vs. depth envelopes

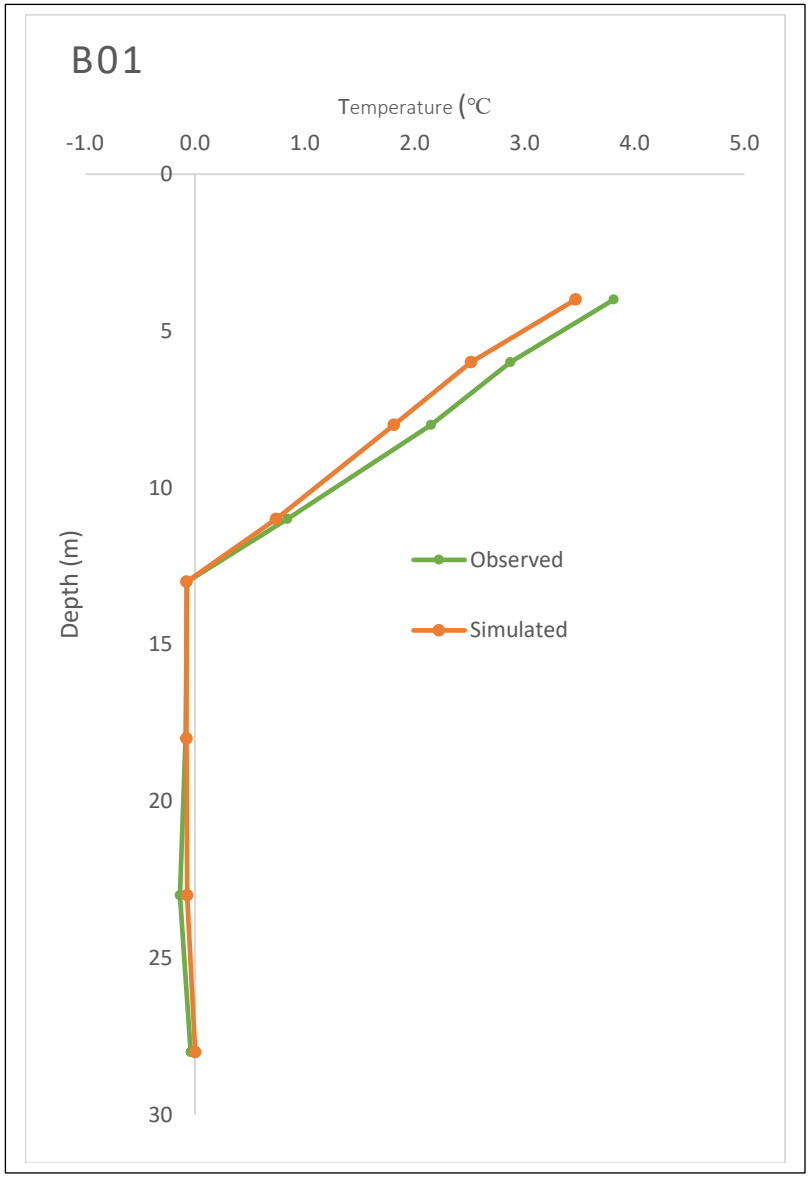

Figure E - 1: Two years average temperature envelopes for B01

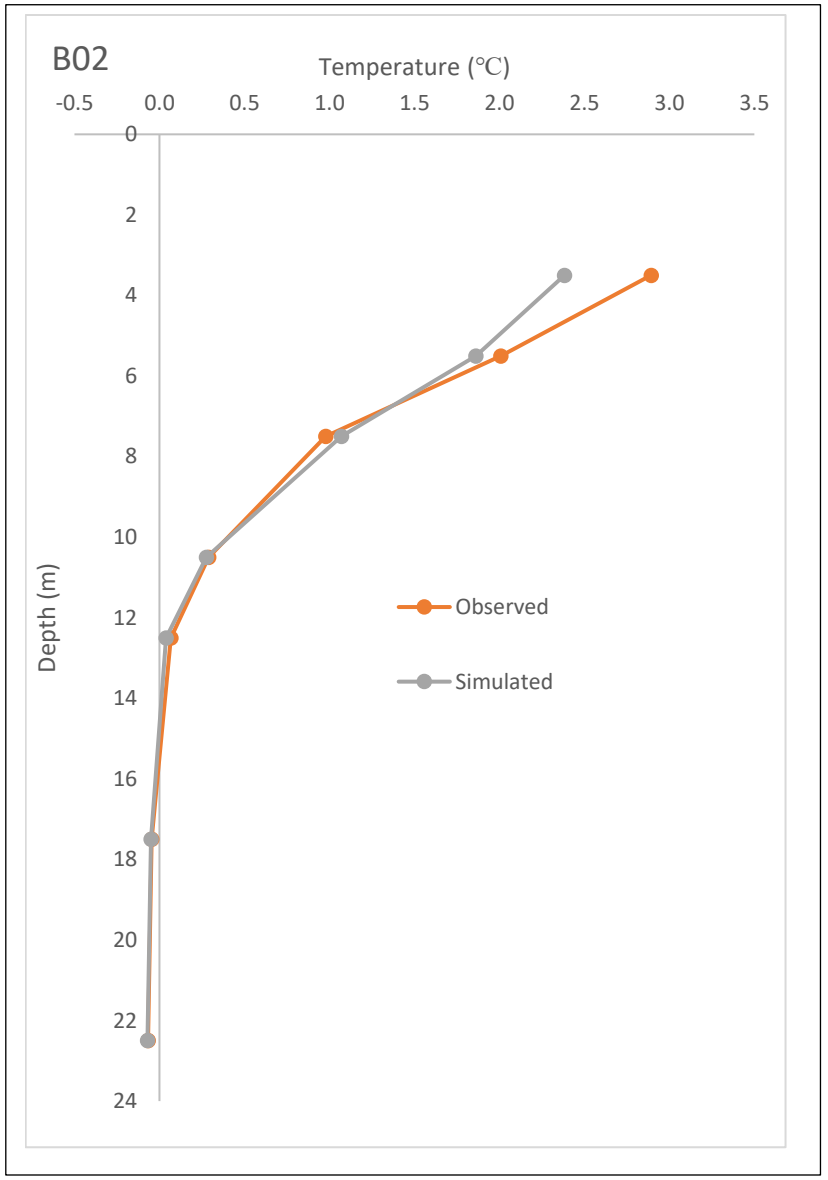

Figure E - 2: Two years average temperature envelopes for B01

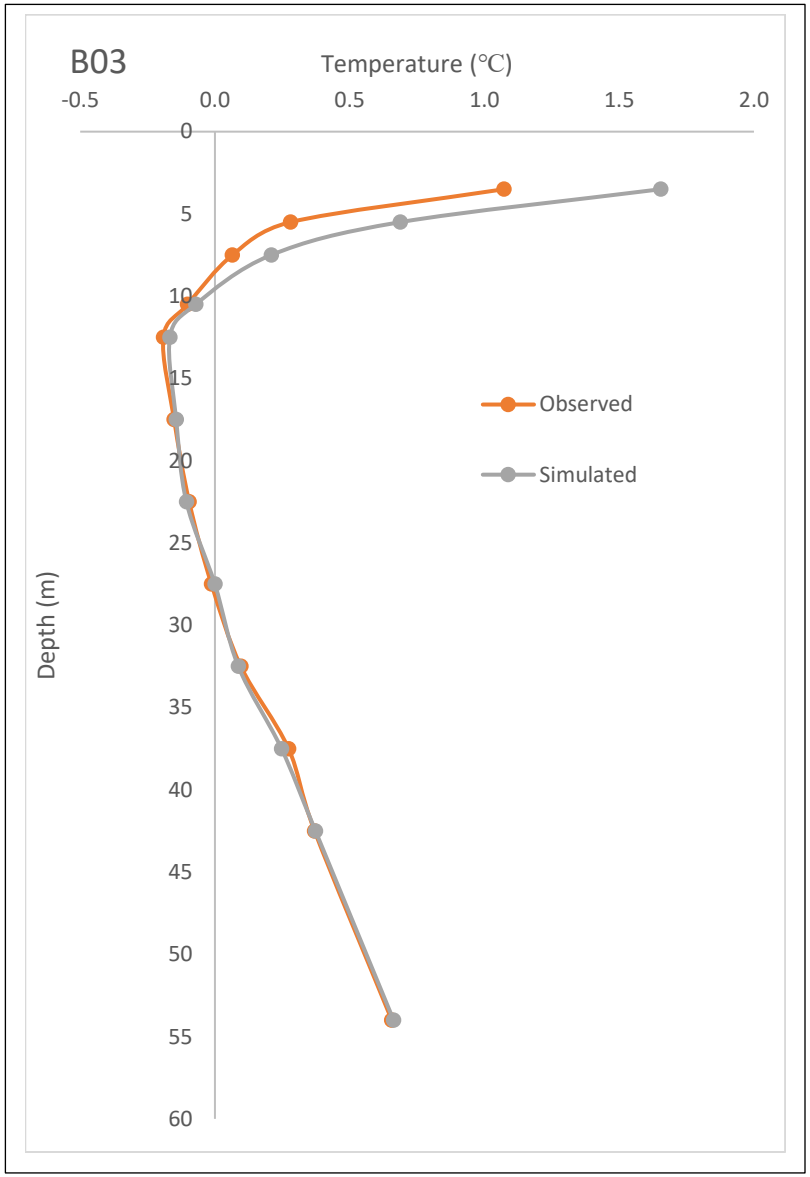

Figure E -3: Two years average temperature envelopes for B04

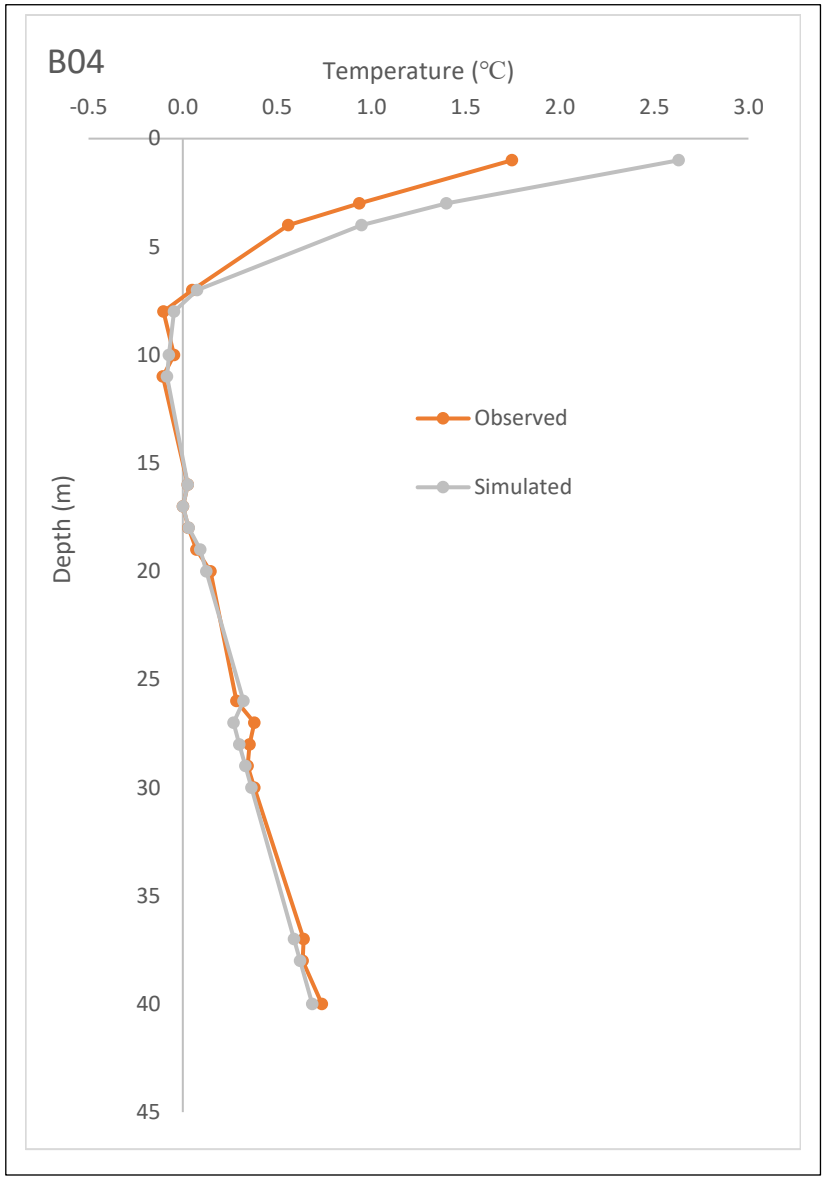

Figure E - 4: Two years average temperature envelopes for B04

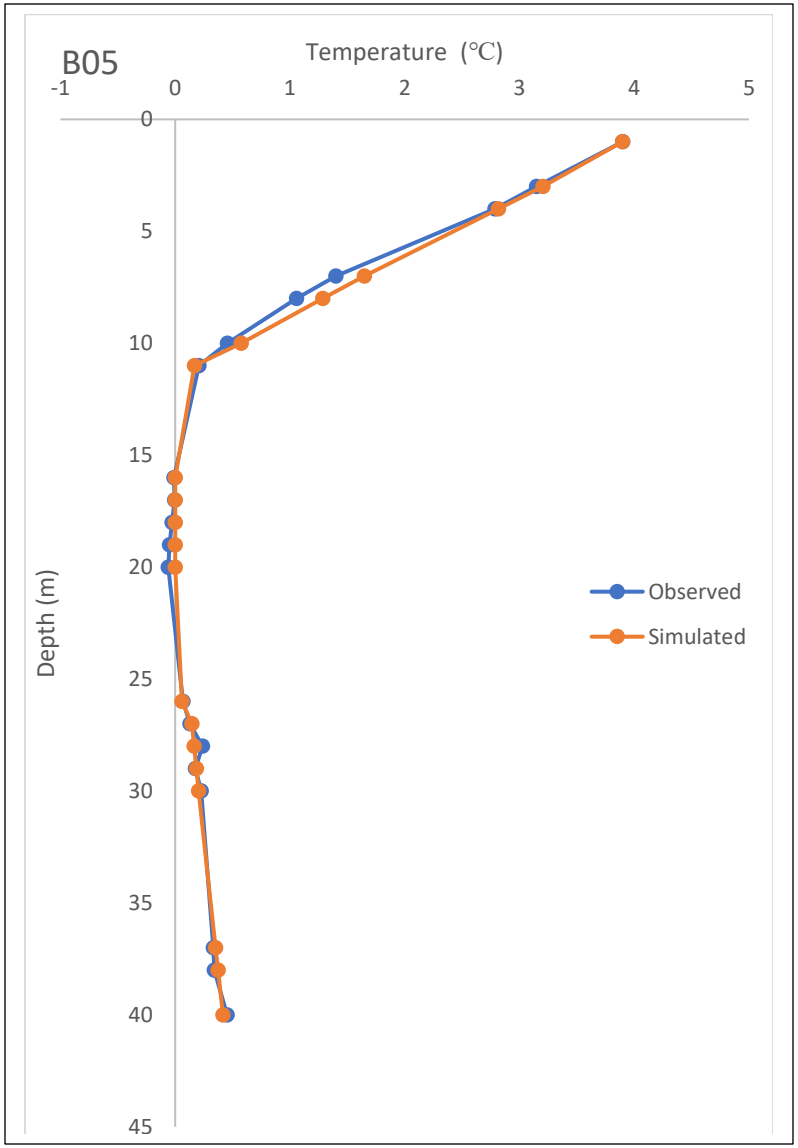

Figure E - 5: Two years average temperature envelopes for B05

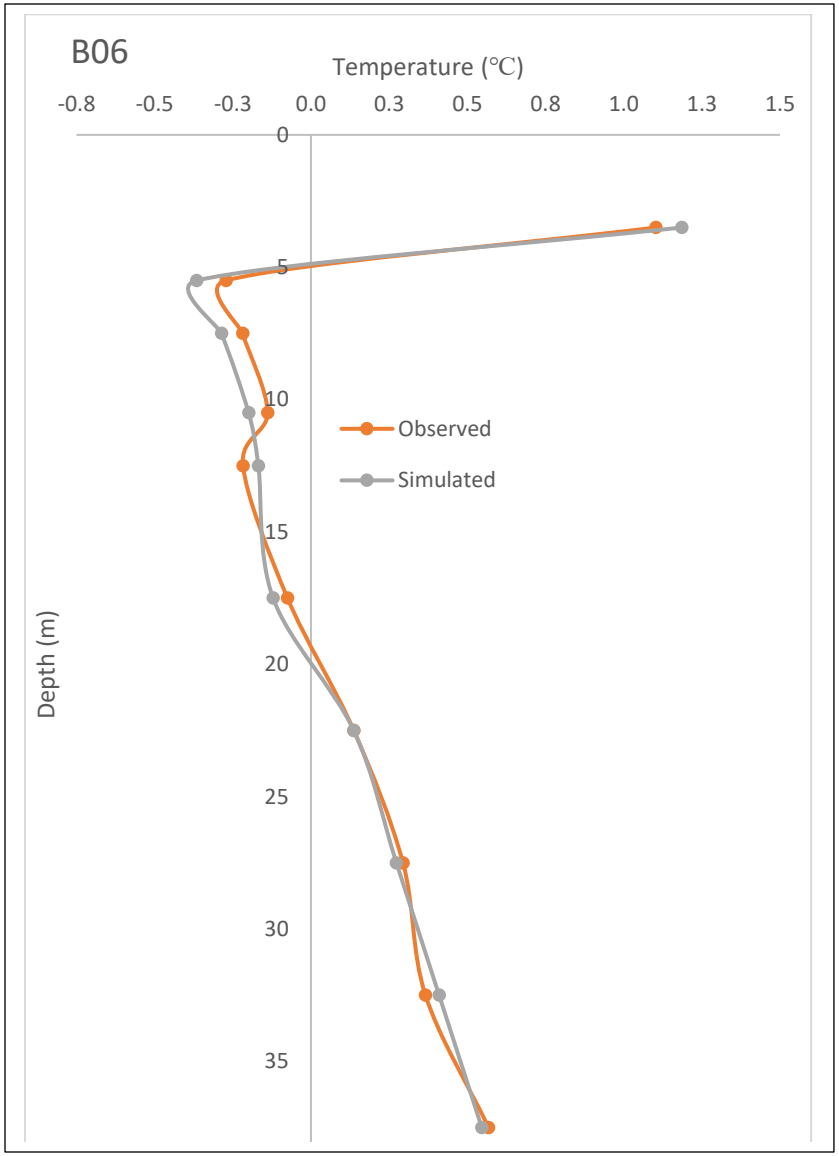

Figure E - 6: Two years average temperature envelopes for B06

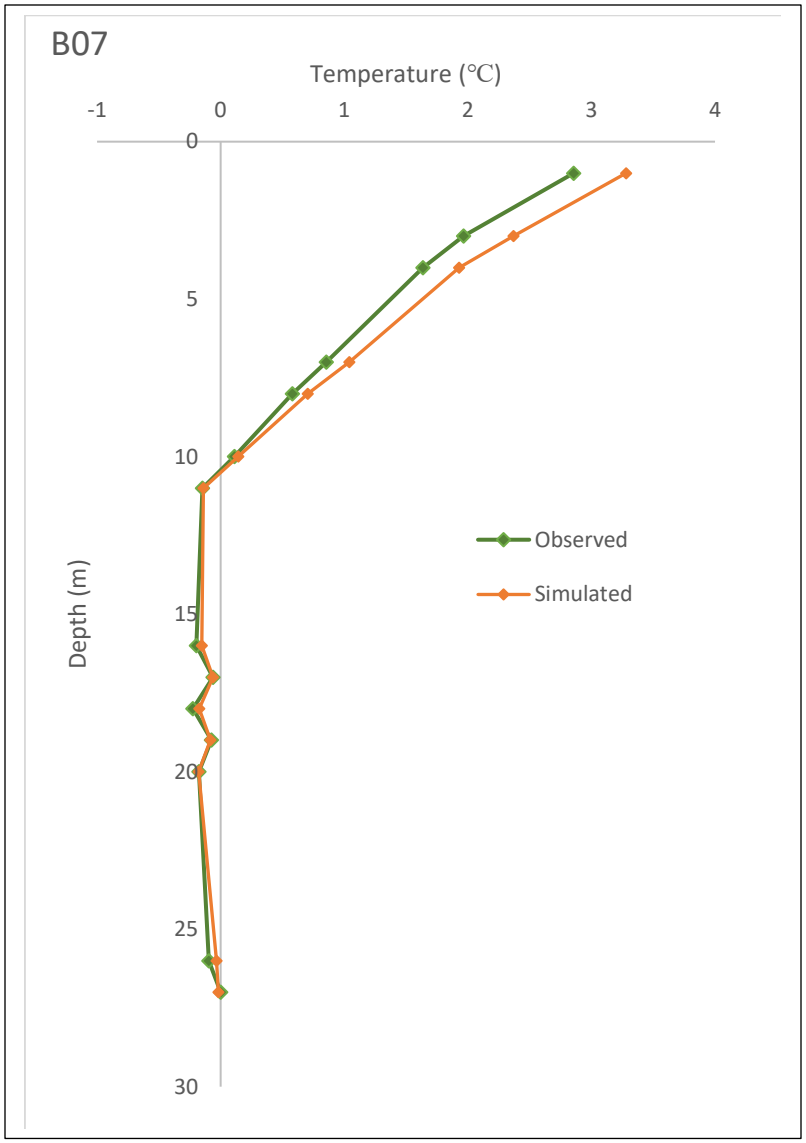

Figure E - 7: Two years average temperature envelopes for B07

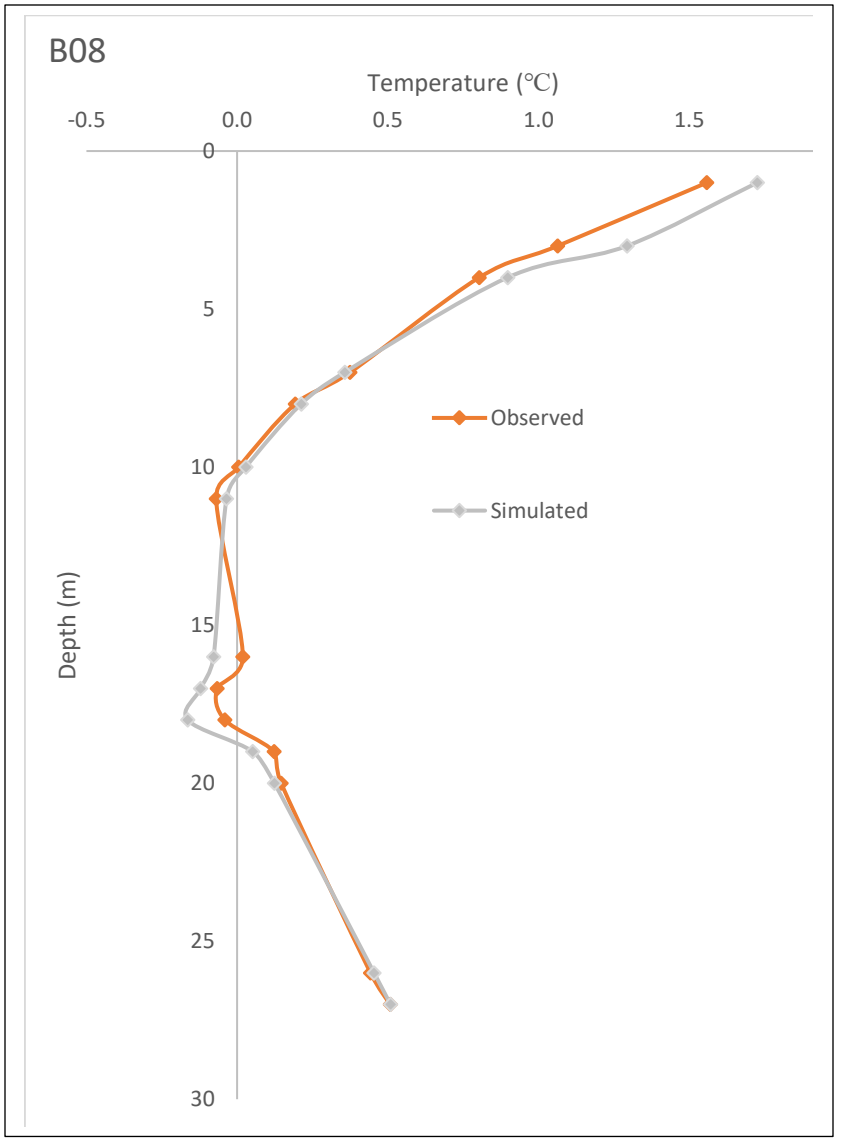

Figure E - 8: Two years average temperature envelopes for B08

Appendix F: Temperature vs depth envelopes for different climate change scenarios

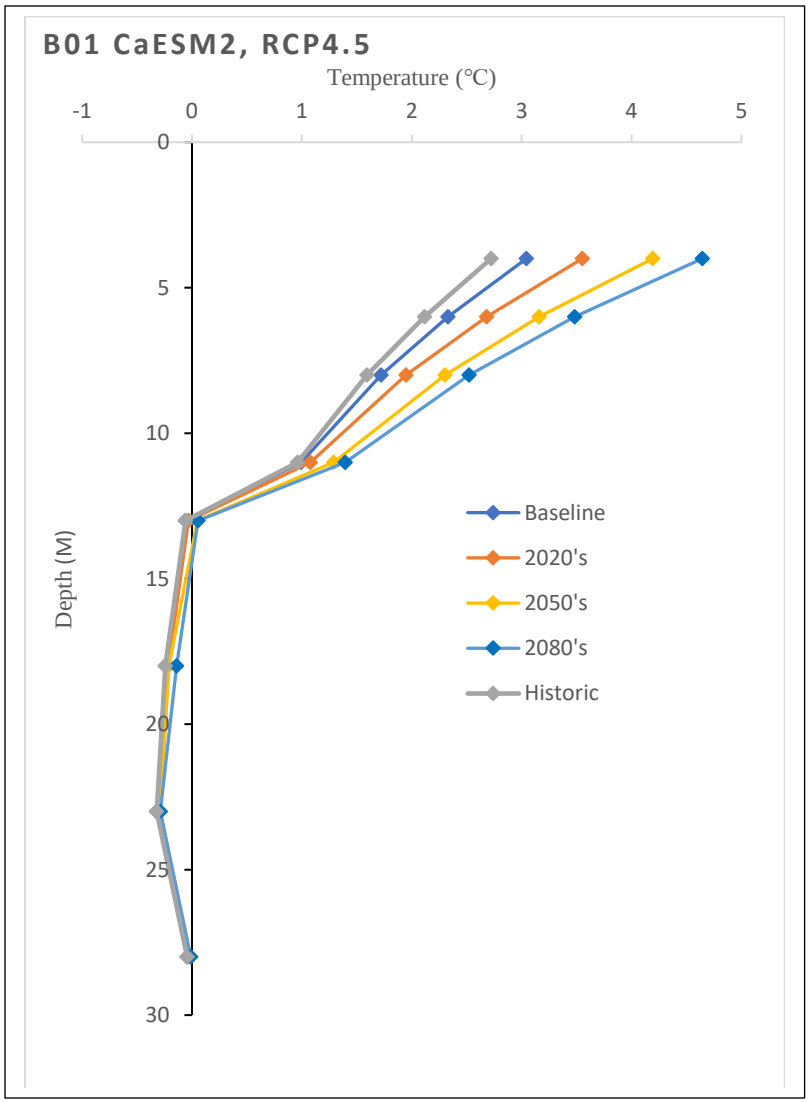

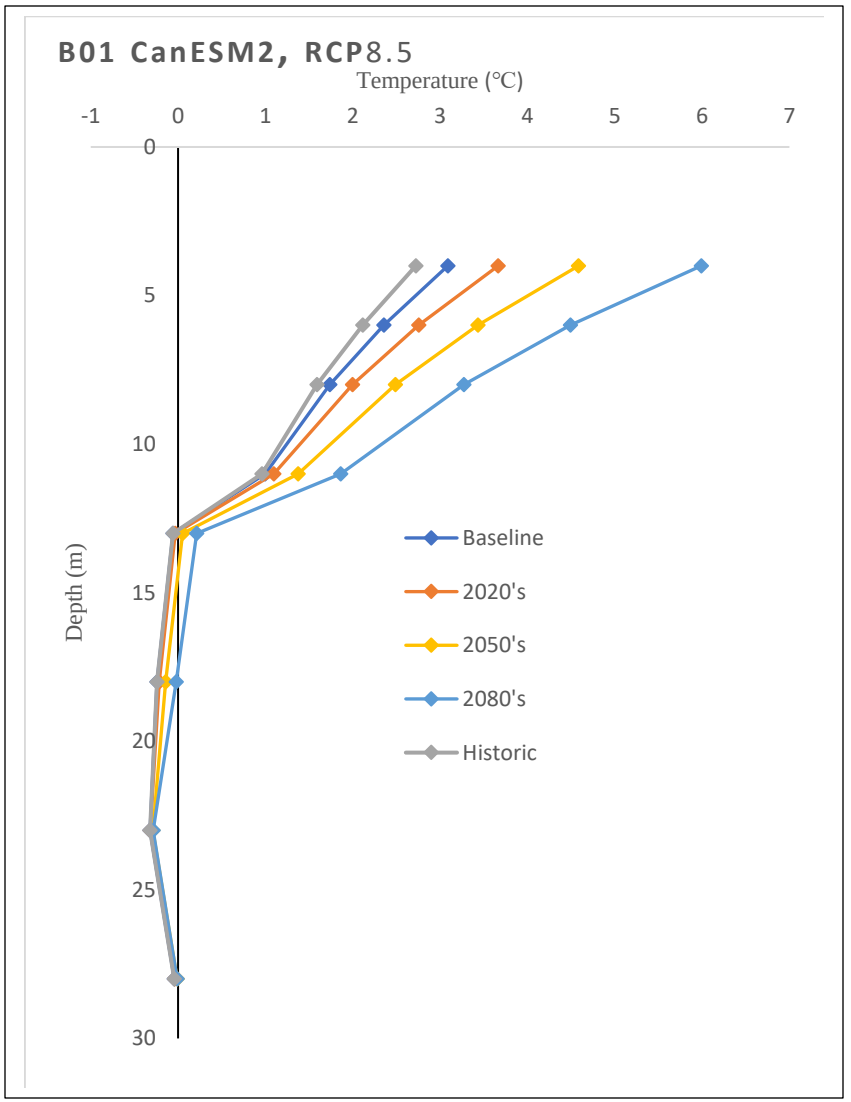

Figure F - 1: Changes in ALT in borehole B01 according to CanESM2 under RCP4.5 and RCP8.5 emission scenarios

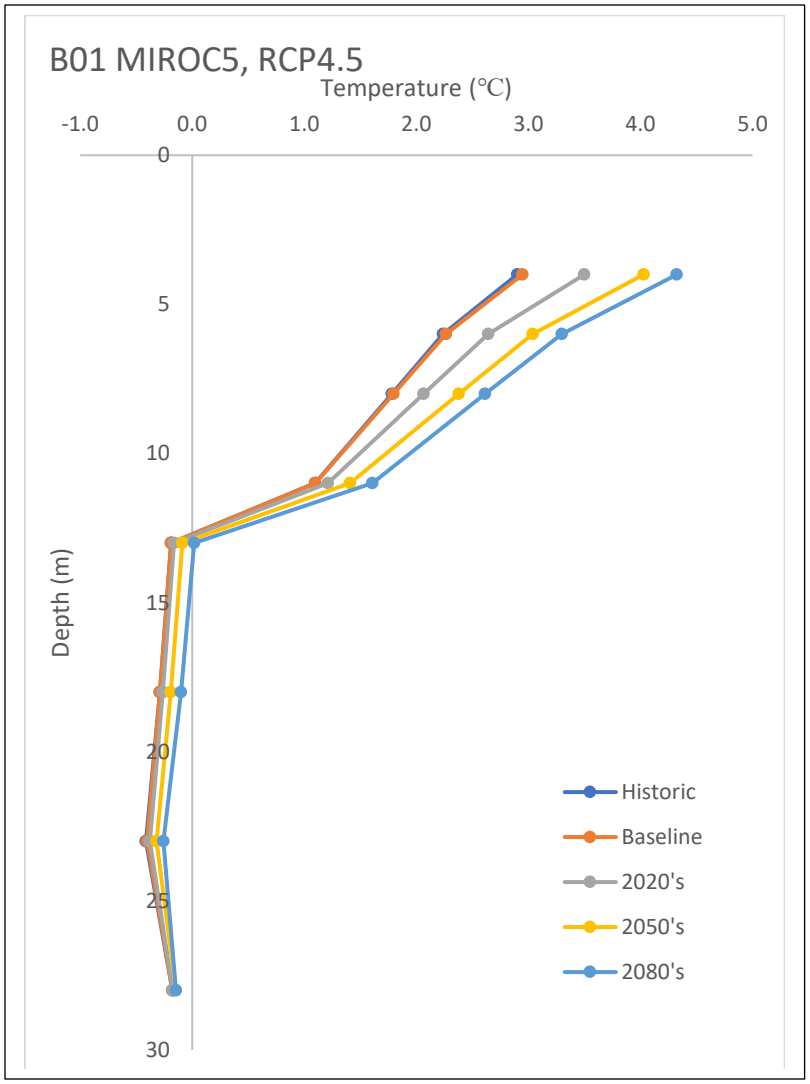

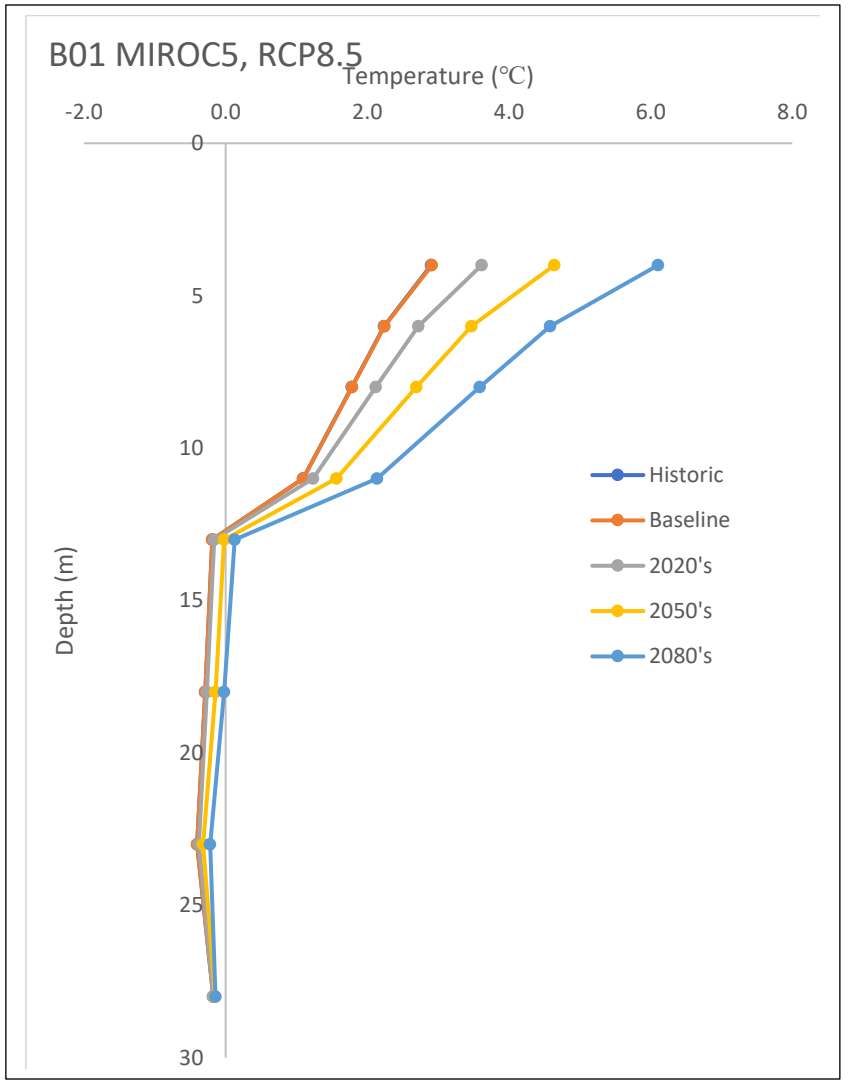

Figure F - 2: Changes in ALT in borehole B01 according to MIROC5 under RCP4.5 and RCP8.5 emission scenarios

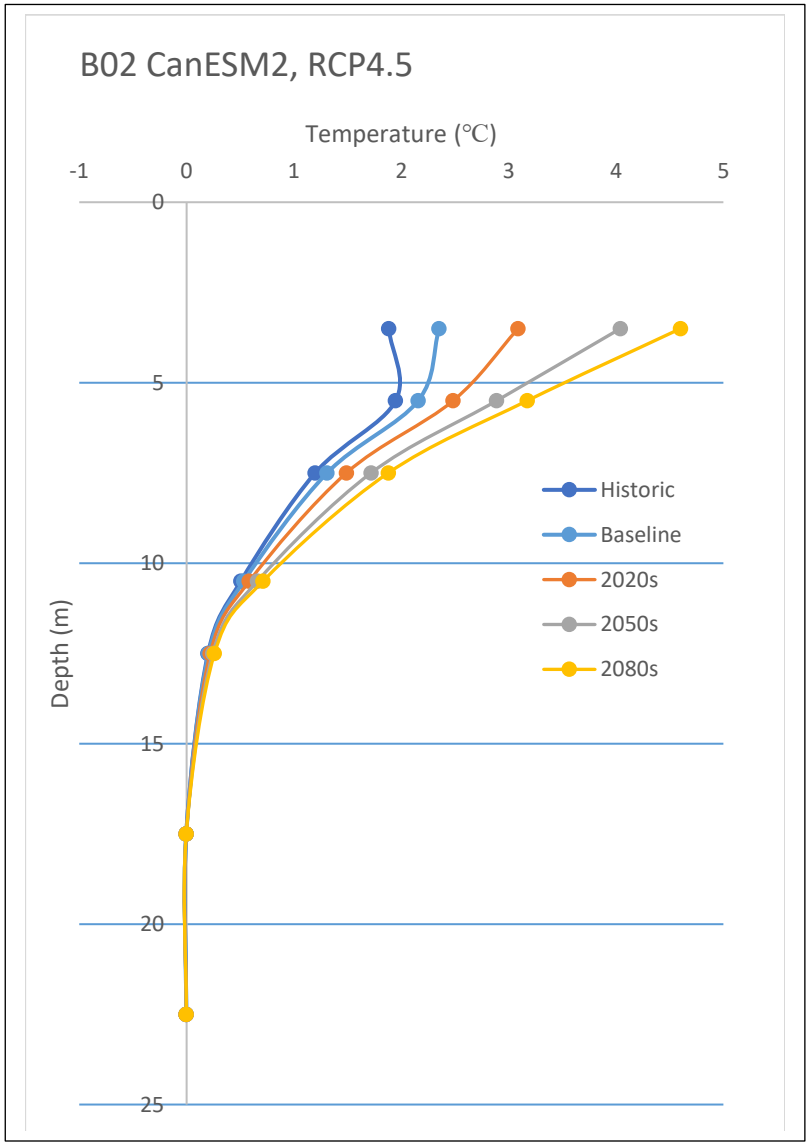

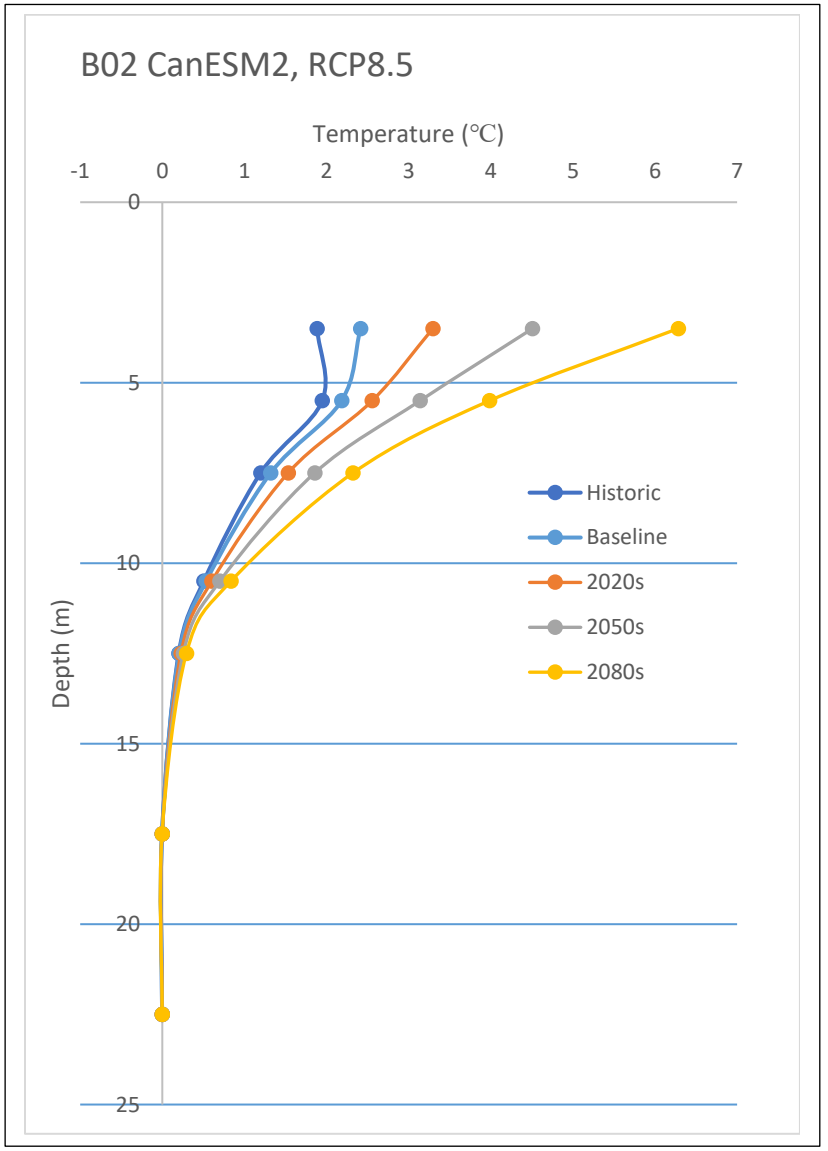

Figure F - 3: Stable ALT in borehole B02 according to CanESM2 under RCP4.5 and RCP8.5 emission scenarios

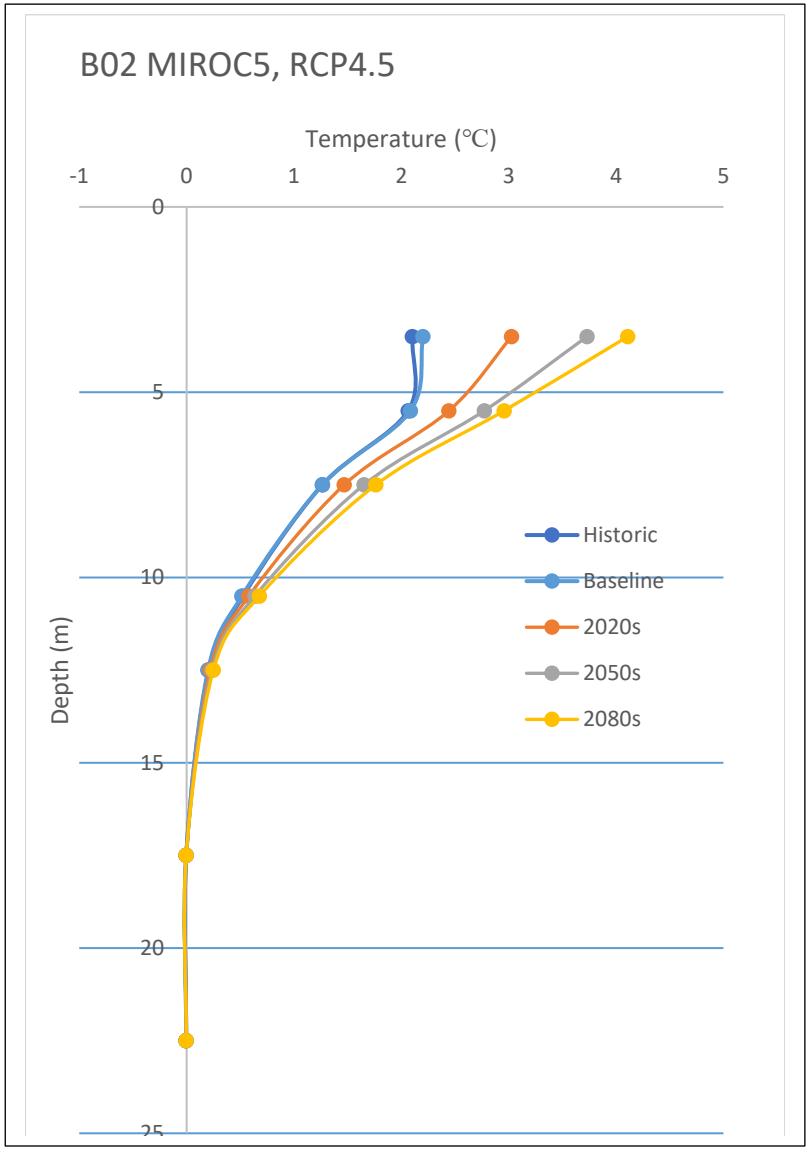

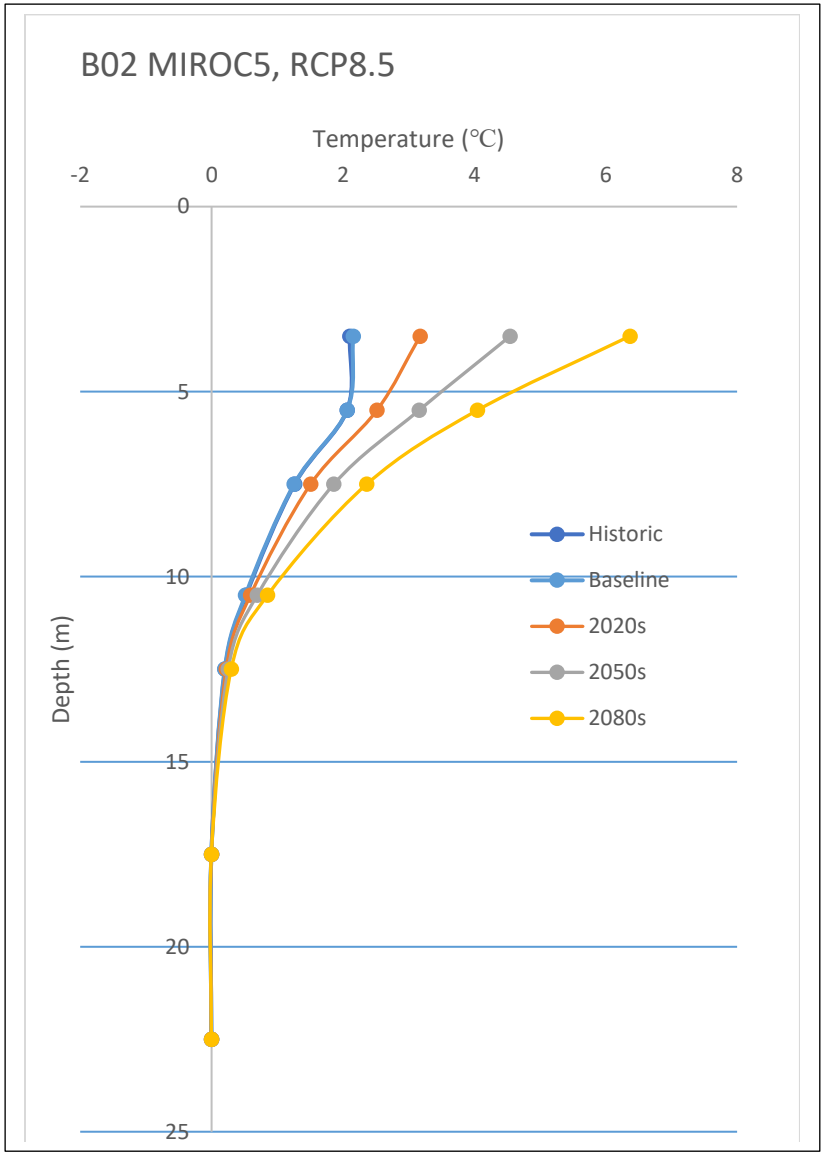

Figure F - 4: Stable ALT in borehole B02 according to MIROC5 under RCP4.5 and RCP8.5 emission scenarios

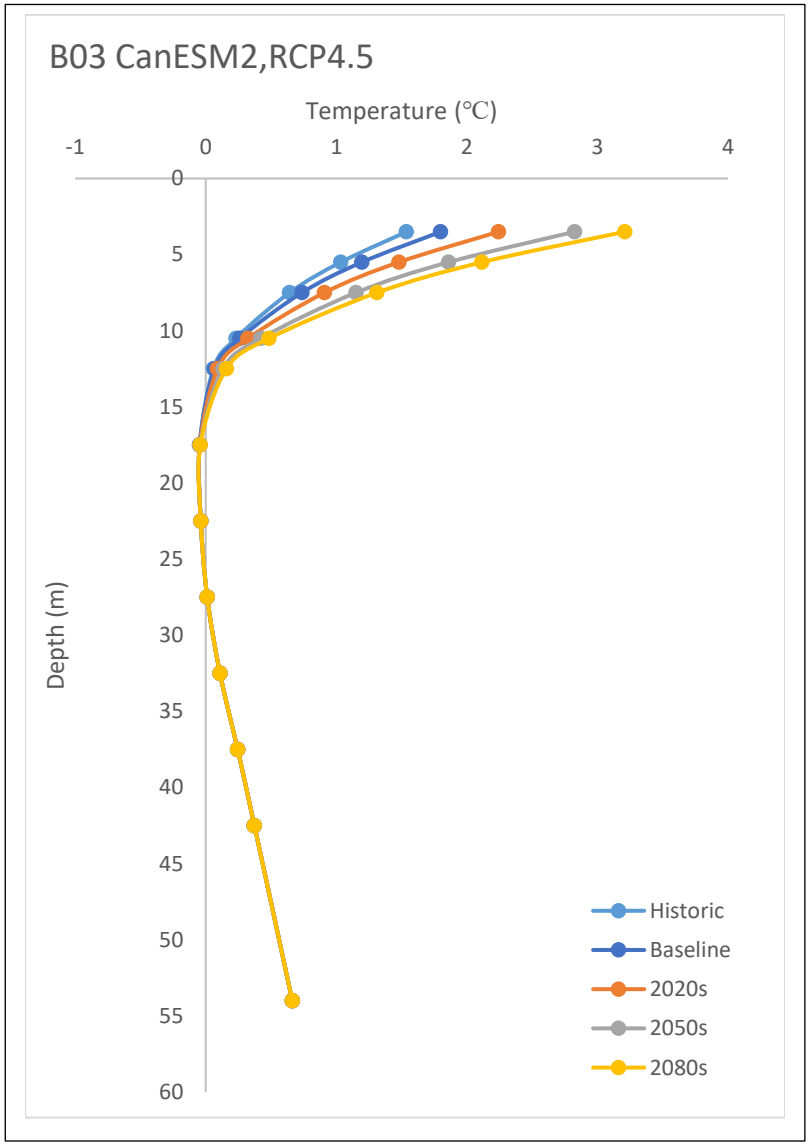

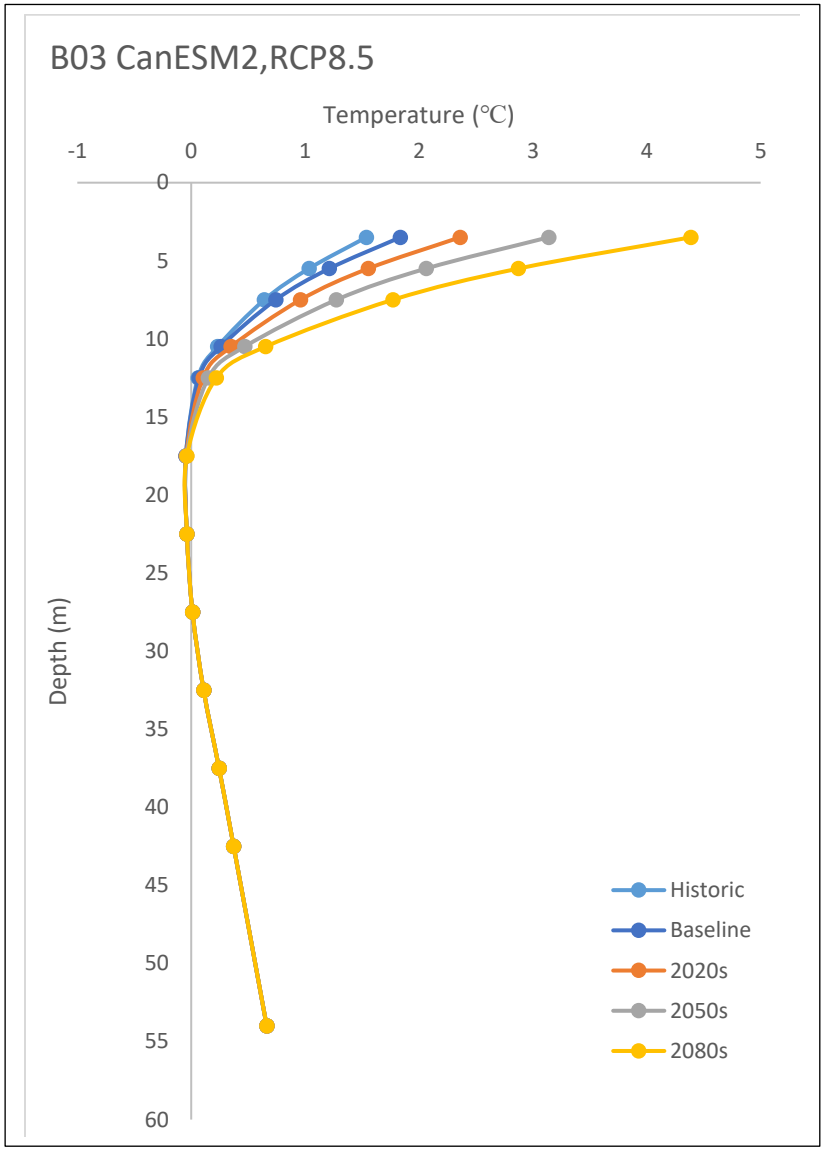

Figure F - 5: Stable ALT in borehole B03 according to CanESM2 under RCP4.5 and RCP8.5 emission scenarios

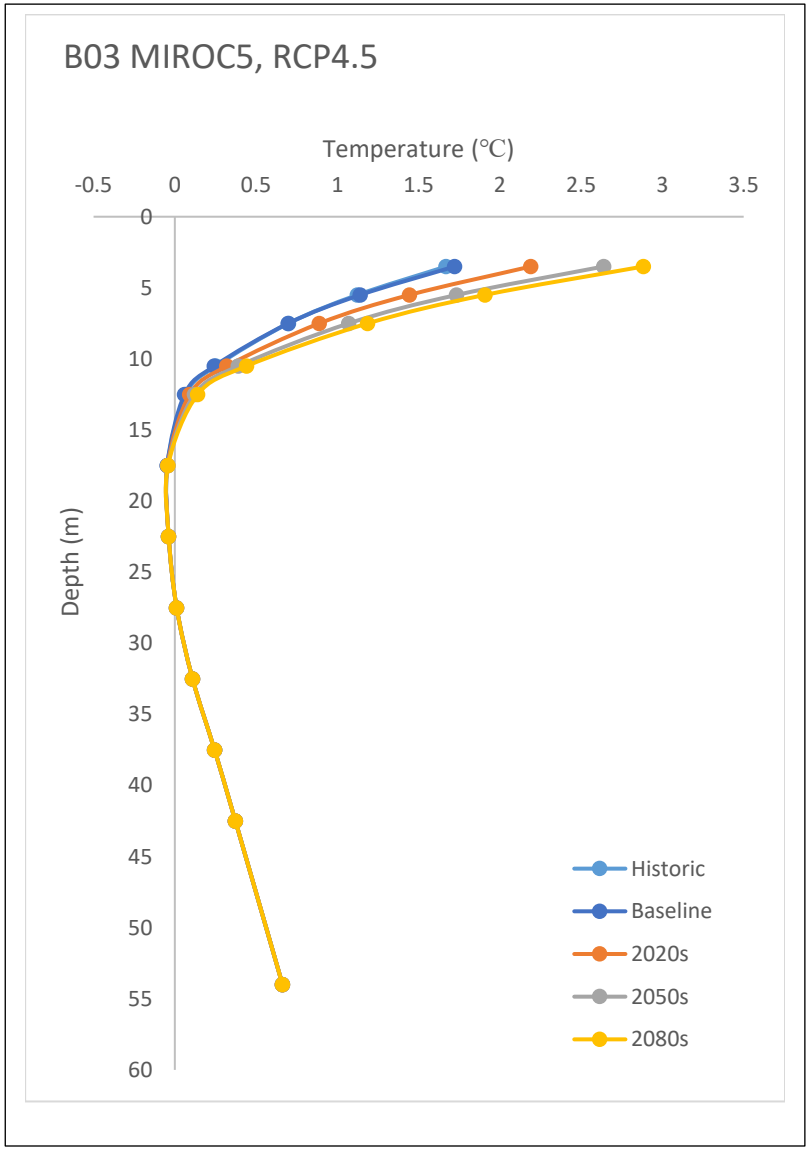

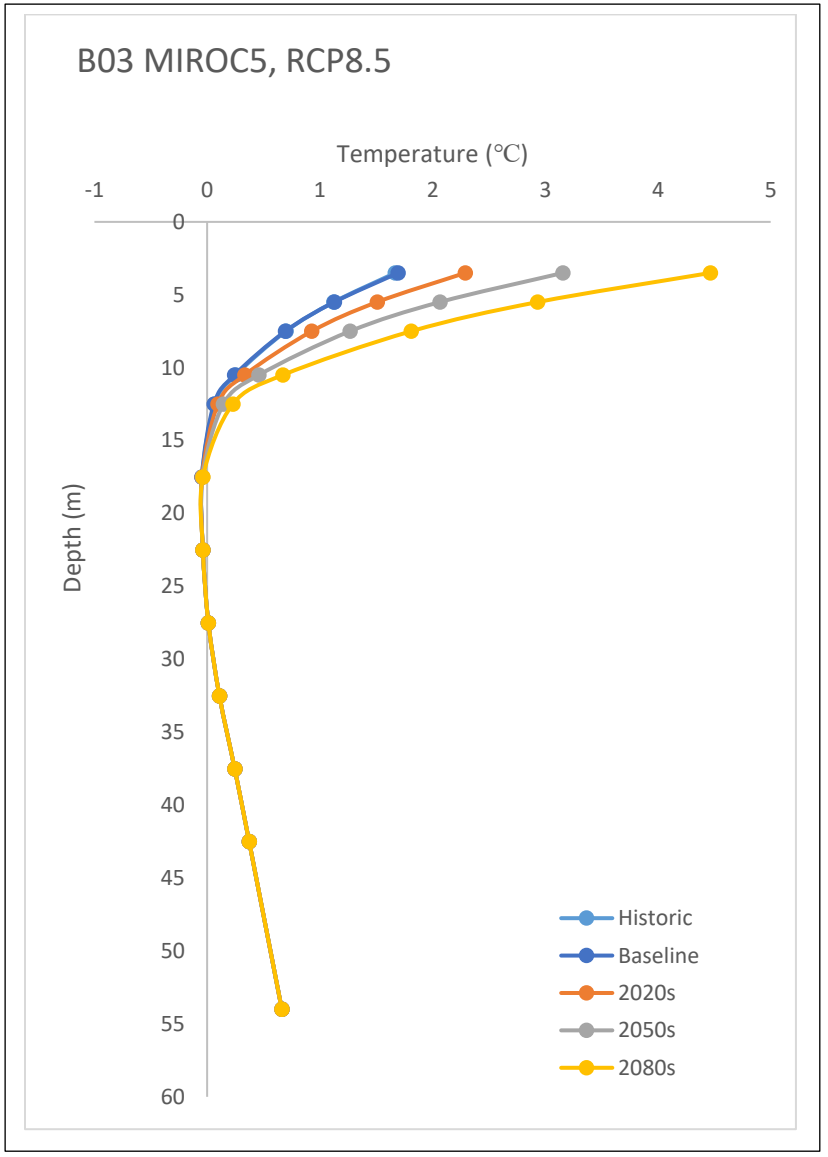

Figure F - 6: Stable ALT in borehole B03 according to MIROC5 under RCP4.5 and RCP8.5 emission scenarios

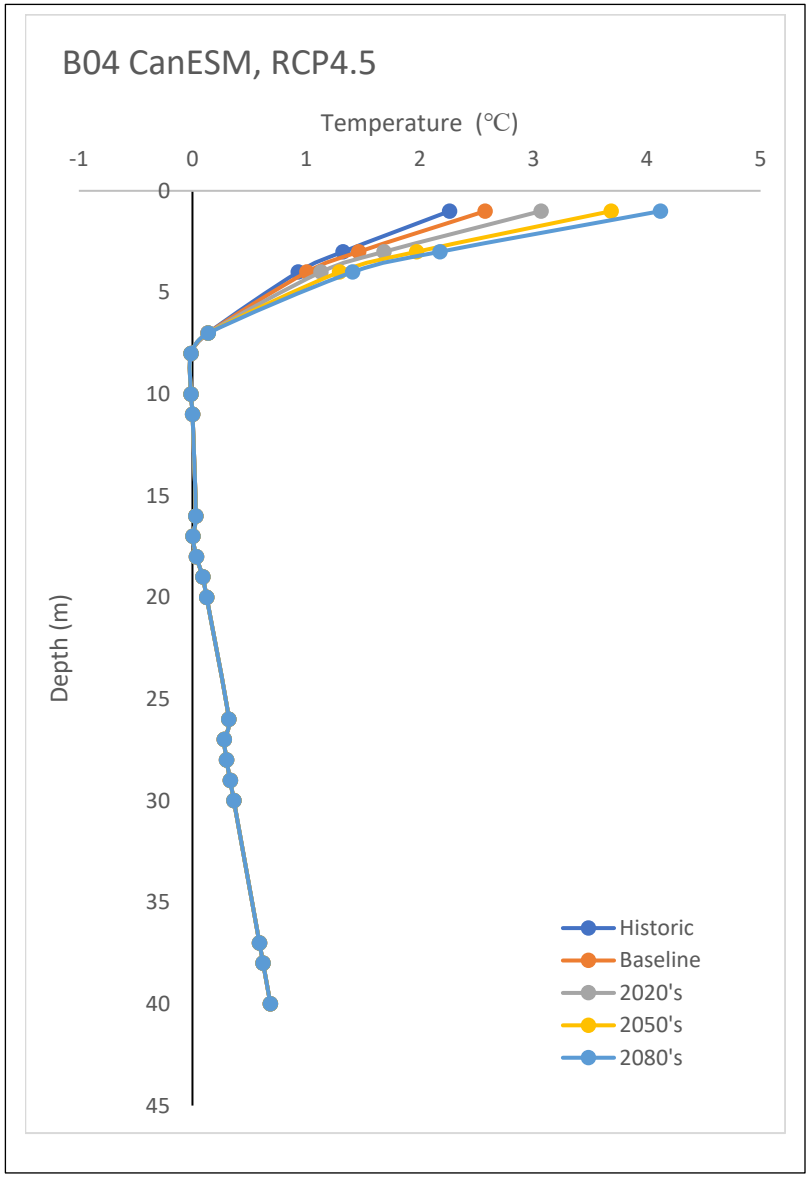

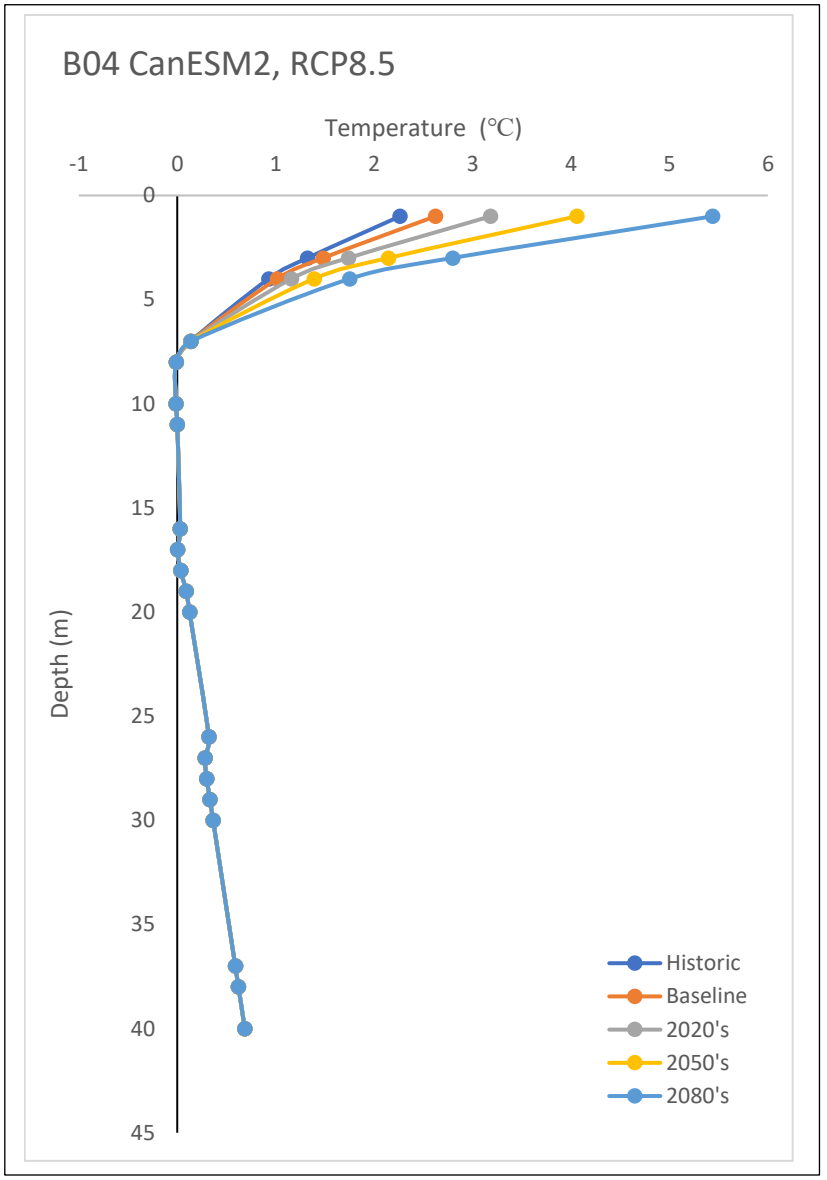

Figure F - 7: Stable ALT in borehole B04 according to CanESM2 under RCP4.5 and RCP8.5 emission scenarios

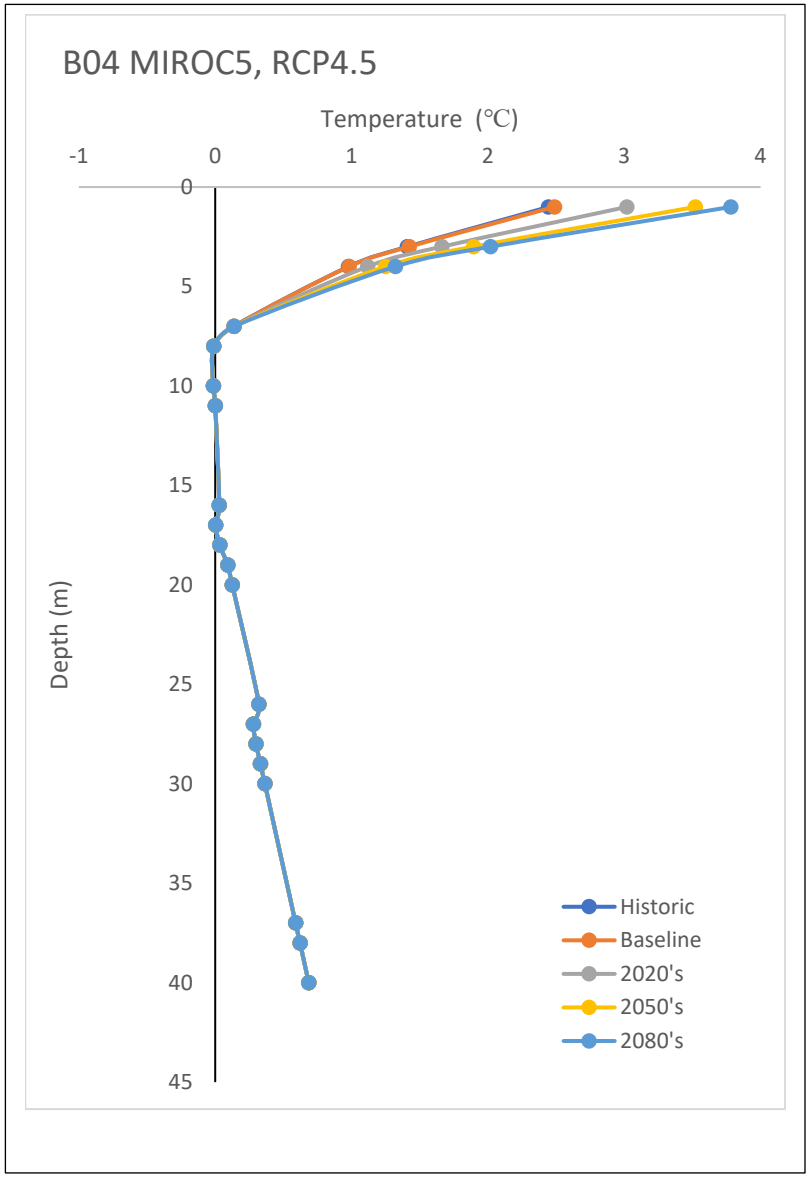

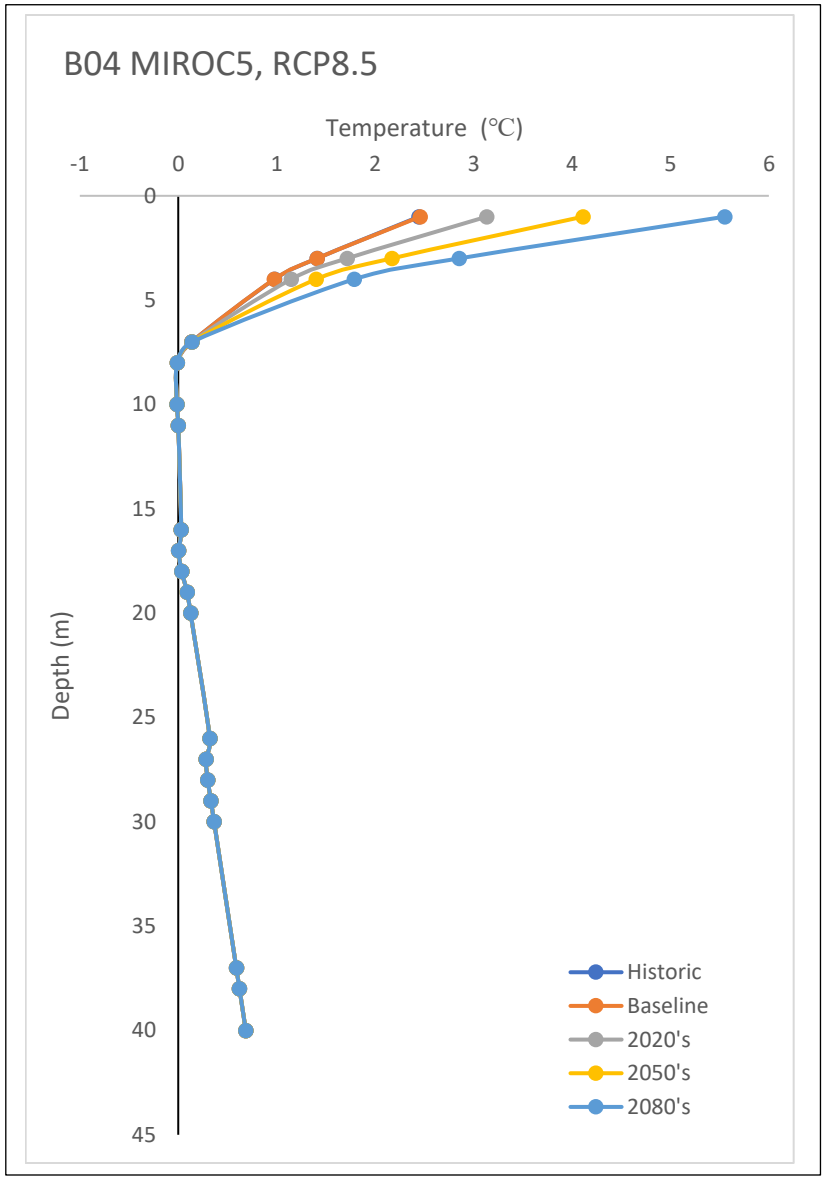

Figure F - 8: Stable ALT in borehole B04 according to MIROC5 under RCP4.5 and RCP8.5 emission scenarios

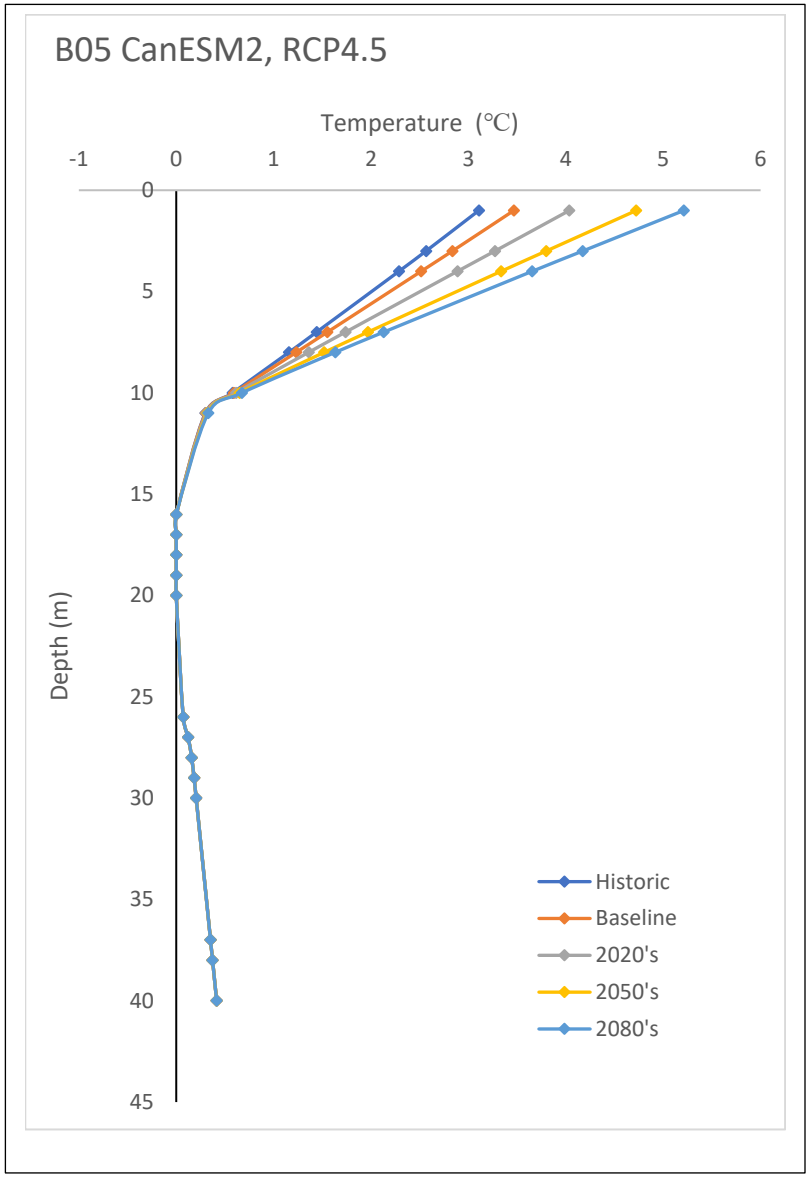

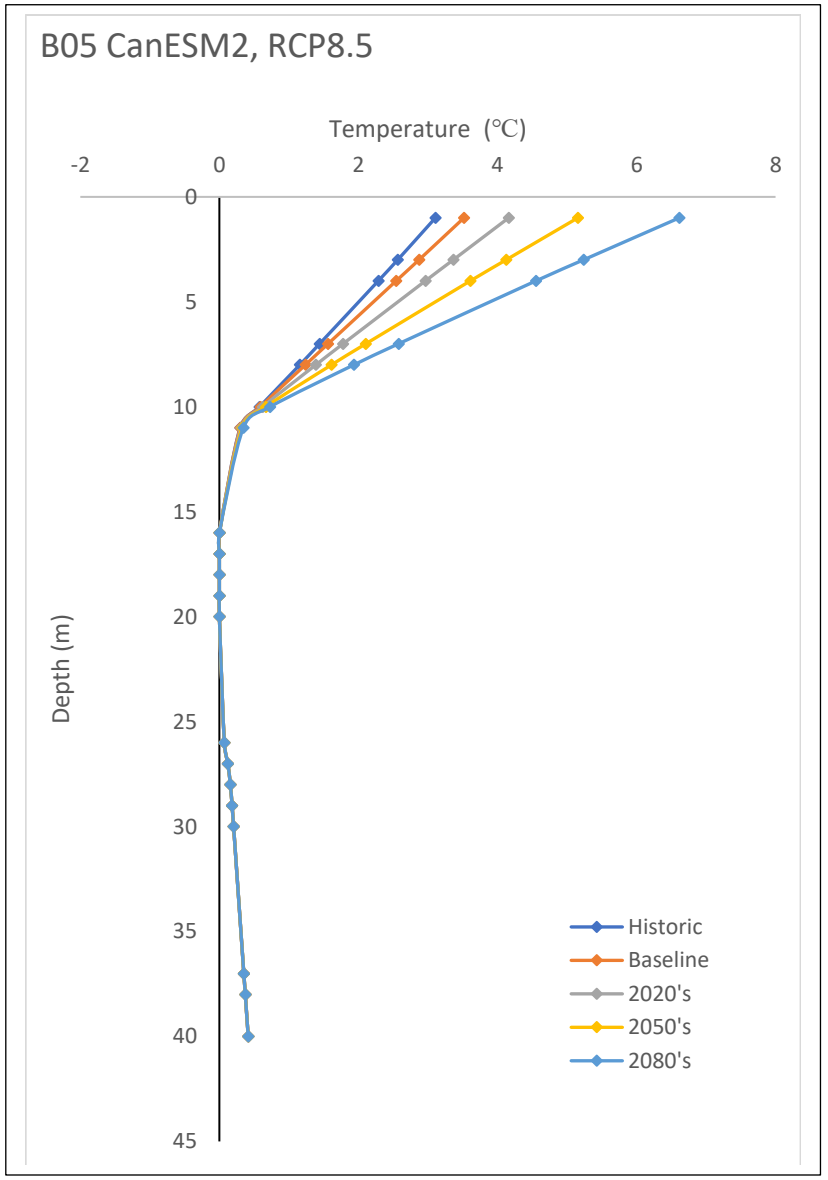

Figure F - 9: Stable ALT in borehole B05 according to CanESM2 under RCP4.5 and RCP8.5 emission scenarios

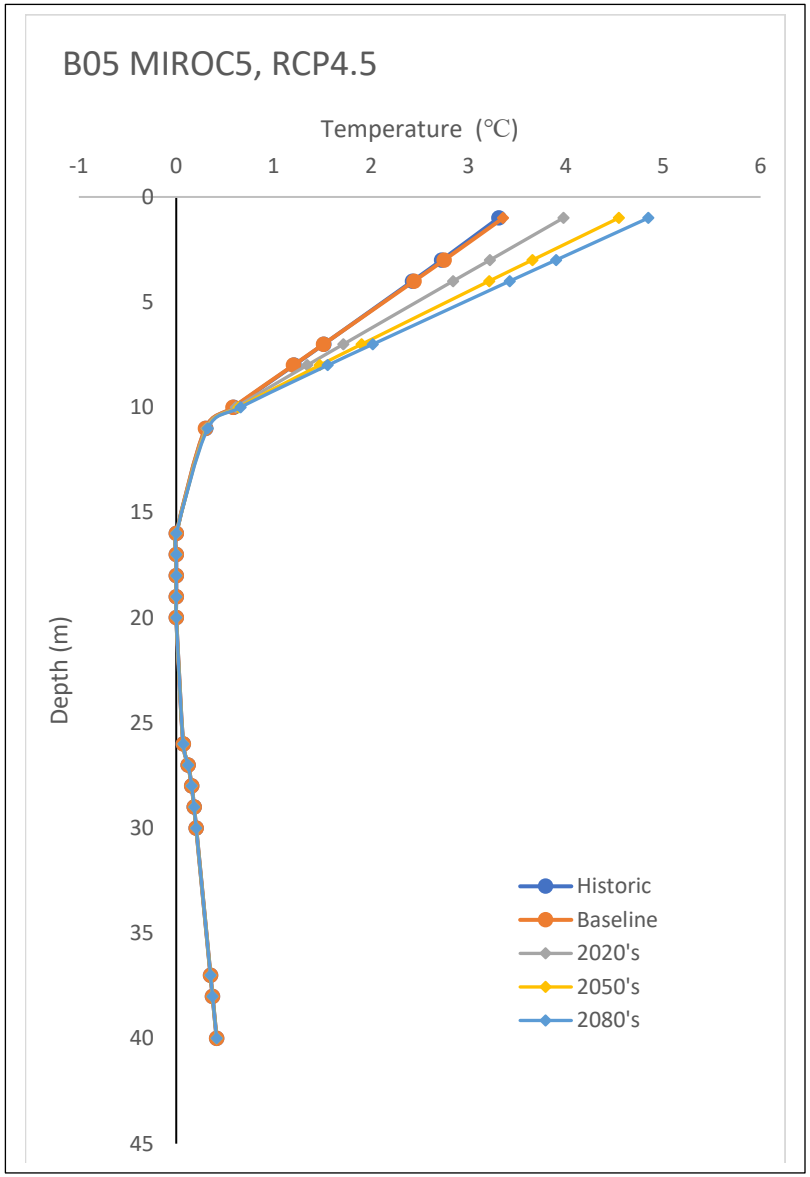

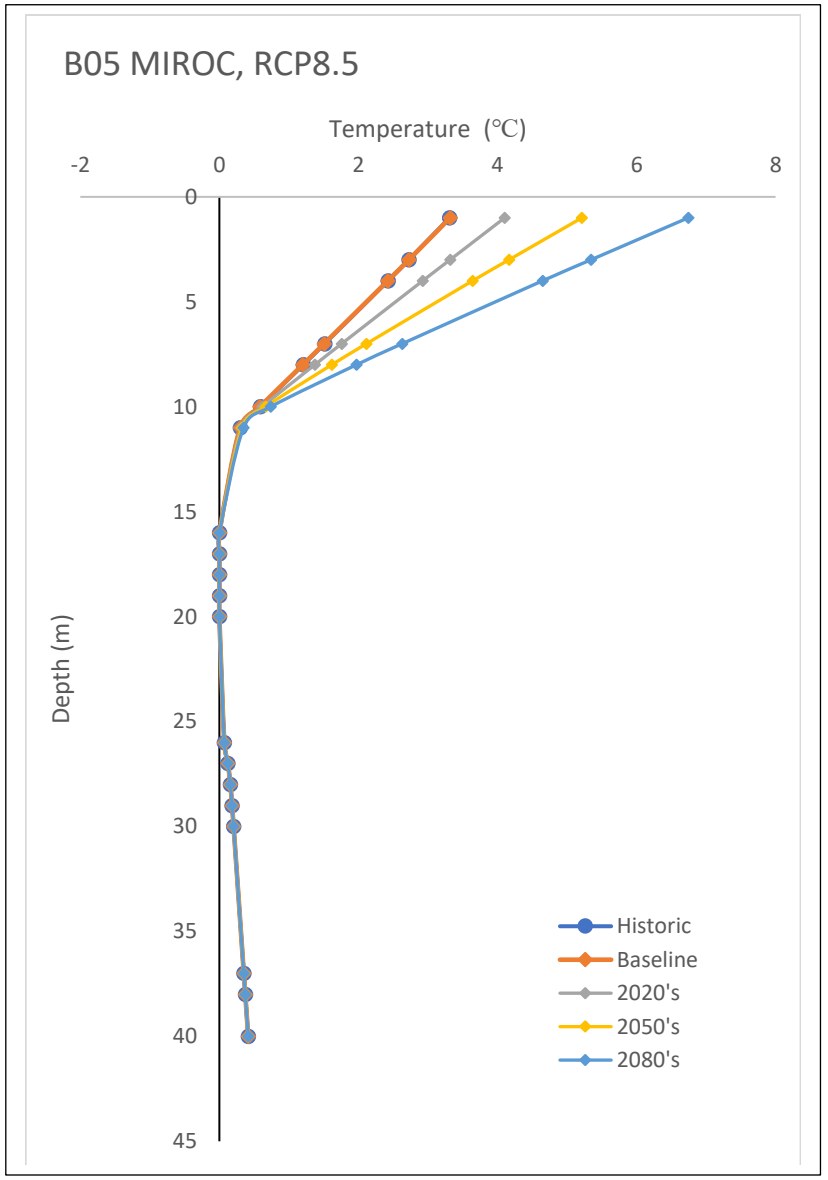

Figure F - 10: Stable ALT in borehole B05 according to MIROC5 under RCP4.5 and RCP8.5 emission scenarios

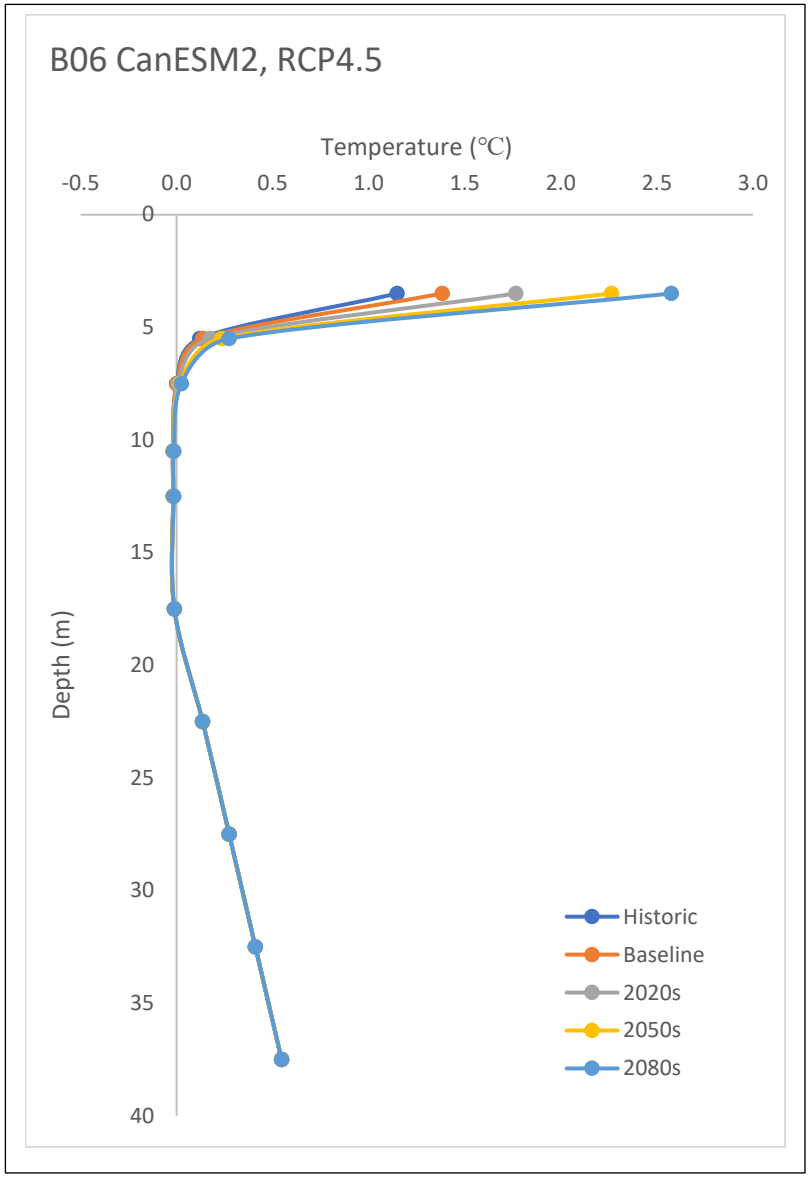

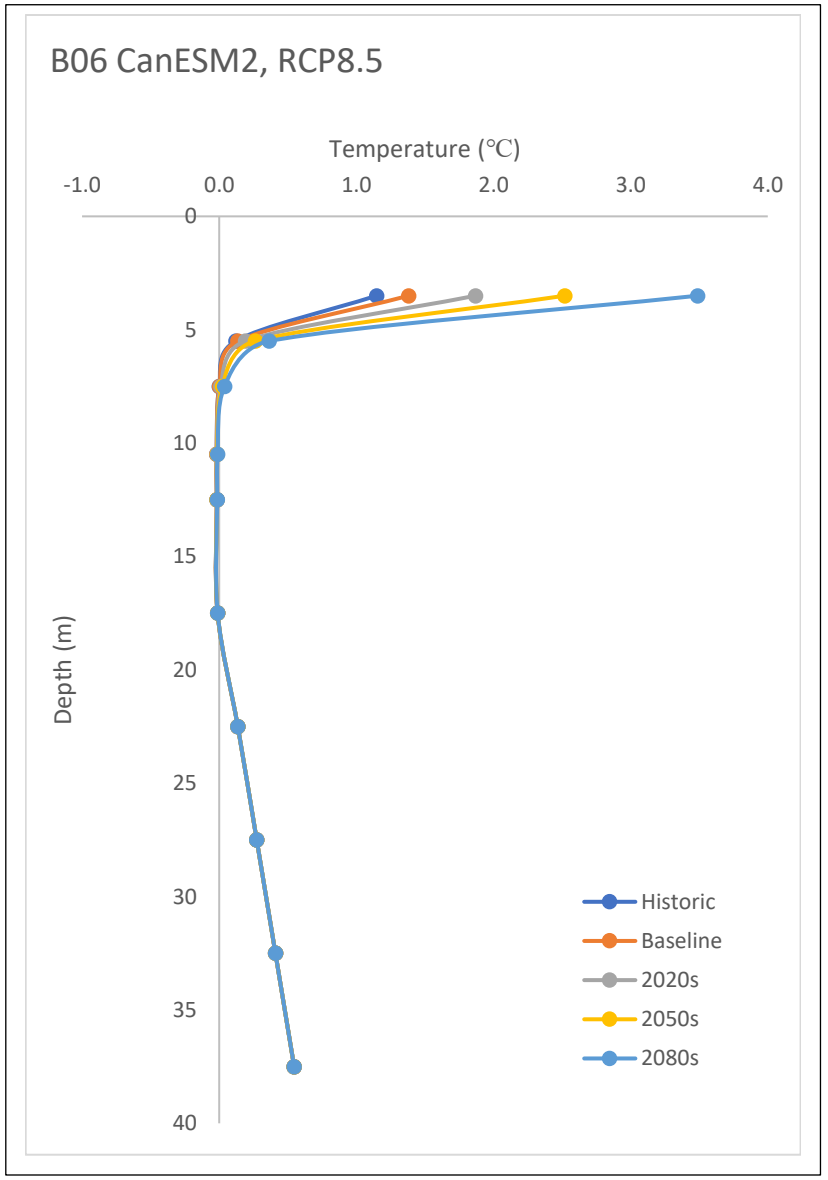

Figure F - 11: Stable ALT in borehole B06 according to CanESM2 under RCP4.5 and RCP8.5 emission scenarios

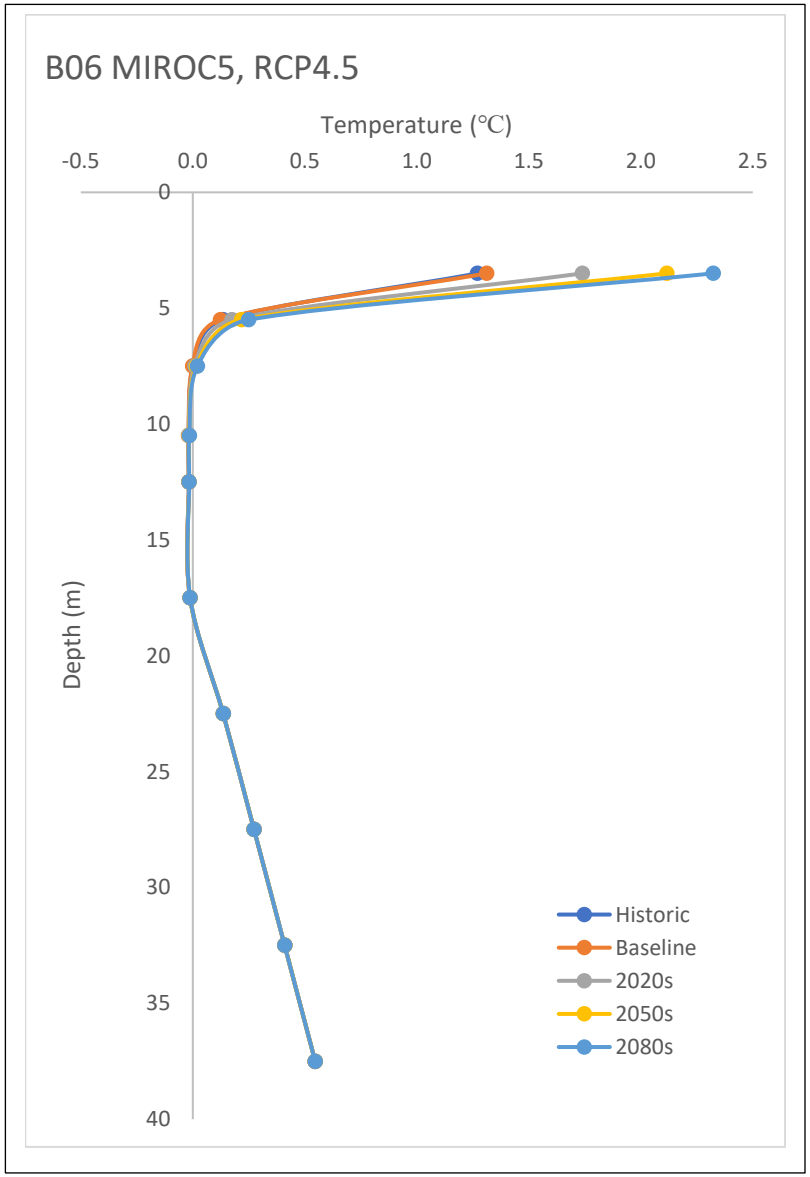

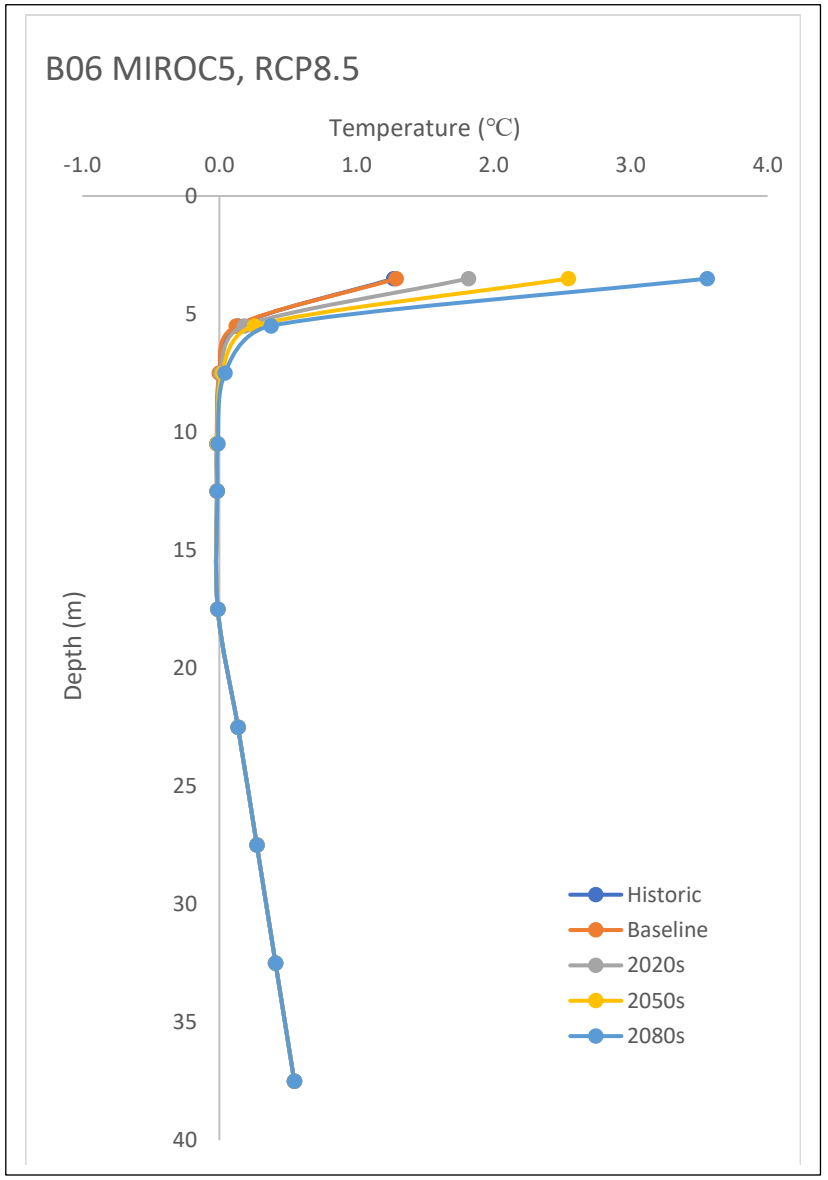

Figure F - 12: Stable ALT in borehole B06 according to MIROC5 under RCP4.5 and RCP8.5 emission scenarios

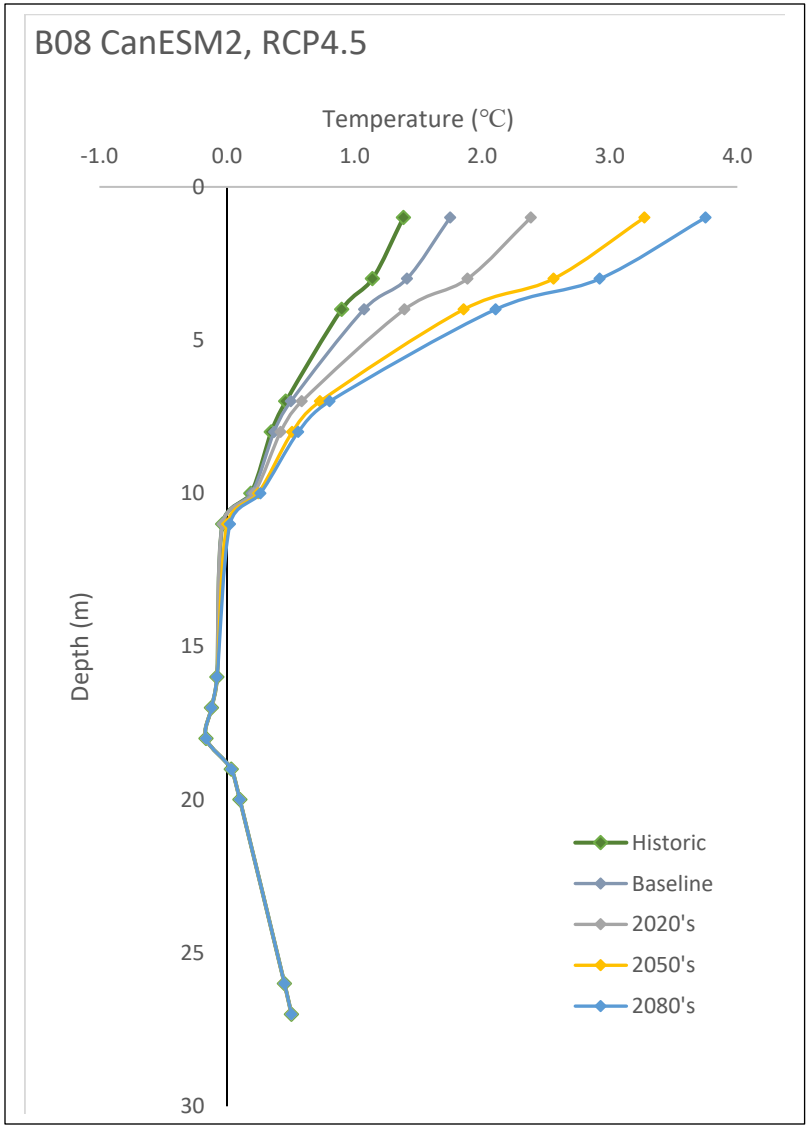

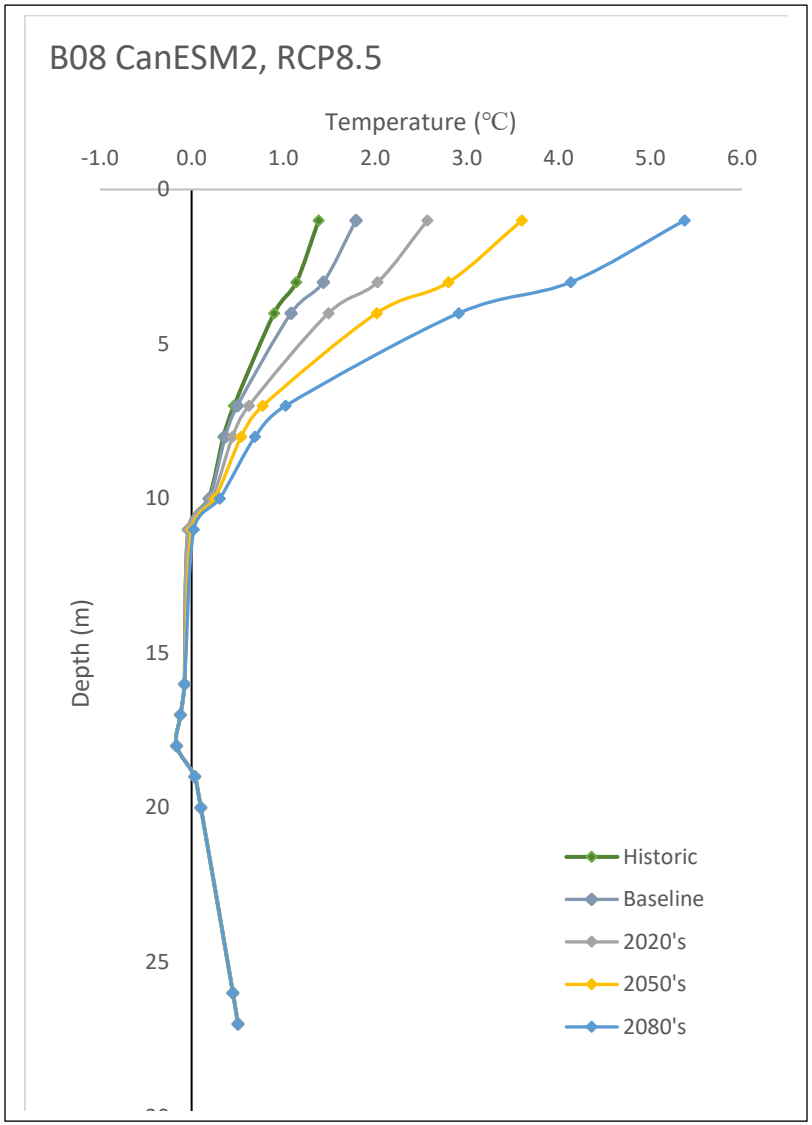

Figure F - 13: Changes in ALT in borehole B08 according to CanESM2 under RCP4.5 and RCP8.5 emission scenarios

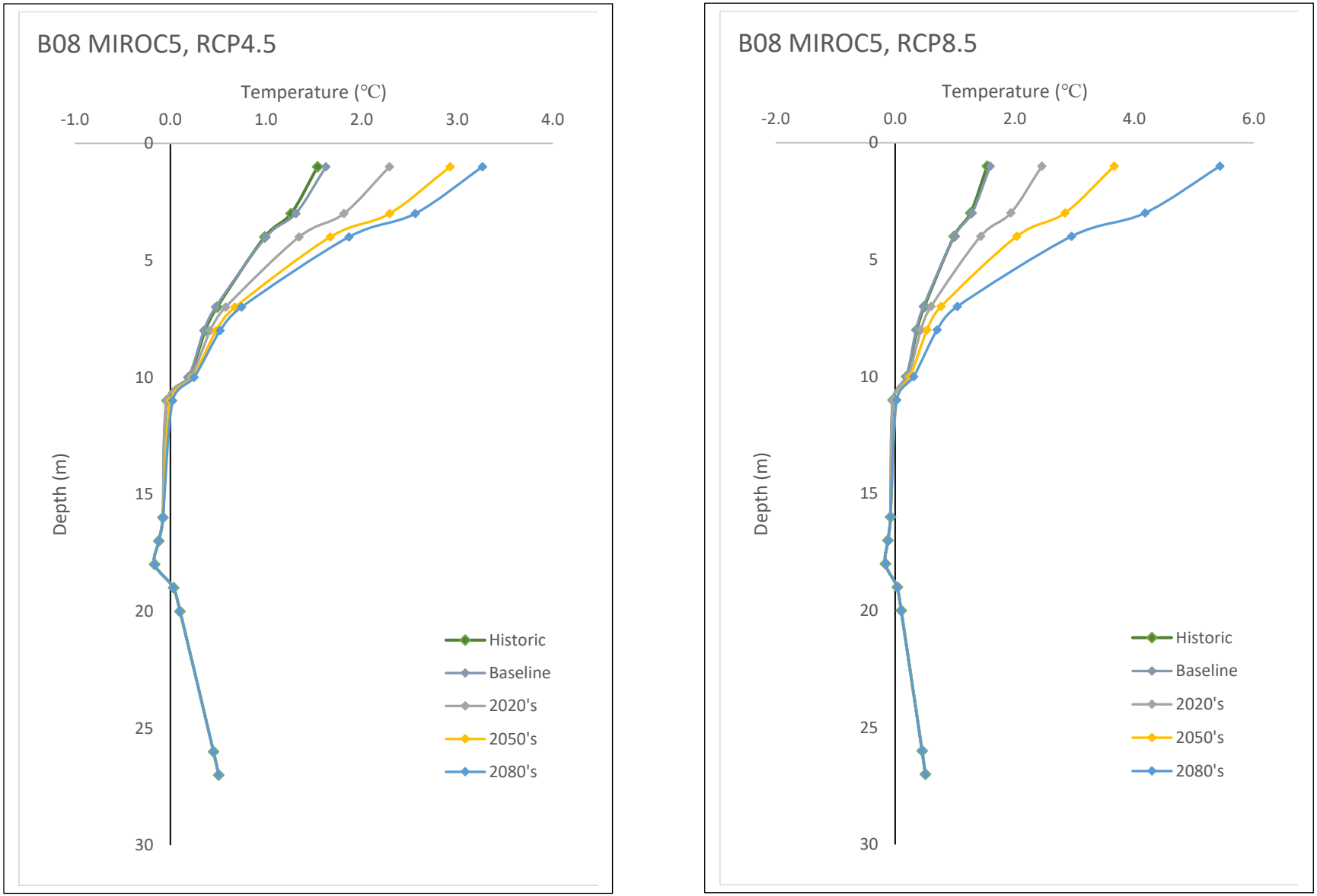

Figure F - 54: Changes in ALT in borehole B08 according to MIROC5 under RCP4.5 and RCP8.5 emission scenario